



## DISCLAIMER

This report was prepared as an account of work sponsored by an agency of the United States Government. Neither the United States Government nor any agency thereof, nor any of their employees, makes any warranty, express or implied, or assumes any legal liability or responsibility for the accuracy, completeness, or usefulness of any information, apparatus, product, or process disclosed, or represents that its use would not infringe privately owned rights. Reference herein to any specific commercial product, process, or service by trade name, trademark, manufacturer, or otherwise, does not necessarily constitute or imply its endorsement, recommendation, or favoring by the United States Government or any agency thereof. The views and opinions of authors expressed herein do not necessarily state or reflect those of the United States Government or any agency thereof.

Printed in the United States of America. Available from:  
National Technical Information Service  
U.S. Department of Commerce  
5285 Port Royal Road  
Springfield, VA 22161

NTIS price codes

Paper copy: **A07**

Microfiche copy: **A01**

DOE/BC/14126-6  
Distribution Category UC-122

ON THE USE OF PRESSURE AND TRACER  
TEST DATA FOR RESERVOIR DESCRIPTION

Supri TR 65

By  
S. Mishra

April 1989

Work Performed Under Contract No. FG19-87BC14126

Prepared for  
U. S. Department of Energy  
Assistant Secretary for Fossil Energy

Thomas B. Reid, Project Manager  
Bartlesville Project Office  
P.O. Box 1398  
Bartlesville, OK 74005

Prepared by  
Stanford University  
Petroleum Research Institute  
Stanford, CA 94305-4042



## ACKNOWLEDGEMENTS

This report by S. Mishra which is based on Mishra's Ph.D. dissertation, is a good example of the close cooperation that occurs between the various research projects in the Petroleum Engineering Department as well as other departments in the School of Earth Sciences at Stanford. The bulk of the funding for this work was through the SUPRI C - Miscible Flooding Industrial Affiliates and DOE Contract No. DE AC21 85MC 22042. However, some of the work was funded through the Stanford Center for Reservoir Forecasting (SCRF), a multidepartmental research effort in the School of Earth Sciences and also a minor amount through SUPRI-A , Thermal Recovery Industrial Affiliates, and DOE Contract No. DE FG19 87BC 14126. It is under the auspices of SUPRI-A that this report is being published.

The results discussed in this report have been made available through publications of the other research organizations mentioned above. However, we know that there are a number of our regular SUPRI-A report readers who are interested in the subject matter of this research, and who would not be likely to see the results of this work if it were not also published through the regular SUPRI-A DOE contract channels.



# TABLE OF CONTENTS

	Page
ACKNOWLEDGEMENTS .....	ii
LIST OF TABLES .....	iv
LIST OF FIGURES .....	v
ABSTRACT .....	vii
1. INTRODUCTION AND SCOPE .....	1
1.1 Introduction .....	1
1.2 Scope and Methodology .....	2
2. REVIEW OF LITERATURE .....	3
2.1 Theoretical Background .....	3
2.1.1 Pressure Test Interpretation .....	3
2.1.2 Tracer Test Interpretation .....	4
2.2 Review of Literature .....	5
2.2.1 Noncommunicating Layered Systems .....	5
2.2.2 Areally Heterogeneous Systems .....	7
2.2.3 Summary of Past Work .....	8
3. WELL TEST ANALYSIS FOR NONCOMMUNICATING LAYERED SYSTEMS .....	9
3.1 Introduction .....	9
3.2 Representation of Heterogeneity .....	9
3.3 Pressure Test Response .....	13
3.3.1 Mathematical Model .....	13
3.3.2 Drawdown Behavior .....	19
3.3.3 Buildup Behavior .....	21
3.4 Tracer Test Response .....	28
3.4.1 Mathematical Model .....	28
3.4.2 Tracer Concentration-time Behavior .....	31
3.5 Discussion of Results .....	35
4. WELL TEST ANALYSIS FOR AREALLY HETEROGENEOUS SYSTEMS .....	37
4.1 Introduction .....	37
4.2 Representation of Heterogeneous Media .....	37
4.3 Pressure Test Response .....	43
4.3.1 Simulation of Pressure Behavior .....	47
4.3.2 Interpretation Methodology .....	48
4.3.3 Analysis of Pressure Test Data .....	50
4.4 Tracer Test Response .....	69
4.4.1 Simulation of Tracer Flow .....	71
4.4.2 Interpretation Methodology .....	74
4.4.3 Analysis of Tracer Test Data .....	74
4.5 Discussion of Results .....	87
5. CONCLUSIONS AND RECOMMENDATIONS .....	87
5.1 Conclusions .....	91
5.2 Recommendations .....	98
NOMENCLATURE .....	101
REFERENCES .....	103
APPENDICES .....	109
A. Calculation of Effective Permeability from Simulated Pressure Data .....	109
B. Effect of Grid Refinement on Simulated Well Test Responses .....	112
C. Computer Program for Generating Auto-correlated Permeability Fields .....	118

## LIST OF TABLES

	Page
3.1 Layer permeabilities for hypothetical stratified systems .....	14
3.2 Rock and fluid properties.....	22
3.3 Dimensionless semi-log slopes from infinite-acting period data.....	22
4.1 Common functional forms for the semi-variogram.....	40
4.2 System data for modeling tracer and pressure response .....	44
4.3 Permeabilities calculated from simulated pressure data, $V_{DP} = 0.35$ .....	62
4.4 Permeabilities calculated from simulated pressure data, $V_{DP} = 0.50$ .....	63
4.5 Permeabilities calculated from simulated pressure data, $V_{DP} = 0.65$ .....	64
4.6 Statistics of dimensionless permeability difference $\Delta k_D$ .....	67
4.7 Effective dispersivity from simulated tracer test data showing Fickian behavior.....	88
4.8 Pseudo-layer parameters from simulated tracer test data showing non-Fickian behavior, $V_{DP} = 0.50$ , $\lambda_D = 16/15$ .....	92
4.9 Pseudo-layer parameters from simulated tracer test data showing non-Fickian behavior, $V_{DP} = 0.65$ , $\lambda_D = 6/15$ .....	93
4.10 Pseudo-layer parameters from simulated tracer test data showing non-Fickian behavior, $V_{DP} = 0.65$ , $\lambda_D = 16/15$ .....	94
B.1 Comparison of effective permeabilities obtained from fine- and coarse-grid simulations .....	113

## LIST OF FIGURES

	Page
3.1 Layering observed in outcrops .....	10
3.2 Well-log schematic, showing stratification along the vertical .....	10
3.3 Idealized <i>layer-cake</i> model in a 5-spot pattern .....	11
3.4 Log-permeability cumulative distribution function.....	12
3.5 Graphical assignment of layer permeabilities for a log-normal cumulative distribution function .....	15
3.6 Verification of model for generating pressure response .....	20
3.7 Effect of layering on drawdown behavior, $V_{DP} = 0.55$ , dimensionless pressure data.....	23
3.8 Effect of permeability contrast on drawdown behavior, 5-layer case, dimensionless pressure data.....	23
3.9 Effect of layering on drawdown behavior, $V_{DP} = 0.55$ , dimensionless pressure derivative data .....	24
3.10 Effect of permeability contrast on drawdown behavior, 5-layer case, dimensionless pressure derivative data.....	24
3.11 Effect of permeability contrast on buildup behavior, 5-layer case, dimensionless Horner graph.....	25
3.12 Effect of permeability contrast on buildup behavior, 5-layer case, dimensionless pressure derivative graph .....	25
3.13 Effect of permeability contrast on buildup behavior, 5-layer case, dimensionless Horner graph, no-flow outer boundary .....	27
3.14 Comparison of buildup responses, 5-layer case, $V_{DP} = 0.75$ , dimensionless Horner graph.....	27
3.15 Mixing in a symmetry element of a repeated 5-spot .....	30
3.16 Tracer breakthrough curve, 5-layer case, $V_{DP} = 0.55$ .....	32
3.17 Tracer breakthrough curve, 10-layer case, $V_{DP} = 0.55$ .....	32
3.18 Tracer breakthrough curve, 5-layer case, $V_{DP} = 0.35$ .....	33
3.19 Tracer breakthrough curve, 5-layer case, $V_{DP} = 0.75$ .....	33
3.20 Tracer breakthrough curve, 5-layer case, $V_{DP} = 0.55$ and $\alpha = 0.1$ ft.....	34
3.21 Tracer breakthrough curve, 5-layer case, $V_{DP} = 0.55$ and $\alpha = 1.0$ ft.....	34
4.1 System schematic, showing a quadrant from a repeated 5-spot.....	38
4.2 Hypothetical semi-variogram with a finite range .....	41
4.3 Hypothetical semi-variogram showing fractal behavior .....	42
4.4 Perspective of simulated permeability field.....	45
4.5 Experimental semi-variogram.....	46
4.6 Flow chart of numerical model simulating pressure behavior .....	49
4.7 Well pressure history, homogeneous case, $k = 10$ md.....	51
4.8 Simulated pressure response, $V_{DP} = 0.35$ and $\lambda_D = 1/15$ .....	52
4.9 Simulated pressure response, $V_{DP} = 0.35$ and $\lambda_D = 6/15$ .....	54
4.10 Simulated pressure response, $V_{DP} = 0.35$ and $\lambda_D = 16/15$ .....	55
4.11 Simulated pressure response, $V_{DP} = 0.50$ and $\lambda_D = 1/15$ .....	56
4.12 Simulated pressure response, $V_{DP} = 0.50$ and $\lambda_D = 6/15$ .....	57
4.13 Simulated pressure response, $V_{DP} = 0.50$ and $\lambda_D = 16/15$ .....	58
4.14 Simulated pressure response, $V_{DP} = 0.65$ and $\lambda_D = 1/15$ .....	59
4.15 Simulated pressure response, $V_{DP} = 0.65$ and $\lambda_D = 6/15$ .....	60
4.16 Simulated pressure response, $V_{DP} = 0.65$ and $\lambda_D = 16/15$ .....	61
4.17 Comparison between calculated and estimated $k_{ss}$ , $V_{DP} = 0.35$ . .....	65
4.18 Comparison between calculated and estimated $k_{ss}$ , $V_{DP} = 0.50$ . .....	65
4.19 Comparison between calculated and estimated $k_{ss}$ , $V_{DP} = 0.65$ . .....	65

4.20	Dimensionless permeability difference $\Delta k_D$ as a function of $V_{DP}$ and $\lambda_D$ .....	68
4.21	Relationship between $\Delta k_D$ and heterogeneity index $\sigma_{ln(k)}^2 \lambda_D$ .....	70
4.22	Flow chart of USGS solute transport simulator .....	75
4.23	Tracer flow simulator verification.....	76
4.24	Tracer breakthrough curve for $V_{DP} = 0.35$ and $\lambda_D = 1/15$ .....	77
4.25	Tracer breakthrough curve for $V_{DP} = 0.35$ and $\lambda_D = 6/15$ .....	78
4.26	Tracer breakthrough curve for $V_{DP} = 0.35$ and $\lambda_D = 16/15$ .....	79
4.27	Tracer breakthrough curve for $V_{DP} = 0.50$ and $\lambda_D = 1/15$ .....	80
4.28	Tracer breakthrough curve for $V_{DP} = 0.50$ and $\lambda_D = 6/15$ .....	81
4.29	Tracer breakthrough curve for $V_{DP} = 0.50$ and $\lambda_D = 16/15$ .....	82
4.30	Tracer breakthrough curve for $V_{DP} = 0.65$ and $\lambda_D = 1/15$ .....	83
4.31	Tracer breakthrough curve for $V_{DP} = 0.65$ and $\lambda_D = 6/15$ .....	84
4.32	Tracer breakthrough curve for $V_{DP} = 0.65$ and $\lambda_D = 16/15$ .....	85
4.33	Influence of heterogeneity index on nature of tracer response .....	89
4.34	Comparison of computed Fickian dispersivities with stochastic theory results.....	90
4.35	Heterogeneity index and correlation length scale (at the Fickian limit) computed for a North Sea oil-field.....	96
A.1	Pressure behavior, example permeability calculation.....	110
A.2	Pressure derivative behavior, example permeability calculation .....	111
B.1	Tracer breakthrough curves for $V_{DP} = 0.35$ and $\lambda_D = 1/15$ .....	114
B.2	Tracer breakthrough curves for $V_{DP} = 0.50$ and $\lambda_D = 6/15$ .....	115
B.3	Tracer breakthrough curves for $V_{DP} = 0.65$ and $\lambda_D = 16/15$ .....	116

## ABSTRACT

This study compares well-to-well tracer test and transient pressure test responses in a 5-spot pattern with permeability variations to examine: (a) the sensitivity of test responses to the presence of heterogeneity, and (b) quantification of permeability variation from the analysis of well test data.

The first part of this research deals with non-communicating layered systems. Analytical models are used to compute pressure and tracer flow behavior for several hypothetical systems. Drawdown and buildup pressure responses are found to be insensitive to the degree of layering and permeability contrast. Because of balanced flooding conditions, differential depletion and the associated humping on a Horner buildup graph do not occur. Thus the pressure buildup behavior is different from that reported for bounded layered systems. Well-to-well tracer test responses are seen to be sensitive to both the degree of layering and permeability contrast. These results suggest that individual layer properties can be calculated by deconvolving tracer test data, while only averaged properties can be obtained from the analysis of conventional pressure test data.

The second part deals with single-layer areally heterogeneous systems. Simulation of transient pressure tests shows that the geometric mean of effective permeabilities around the injection and production wells is a good approximation for the steady-state interwell permeability. A dimensionless permeability difference defined in terms of these quantities can be correlated with a heterogeneity index, defined as the product of permeability variance and a dimensionless correlation length scale. Simulation of well-to-well tracer flow indicates that tracer test data can be matched with solutions of the convection-diffusion equation to calculate effective dispersivities only when the heterogeneity index is small. When the heterogeneity index is large, preferential flow paths are generated in the system, which requires a *pseudo-layered* model to match tracer test data. A reservoir description procedure, based on the heterogeneity index and a combined analysis of pressure and tracer test data, is proposed.



# 1. INTRODUCTION AND SCOPE

*A brief background on the use of well test data for reservoir description is presented. The motivation for this research is described, and its scope and methodology are outlined.*

## 1.1. INTRODUCTION

The overall efficiency of a fluid injection program for enhanced oil recovery (EOR) depends on two factors - the volumetric conformance of the process, and its local displacement efficiency. Displacement efficiency depends on the interaction between the injected fluid and the oil in-situ, while volumetric conformance depends on the heterogeneity of the reservoir rock and the mobility contrast between injected and in-place fluids. For the simple case of water displacing oil, reservoir heterogeneity can be responsible for reducing volumetric sweep, and hence, overall process efficiency. For the more complex case of carbon dioxide displacing oil, heterogeneity may interact with phase behavior, and also aggravate viscous instability, thereby lowering displacement efficiency as well. Thus it is necessary to determine what kinds of heterogeneities might be present in a reservoir with EOR potential, so that these may be properly represented in performance forecasting models.

Unlike process description, i.e., aspects related to fluid mixing and phase behavior which can be developed on the basis of laboratory experiments, reservoir description, i.e., enumeration of the nature of variations in porous media properties (e.g., permeability), is possible only through indirect means. Typically, some disturbance is imposed on the physical system, and the resultant response is analyzed to obtain a qualitative and/or quantitative description of the material properties of the system. Thus the detection of formation heterogeneities for reservoir characterization and modeling represents a classic inverse problem.

Two kinds of well tests are commonly used for this purpose: (a) well-to-well tracer testing, and (b) transient pressure testing. Interwell tracer tests are used to track subsurface fluid movement and infer formation characteristics (Brigham and Abbaszadeh-Dehghani, 1987). Such a test involves injecting a tracer slug driven by a chase fluid, and monitoring the tracer concentration at an adjacent producer. Pressure transient tests are used to estimate average formation properties and wellbore conditions, and detect barriers for fluid flow (Ramey, 1982). Such a test is carried out by perturbing the flow rate at one well and monitoring the resultant pressure response at the same or adjacent wells.

The influence of heterogeneities on pressure and tracer test responses has been the subject of several studies, both in the petroleum and groundwater literature. A majority of these studies have sought to characterize heterogeneities through lumped parameter modeling, i.e. by computing some *effective* medium property (e.g., permeability, dispersivity) corresponding to a fictitious homogeneous system, whose behavior matches that of the real heterogeneous system. However, if distributed heterogeneities are to be detected qualitatively and/or quantitatively by well tests, some knowledge of the relationship between these effective parameters and system heterogeneities is required. An associated question of importance is the definition of conditions under which such effective medium approximations can be used for describing heterogeneous media. It is also useful to know the relationship between tracer and pressure test responses for the same system, so that information from both tests can be integrated.

The need to synthesize information from different sources becomes more obvious if one recognizes the possibility that the sensitivity of pressure and tracer test responses to heterogeneities may be different. As pointed out by Ramey (1983), one observation from

pressure test analysis to date is that field data often match mathematical models derived for homogeneous systems. This is frequently found to be the case even when *a priori* information about the reservoir indicates the system to be heterogeneous. This suggests that pressure data as presently interpreted may not contain detailed information concerning certain reservoir heterogeneities. Tracer tests, on the other hand, may be more sensitive to the presence of heterogeneous elements in the reservoir because of the convective nature of the flow test.

## 1.2. SCOPE AND METHODOLOGY

In this context, this research seeks to contribute in two major areas. The first is in providing a comparative assessment of pressure and tracer test responses when heterogeneities are present in the system. The second is in developing methods for computing simple measures of heterogeneity from the analysis of well test data. For the purposes of this study, the problem of detecting, identifying and representing heterogeneities based on well test analysis can be posed as follows:

- (1) Given a reservoir description (i.e. a distributed permeability field), what are the pressure and tracer test responses?
- (2) How are these responses affected by heterogeneities? To what extent can heterogeneous systems be represented as effectively homogeneous media?
- (3) Can distributed heterogeneities be identified, and/or an integrated measure of heterogeneity computed, from the analysis of well test data?

The flow geometry of interest is a 5-spot pattern within a repeated and balanced injection-production pattern, where permeability variation is assumed to be the only source of heterogeneity. This research is restricted to two simple kinds of nonidealities in the formation: (a) vertical permeability variations in a layered system with noncommunicating strata, which can be modeled as a stack of permeable layers with no interlayer crossflow (i.e., *alayer-cake* system), and (b) areal permeability variations in a single-layer system, where a spatially continuous permeability field can be discretized into a set of grid-block permeabilities.

In order to achieve the objectives of this work, several hypothetical heterogeneous media will be generated with assumed statistics of permeability variation. Pressure and tracer test responses for these systems will then be simulated using analytical or numerical models as appropriate. Simulated well test data will be analyzed to examine the sensitivity of the responses to heterogeneities. The possibility of inferring simple measures of heterogeneity from pressure and tracer test data will be investigated.

The rest of this dissertation is organized in four major sections. In Section 2, a brief review of pertinent past work is presented. Sections 3 and 4 deal with well test analysis for noncommunicating layered media and areally heterogeneous systems respectively. Finally, conclusions and recommendations from this study are presented in Section 5.

## 2. REVIEW OF LITERATURE

*The theory of pressure and tracer test interpretation is reviewed. Previous work relating to the analysis of well test data from noncommunicating layered systems and areally heterogeneous systems is summarized.*

### 2.1. THEORETICAL BACKGROUND

Pressure behavior during single-phase fluid flow in porous media is described by the pressure-diffusion equation, whereas tracer flow is described by the convection-diffusion equation. The derivation of these equations and their application in pressure and tracer test analysis is presented briefly in the following.

#### 2.1.1. Pressure Test Interpretation

The partial differential equation governing fluid flow (and pressure behavior) in a porous medium, which can be derived by combining a mass balance expression (equation of continuity), an equation of state (density-pressure relation), an equation of motion (Darcy's law), and assuming small and constant compressibility, is:

$$\nabla \cdot \left[ \mathbf{k} \cdot \nabla p \right] = \phi \mu c_t \frac{\partial p}{\partial t} \quad (2.1.1)$$

where  $p$  is the pressure,  $\mathbf{k}$  the permeability tensor,  $\phi$  the porosity,  $\mu$  the fluid viscosity, and  $c_t$  the total system compressibility. This equation is analogous to those governing heat conduction (Carslaw and Jaeger, 1959) and chemical diffusion (Crank, 1957), and is generally referred to as the diffusivity equation. The transmission of a pressure pulse being a diffusional process, Eq. 2.1.1 is also described as the pressure-diffusion equation.

For single-phase radial flow to a well in a homogeneous and isotropic porous medium, Eq. 2.1.1 reduces to:

$$\frac{\partial^2 p}{\partial r^2} + \frac{1}{r} \frac{\partial p}{\partial r} = \frac{\phi \mu c_t}{k} \frac{\partial p}{\partial t} \quad (2.1.2)$$

With appropriate initial and boundary conditions, this equation can be solved to yield pressure as a function of radial distance and time. As an example, the solution for constant flow rate to a line-source well in an infinite medium is:

$$p_{wf} = p_i + \frac{q\mu}{4\pi kh} Ei \left\{ - \frac{\phi \mu c_t r_w^2}{4kt} \right\} \quad (2.1.3)$$

where  $Ei$  denotes the exponential integral:

$$- Ei(-x) = \int_x^{\infty} \frac{e^{-u}}{u} du \quad (2.1.4)$$

Similar solutions for different initial and boundary conditions, as well as different system geometries, have been summarized by Matthews and Russell (1967), Ramey et al. (1973), Earlougher (1977) and Lee (1983).

Pressure test interpretation involves matching pressure-time data with an appropriate solution of the pressure-diffusion equation to extract values of effective permeability, initial (or average) pressure in the system, a measure of wellbore damage, etc. Such a process can be either graphical, using straight line graphs, dimensionless solutions or type-curves (e.g., Ramey, 1976), or automatic, using nonlinear regression methods (e.g., Rosa and Horne, 1983). Interpretation methodology for a variety of well-reservoir configurations has been described in the recent literature (Gringarten, 1985).

### 2.1.2. Tracer Test Interpretation

The partial differential equation governing transport of a conservative and nonreactive solute in a fluid of constant density and viscosity is:

$$\frac{\partial C}{\partial t} + \nabla \cdot \{ \mathbf{V} C \} = \nabla \cdot \{ \mathbf{D} \cdot \nabla C \} \quad (2.1.5)$$

and is known as the convection-diffusion equation. Here  $C$  is the solute concentration,  $\mathbf{V}$  the interstitial velocity vector, and  $\mathbf{D}$  the dispersion coefficient tensor. In this equation, total solute flux is represented as the sum of two components, the convective flux (the flux term on the left hand side) and the dispersive flux (the flux term on the right hand side). Dispersive transport is assumed to be Fickian, i.e., the dispersive mass flux is assumed to be proportional to the concentration gradient in analogy to molecular diffusion.

As used in the preceding, convection refers to bulk fluid flow, and dispersion to spreading of the solute due to a combination of molecular diffusion and local velocity fluctuations (mechanical dispersion). Diffusional effects are important only at the pore-scale, and/or at low displacement velocities (Perkins and Johnston, 1963). Consequently, it is customary to lump all dispersive factors into one transport parameter, the dispersion coefficient,  $D$ . Based on laboratory measurements,  $D$  is generally expressed as the product of displacement velocity,  $v$ , and a constant,  $\alpha$ , known as dispersivity and taken to be a characteristic of the medium (Bear, 1972).

Laboratory experiments have demonstrated that the convection-diffusion equation is often satisfactory for matching core-scale displacements. In such cases, the one-dimensional version of Eq. (2.1.5) is usually solved with appropriate initial and boundary conditions. Experimental data is fitted to the proper solution to compute effective dispersivity. Several methods can be used for this purpose : (a) the graphical procedure suggested by Brigham *et al.* (1961), (b) the method of moments (e.g., Fischer *et al.*, 1979), or (c) conventional nonlinear regression methods (e.g., Beck and Arnold, 1977).

Application of the one-parameter convection-diffusion equation to field-scale problems (i.e., for tracer test interpretation) has often yielded inconsistent results, particularly with respect to dispersivity. Field dispersivities have been found to be orders of magnitude higher than those measured in the laboratory, even for similar media. Moreover, dispersivity has also been observed to be dependent on the scale of displacement. Such scale-dependence has been

ascribed to large-scale formational heterogeneities, which are successively encountered as tracer transport progresses in space. *Gelhar et al.* (1985) provide an excellent review of pertinent field evidence.

While the one-parameter convection-diffusion equation is adequate for fairly homogeneous cores (e.g., sandstones), experience indicates that it has to be modified in order to explain the long tailing observed in displacements from carbonate cores. One way of matching such experiments is to use a model which partitions the pore space into flowing and stagnant fractions with mass transfer between the fractions, as suggested by Coats and Smith (1964). While such a bi-continuum model is the simplest one available for this purpose, it has little physical basis, and moreover, scaling of model parameters to actual field-scale conditions has not been demonstrated.

## 2.2. REVIEW OF LITERATURE

This review is divided into two major parts. The first part deals with noncommunicating layered systems, and the second with areally heterogeneous systems. In each part, the literature pertaining to pressure and tracer testing is summarized in separate sub-sections.

### 2.2.1. Noncommunicating Layered Systems

#### Pressure Test Response

The pressure behavior of layered systems with noncommunicating strata (i.e., systems made up of several isolated homogeneous layers of different permeability) has been studied by many investigators. Lefkovits *et al.* (1961) presented analytical solutions describing the pressure behavior of bounded multi-layered systems. They showed that the drawdown behavior of multi-layered systems is similar to that of single-layer systems, with three distinct periods corresponding to infinite-acting, late-transient and pseudo steady-state flow. The thickness averaged formation flow capacity can be determined from the slope of a semi-log straight line of the early-time data, as in the single-layer case. Moreover, the duration of the late-transient period may be orders of magnitude longer than that for single-layer systems. They further observed that during buildup the shut-in pressure is initially influenced by the more-depleted (high transmissivity) layer(s), which results in an early flattening of the buildup data. Subsequently, with crossflow taking place from the less-depleted to the more-depleted layer(s) through the wellbore, there is repressurization and the pressure begins to rise. This causes a hump in the buildup pressure-time graph, which is recognized as a diagnostic feature of bounded layered systems without interlayer crossflow.

Cobb *et al.* (1972) used the solutions of Lefkovits *et al.* in a detailed study of the buildup behavior of a bounded two-layer reservoir, where only the permeability contrast between the two zones was allowed to vary. Buildup behavior was studied using single-layer analysis methods proposed by Muskat (1937), Miller *et al.* (1950) and Horner (1951). Under well defined conditions, all methods could be applied to calculate total system transmissivity and average reservoir pressure. Raghavan *et al.* (1974) extended the study of Cobb *et al.* to systems with two layers of varying thickness and permeability. They suggested using the Horner graph to calculate average pressure, and proposed a method to calculate the layer permeability ratio, provided the thickness of the layers was known.

Earlougher *et al.* (1974) included the effects of wellbore storage and skin in their model. They concluded that wellbore storage in multi-layered systems had an effect identical to that in the single-layer case. They also observed that only under certain conditions would the buildup behavior have distinctive layered system characteristics, and in general, no guidelines could be established regarding typical layered system behavior.

Tariq (1977), in making a comprehensive study of bounded multi-layered systems, considered differences in permeability, thickness, skin effect and outer radius. He found that false wellbore storage effects could appear when the permeability contrast was high, and a higher permeability layer had a smaller outer radius than the low permeability layer(s). He also found that layered system data could be analyzed under some ideal circumstances to yield information about the permeability ratio and the outer radii of the layers.

Larsen (1981) studied the pressure behavior of multi-layered systems with unequal initial pressures and skin factors in various layers. He observed that the slope of the infinite-acting semi-log straight line could be a function of time for unequal layer properties and nonzero skin factors. Since this slope is always greater than the theoretical value of 1.151, formation flow capacity computed from the slope of any apparent straight line will be underestimated. Larsen also quantified conditions under which the behavior of multi-layered systems would be indistinguishable from that of single-layer systems.

Ehlig-Economides and Joseph (1985) examined transient pressure and flow rate responses of multi-layered systems with variable interlayer crossflow. They developed a procedure for estimating layer permeabilities, skin factors and effective vertical permeability. This method requires the combined analysis of wellbore pressure and individual layer flow rate data.

#### Tracer Test Response

Work on the quantitative analysis of well-to-well tracer tests in layered reservoirs has been reported by several workers. Brigham and Smith (1965) derived equations to compute tracer response (for a slug injection) in a homogeneous, developed 5-spot by combining tracer dispersion and areal sweep effects. Dispersion was evaluated by assuming radial flow towards the producing well. This solution was extended to the case of noncommunicating stratified systems by volumetrically adding the tracer arrival curves from different layers to obtain the overall tracer breakthrough curve. This model was used to analyze a field test with a trial-and-error procedure being utilized to estimate layer permeabilities and thicknesses. Baldwin (1966) also analyzed the same field tracer test data reported by Brigham and Smith. He used equations for radially convergent-divergent flow to calculate the effects of tracer dispersion.

Yuen *et al.* (1979) revised the analytical solution of Brigham and Smith to include the effects of converging-diverging flow on dispersion. They developed a computer program which could decompose an overall tracer breakthrough curve from a multi-layered system, and compute layer properties (e.g., fractional layer porosity-thickness and permeability-thickness). The curve-matching was done by a trial-and-error procedure.

Abbaszadeh-Dehghani and Brigham (1982) developed equations for computing tracer breakthrough curves in several developed flooding patterns by analytically formulating tracer dispersion effects. They also proposed a nonlinear regression technique to deconvolve tracer concentration-time data from multi-layer systems and calculate layer properties.

## 2.2.2. Areal Heterogeneous Systems

### Pressure Test Response

The effects of a distributed permeability field on pressure behavior has been examined by several workers in the petroleum and groundwater literature using stochastic methods. The pioneering study in this area was presented by Warren and Price (1961). They investigated the effect of permeability variation on steady-state and transient pressure behavior in a discretized three-dimensional system. Individual block permeabilities were drawn randomly from specified probability distribution functions. For a log-normal permeability distribution with no spatial correlation, they found that the most probable behavior of a heterogeneous system approaches that of a homogeneous system with an effective permeability equal to the geometric mean of the input distribution. This value was also found to be approximated by the permeability obtained from a transient buildup test.

Several workers in the field of groundwater hydrology have arrived at the same relation for steady-state flow in two space dimensions when permeability is log-normally distributed and has an isotropic spatial correlation structure (e.g. Gutjahr *et al.*, 1978; Dagan, 1979). For three-dimensional media, Gelhar and Axness (1983) evaluated the components of the effective permeability tensor using spectral analysis and found that the geometric mean is a first-order approximation for the effective permeability in isotropic systems only for small permeability variances (such as those used by Warren and Price).

Recent studies have indicated that such logarithmic averaging of permeabilities (i.e., the geometric mean relationship) may be invalid when permeability does not have a univariate frequency distribution, such as in sand-shale sequences (Desbarats, 1987), or discrete fracture networks (Long *et al.*, 1982).

### Tracer Test Response

Several stochastic studies have dealt with the problem of tracer transport in a distributed permeability field. Warren and Skiba (1964) extended the study of Warren and Price to investigate the effects of tracer dispersion (spreading) due to macroscopic permeability variations over a discrete three-dimensional grid. Grid block permeabilities were drawn from a log-normal probability distribution and were assumed to be uncorrelated. By matching simulated tracer breakthrough behavior with a simple one-dimensional solution of the convection-diffusion equation, they computed effective dispersion coefficients and related these to the variability of the permeability distribution. One of their important conclusions was that the effects of field-scale heterogeneities cannot be simulated at the laboratory scale.

Schwartz (1977) considered the case of one-dimensional solute transport with heterogeneities randomly inserted as low permeability inclusions in a high permeability medium. He found that under certain conditions, it may not be possible to obtain an effective dispersivity. He also observed that the magnitude of dispersion is strongly dependent on the contrast between the high and low permeability elements comprising the medium.

Gelhar *et al.* (1979) were concerned with longitudinal dispersion produced as a result of vertical variations in hydraulic conductivity in a stratified aquifer. Using spectral analysis to solve the resulting stochastic partial differential equation, they showed that the dispersive process has a transient part, during which it is non-Fickian. At large times, the longitudinal dispersivity becomes constant and is proportional to the variability and correlation length scale of the permeability field.

Smith and Schwartz (1980) expanded upon the earlier work of Schwartz to add the effects of two-dimensional flow and spatial correlation in permeability. They concluded that over finite domains, diffusional models may be inadequate to describe tracer transport because of insufficient spatial averaging. Their sensitivity studies indicated that considerable uncertainty may be present in Monte-Carlo simulation results, even when statistical features of the porous medium are known.

Gelhar and Axness (1983) used spectral analysis to calculate the components of the macroscopic dispersion tensor, based on the statistics of permeability variation. Their three-dimensional theory is quite general in that it includes the effects of local dispersion as well as anisotropy in the permeability field.

Smith and Brown (1984) used an approach similar to that of Smith and Schwartz to study dispersion in a two-dimensional cross section for a developed 5-spot. They matched their breakthrough curves to a one-dimensional solution of the convection-diffusion equation, and correlated longitudinal dispersivity with statistical parameters of the permeability distribution.

Arya *et al.* (1985) investigated the behavior of grid-block scale and inter-well scale dispersion for two-dimensional flow. They found that the degree of autocorrelation in the permeability field determines whether or not interwell scale dispersivity can be uniquely defined. If the correlation length scale is large compared to medium dimensions, dispersivity grows with distance. For small correlation lengths, dispersivity stabilizes at some constant value which depends on permeability variance. They also showed that the medium acts as effectively layered when the correlation length scale is comparable to system dimensions.

### 2.2.3. Summary of Past Work

As stated in the introductory section, a major objective of this study is to compare pressure and tracer test responses in a balanced flooding pattern, where permeability varies either vertically or areally. For the stratified system case, a model for computing tracer flow behavior is available (Abbaszadeh-Dehghani and Brigham, 1982). However, none of the previous studies on transient pressure testing have considered the case of layered systems with a constant pressure outer boundary, which is the proper boundary condition for the injection case. Therefore, one objective of this research will be to develop a theory to compute pressure behavior in such systems, and examine the effect of stratification on drawdown and buildup pressure response.

For the areally heterogeneous system case, the scope of most studies on pressure behavior has been on estimating steady-state effective permeabilities. Detailed analysis of averaging effects during transient flow conditions (prevailing during drawdown or buildup tests) has been dealt with only briefly. Moreover, the problem of obtaining some measure of permeability variation from single or multi-well pressure data does not appear to have been addressed in the literature. Hence, these aspects will be emphasized in this research. As far as tracer flow in such systems is concerned, a 5-spot pattern geometry has not been considered by previous workers. Such a study should be useful in examining the extent to which analytical solutions derived by Abbaszadeh-Dehghani and Brigham for homogeneous media can be used to analyze tracer breakthrough curves from heterogeneous systems.

### 3. WELL TEST ANALYSIS FOR NONCOMMUNICATING LAYERED SYSTEMS

*Analytical models for simulating pressure and tracer tests in noncommunicating layered systems are described. The effect of heterogeneities on well test data is analyzed, and the problem of quantifying permeability variation is examined.*

#### 3.1. INTRODUCTION

Petroliferous formations are generally sedimentary in nature, the sedimentation process occurring over geologic time. Because of the cyclic nature of the depositional process, different kinds of rock-forming material may be deposited at different times, thus resulting in a stratified (or layered) system upon compaction and/or diagenesis. Layering, which is observed in many outcrops (Fig. 3.1) as well as in well logs (Fig. 3.2), is a common feature of sandstone formations. Usually, complex stratigraphic sequences are not used in geologic model descriptions for reservoir performance calculations. Simple models which consider the physical system to be composed of a combination of permeable (e.g., sandstone) and impermeable (e.g., shale) strata, as shown in Fig. 3.3, are used more frequently as idealizations of actual reservoirs - particularly in analytical methods for computing displacement performance (e.g., Dykstra and Parsons, 1950).

In this section, systems such as those described in the preceding paragraph are considered. The flow geometry of interest is a layered system, comprised of homogeneous permeable sand strata and impermeable shale strata so that there is no interlayer crossflow, within a developed and balanced 5-spot pattern. The sand layers are assumed to have different permeabilities, which causes the system to be heterogeneous.

#### 3.2. REPRESENTATION OF HETEROGENEITY

Field evidence, based on core measurements, indicates that permeability can vary over several orders of magnitude. In many cases, the log-normal distribution has been found to match the permeability histogram well, particularly when the frequency distribution is unimodal (e.g., Law, 1944; Warren et al., 1961). A convenient measure of permeability variation is then given by the Dykstra-Parsons permeability variation coefficient (Dykstra and Parsons, 1950):

$$V_{DP} = \frac{\bar{k} - k_{\sigma}}{\bar{k}} \quad (3.2.1)$$

Here  $\bar{k}$  is the median (i.e., the 50 percent value) and  $k_{\sigma}$  the permeability at one standard deviation (i.e. the 84.1 percent value) on a log-permeability cumulative probability distribution function (CDF) graph. Fig. 3.4 shows an idealized permeability CDF on log-probability paper, and the graphical computation of  $V_{DP}$ .

Distributions other than log-normal have also been used to describe permeability data (e.g., Bennion and Griffiths, 1966; Jensen *et al.*, 1985). Bennion and Griffiths found the normal distribution to be more appropriate for some data sets. Jensen *et al.* suggested using a power transformation to convert the raw data and fit a normal distribution, and showed that the log-normal distribution is just one member of this family of transformations. However, for the purposes of this study such models offer no particular advantage, and hence the assumption of log-normality will be made primarily for convenience.



Fig. 3.1 Layering observed in outcrops.

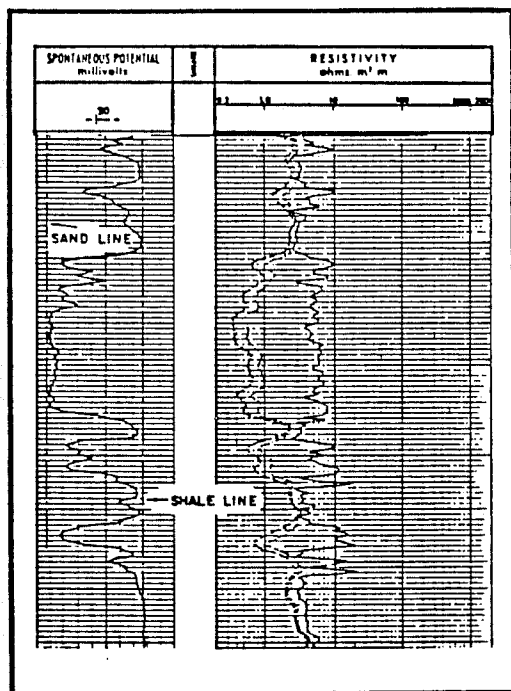


Fig. 3.2 Well-log schematic, showing stratification along the vertical.

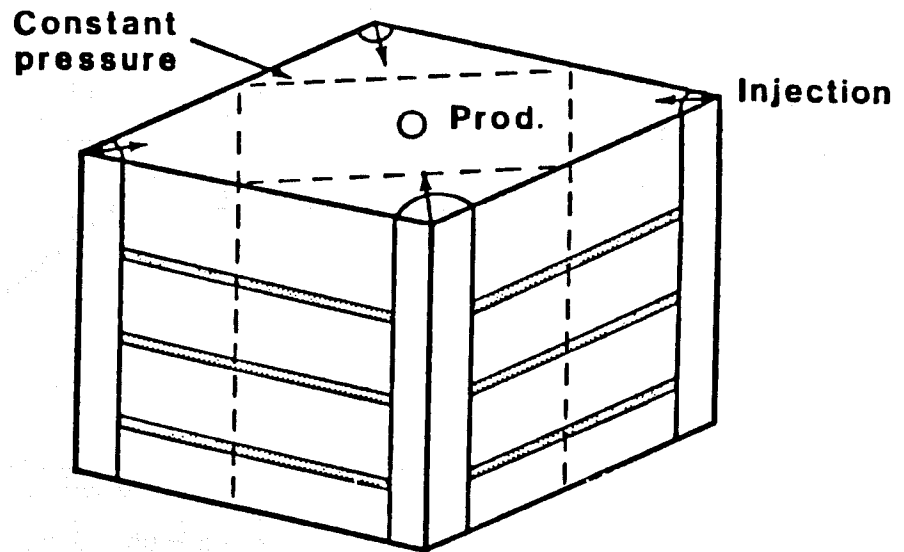


Fig. 3.3 Idealized *layer-cake* model in a 5-spot pattern.

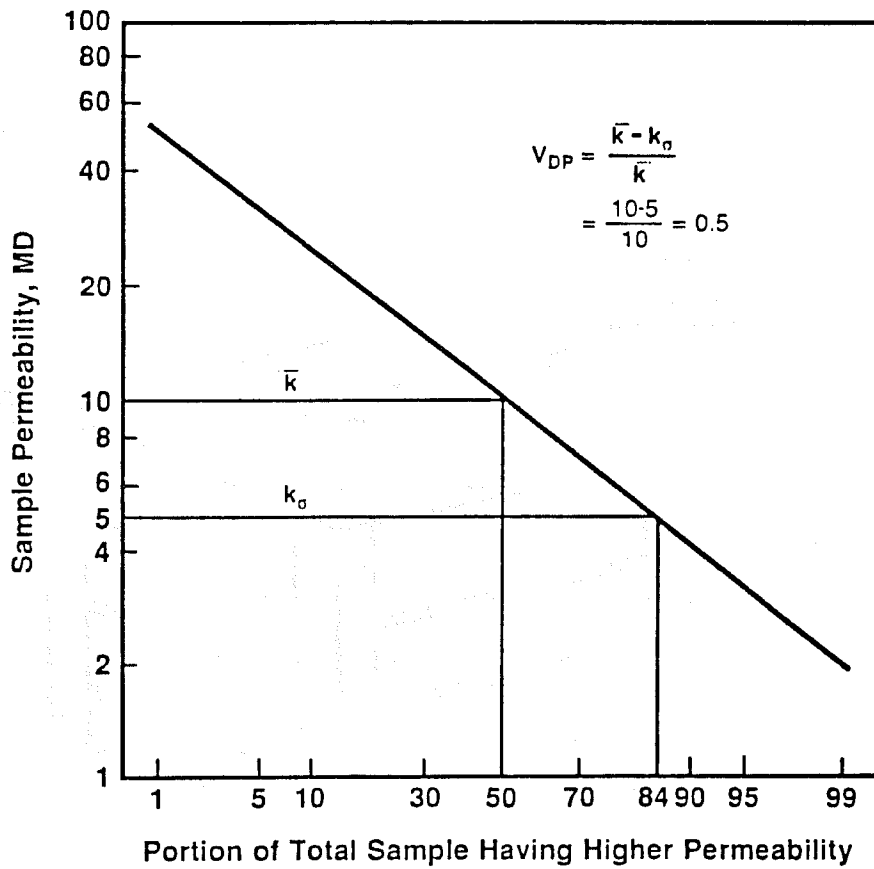


Fig. 3.4 Log-permeability cumulative distribution function.

In reality, the permeability distribution should usually be continuous. However, when a real system is approximated by a layer-cake model (Fig. 3.3), it is necessary to reduce the continuous permeability distribution to a discrete form. When  $V_{DP}$  and  $\bar{k}$  are known,  $k_{\sigma}$  can be calculated from Eq. 3.2.1, and a continuous log-normal CDF can be constructed by drawing a line on log-probability paper which passes through  $\bar{k}$  and  $k_{\sigma}$ . For a system with a finite number of layers, assignment of layer permeabilities should then be made so as to honor the CDF. Willhite (1986) suggests a graphical procedure for this purpose, where the CDF is first divided into several intervals (equal to the number of layers required), and then the permeability of the layer is selected at the mid-point of the interval. Permeabilities thus assigned can be checked for internal consistency because the geometric mean is equal to the median value. Figure 3.5 demonstrates this technique for a 10-layer system with  $V_{DP} = 0.55$ , and  $\bar{k} = 35$  md. The layer permeabilities are selected at the 5%, 15%, 25%, etc. points to correspond to the midpoint of each of the layer ranges. This simple procedure reproduces the distribution reasonably, since the computed geometric mean is 35.2 md and compares well with the input median of 35 md. Layer permeabilities thus calculated for other cases are tabulated in Table 3.1. Corresponding rock and fluid properties for these systems are given in Table 3.2, and will be used later as input to pressure and tracer test models.

A one-parameter representation of heterogeneity (using the Dykstra-Parsons coefficient  $V_{DP}$ ) characterizes only spatial variability. A proper description of permeability variation should also include some measure of the spatial correlation structure of permeability. Fortunately, in dealing with layered media, the ordering of layer permeability values is important only if gravity effects are considered. When gravity is neglected, as in this study (as well as in most theoretical models of pressure and tracer test analysis) - the use of  $V_{DP}$  to describe heterogeneity is sufficient.

### 3.3. PRESSURE TEST RESPONSE

A review of pertinent literature (Section 2.2.1) indicates that none of the studies consider the case of layered systems with a constant pressure outer boundary, which is the proper boundary condition in a balanced flooding pattern (e.g., Fig. 3.3). Therefore, the focus here will be to develop a theory for computing the pressure behavior in such systems, and use it to examine the effect of stratification on drawdown and buildup pressure response for several hypothetical systems.

#### 3.3.1. Mathematical Model

The physical system of interest is shown in Fig. 3.3. Because of the balanced 5-spot pattern, the drainage boundary of each production well is a constant pressure square. With little loss of generality, this square can be replaced with a circle having the same area. Furthermore, the radius of the constant pressure circle is assumed to be the same for all layers. Other assumptions of importance are:

1. Single-phase flow in radial geometry,
2. Layered system with noncommunicating strata,
3. Commingling only at the wellbore,
4. Constant total surface rate,

**TABLE 3.1**

**LAYER PERMEABILITIES FOR HYPOTHETICAL STRATIFIED SYSTEMS**

Layer	$V_{DP} = 0.35$		$V_{DP} = 0.55$		$V_{DP} = 0.75$	
	$NL = 5$	$NL = 10$	$NL = 5$	$NL = 10$	$NL = 5$	$NL = 10$
1	60	70	98	130	195	330
2	43	54	54	80	70	140
3	35	46	35	60	35	86
4	28	41	23	48	17	58
5	20	36	13	38	6	41
6		33		32		29
7		29		26		20
8		26		21		18
9		22		15		8
10		17		9.8		4
$\bar{k}$	34.7	34.5	35.4	35.2	34.5	35.5

**TABLE 3.2**

**ROCK AND FLUID PROPERTIES**

Area, $A$	20 acres
Outer radius, $r_e$	372.5 ft
Wellbore radius, $r_w$	0.25 ft
Porosity, $\phi$	0.25
Thickness, $h$	100 ft
Median perm, $\bar{k}$	35 md
Water saturation, $S_w$	0.50
Dispersivity, $\alpha$	0.1 ft
Tracer injected, $V_{TR}$	0.1 Pore volume

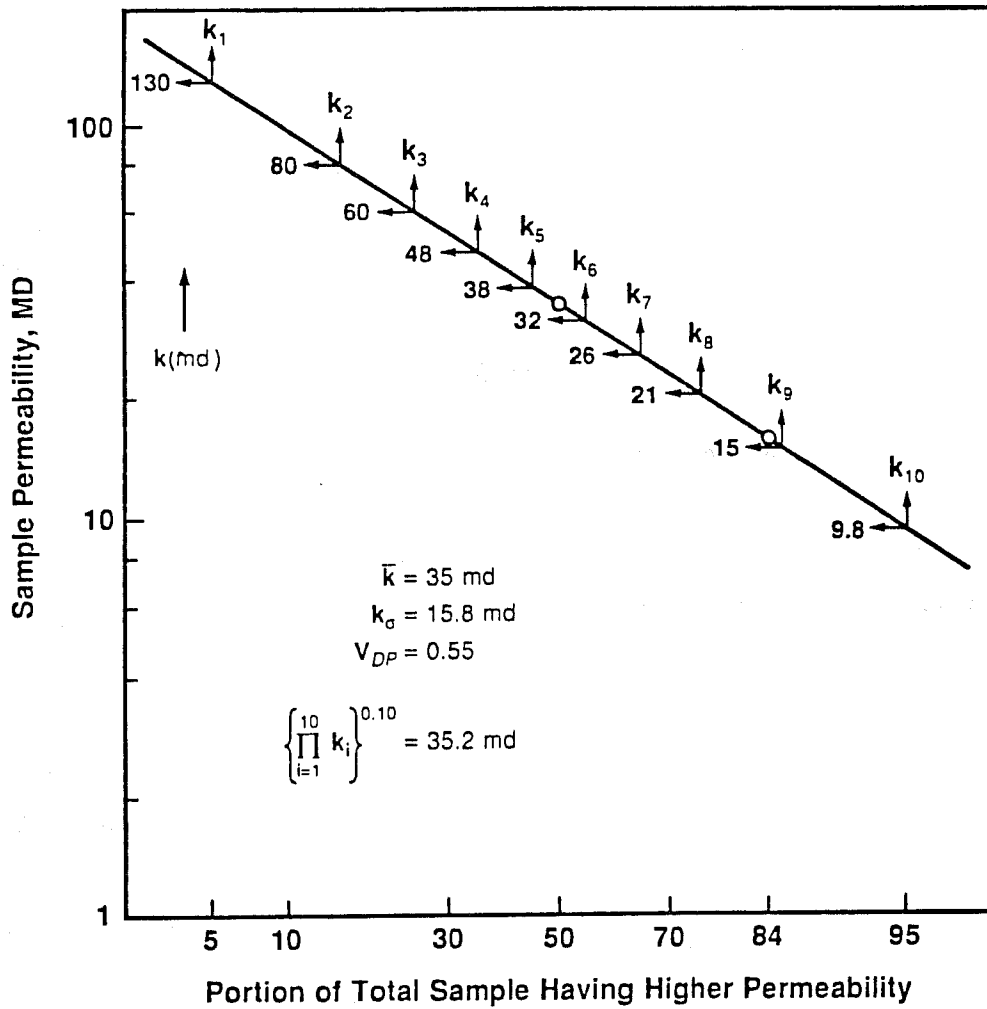


Fig. 3.5 Graphical assignment of layer permeabilities, log-normal distribution.

5. Constant wellbore storage coefficient,
6. Each layer homogeneous, uniform and isotropic with respect to  $k$ ,  $\phi$  and  $h$ ,
7. Slightly compressible fluid with constant  $\mu$  and  $c_p$ ,
8. Wellbore radius and instantaneous sandface pressure the same for all layers, and
9. Outer boundary at constant pressure.

The diffusivity equation for layer  $j$  is :

$$\frac{\partial^2 p_j}{\partial r^2} + \frac{1}{r} \frac{\partial p_j}{\partial r} = \frac{S_j}{T_j} \frac{\partial p_j}{\partial t} \quad (3.3.1)$$

where storativity  $S_j = (\phi c_p h)_j$  and transmissivity  $T_j = (kh/\mu)_j$ . Initially, the system is in pressure equilibrium:

$$p_j(r,0) = p_i \quad (3.3.2)$$

The outer boundary is at constant pressure:

$$p_j(r_e, t) = p_i \quad (3.3.3)$$

An infinitesimally thin skin causes a pressure drop at the inner boundary:

$$p_{wf}(t) = p_j(r_w, t) - s_j \left\{ r \frac{\partial p_j}{\partial r} \right\}_{r_w} \quad (3.3.4)$$

The total surface flow rate is constant, but the sandface rate may be time variant due to wellbore storage:

$$q = - C \frac{dp_{wf}}{dt} + \sum_{j=1}^{NL} 2\pi T_j \left\{ r \frac{\partial p_j}{\partial r} \right\}_{r_w} \quad (3.3.5)$$

where  $NL$  is the total number of permeable layers in the system. The following dimensionless variables are now defined:

$$p_{Dj} = \frac{2\pi T_i}{q} [ p_i - p_j ] \quad (3.3.6)$$

$$t_D = \frac{T_i}{S_i} \frac{t}{r_w^2} \quad (3.3.7)$$

$$r_D = \frac{r}{r_w} \quad (3.3.8)$$

$$C_D = \frac{C}{2\pi S_t r_w^2} \quad (3.3.9)$$

where total transmissivity,  $T_t$ , and total storativity,  $S_t$ , are defined as:

$$T_t = \sum_{j=1}^{NL} T_j = \sum_{j=1}^{NL} \left\{ \frac{kh}{\mu} \right\}_j \quad (3.3.10)$$

$$S_t = \sum_{j=1}^{NL} S_j = \sum_{j=1}^{NL} \left\{ \phi c_t h \right\}_j \quad (3.3.11)$$

Rewriting Eqs. 3.3.1 - 3.3.5 in terms of the dimensionless variables gives:

$$\frac{1}{r_D} \frac{\partial}{\partial r_D} \left\{ r_D \frac{\partial p_{Dj}}{\partial r_D} \right\} = \frac{S_j / S_t}{T_j / T_t} \frac{\partial p_{Dj}}{\partial t_D} = \frac{f_{1j}}{f_{2j}} \frac{\partial p_{Dj}}{\partial t_D} = f_j \frac{\partial p_{Dj}}{\partial t_D} \quad (3.3.12)$$

$$p_{Dj}(r_D, 0) = 0 \quad (3.3.13a)$$

$$p_{Dj}(r_{eD}, t_D) = 0 \quad (3.3.13b)$$

$$p_{wD} = \left[ p_{Dj} - s_j \frac{\partial p_{Dj}}{\partial r_D} \right]_{r_D=1} \quad (3.3.14)$$

$$1 = C_D \frac{dp_{wD}}{dt_D} - \sum_{j=1}^{NL} f_{2j} \left\{ \frac{\partial p_{Dj}}{\partial r_D} \right\}_{r_D=1} \quad (3.3.15)$$

Here  $f_{1j} = S_j / S_t$  is the fractional layer storativity,  $f_{2j} = T_j / T_t$  the fractional layer transmissivity, and  $f_j = f_{1j} / f_{2j}$ . This set of equations, i.e., Eqs. 3.3.12 - 3.3.15, was solved using the method of Laplace transformation. The Laplace transformation is defined as:

$$\bar{p}_{wD}(l) = \int_0^{\infty} e^{-l\tau} p_{wD}(\tau) d\tau \quad (3.3.16)$$

where  $l$  is the Laplace space variable. First, Eq. 3.3.12 is transformed using the initial condition of Eq. (3.3.13a):

$$\frac{d^2 \bar{p}_{Dj}}{dr_D^2} + \frac{1}{r_D} \frac{d\bar{p}_{Dj}}{dr_D} = lf_j \bar{p}_{Dj} \quad (3.3.17)$$

The transformed boundary conditions are then obtained as:

$$\bar{p}_{Dj}(r_{eD}) = 0 \quad (3.3.18)$$

$$\bar{p}_{wD} = \left[ \bar{p}_{Dj} - s_j \frac{d\bar{p}_{Dj}}{dr_D} \right]_{r_D=1} \quad (3.3.19)$$

$$\frac{1}{l} = C_{Dl} \bar{p}_{wD} - \sum_{j=1}^{NL} f_{2j} \left[ \frac{d\bar{p}_{Dj}}{dr_D} \right]_{r_D=1} \quad (3.3.20)$$

A general solution to Eq. 3.3.17 can be written in the form:

$$\bar{p}_{Dj} = A_j I_0(r_D \beta_j) + B_j K_0(r_D \beta_j) \quad (3.3.21)$$

where  $\beta_j = \sqrt{l f_j}$ . Substitution of this expression in Eqn. (3.3.19) yields:

$$\bar{p}_{wD} = A_j I_0(\beta_j) + B_j K_0(\beta_j) - s_j A_j \beta_j I_1(\beta_j) + s_j B_j \beta_j K_1(\beta_j) \quad (3.3.22)$$

Defining two new expressions:

$$\delta_I = I_0(\beta_j) - s_j \beta_j I_1(\beta_j) \quad (3.3.23a)$$

$$\delta_K = K_0(\beta_j) + s_j \beta_j K_1(\beta_j) \quad (3.3.23b)$$

Equation 3.3.22 can be simplified to:

$$\bar{p}_{wD} = A_j \delta_I + B_j \delta_K \quad (3.3.24)$$

Substitution of Eq. 3.3.21 in Eq. 3.3.18 yields:

$$0 = \bar{p}_{Dj}(r_{eD}) = A_j I_0(\gamma_j) + B_j K_0(\gamma_j) \quad (3.3.25)$$

where  $\gamma_j = r_{eD} \beta_j$ . This leads to the relationship:

$$A_j = - B_j \frac{K_0(\gamma_j)}{I_0(\gamma_j)} \quad (3.3.26)$$

This expression can be substituted in Eq. 3.3.24 in order to evaluate the coefficients  $A_j$  and  $B_j$ , which are obtained as:

$$A_j = \frac{-\bar{p}_{wD} K_0(\gamma_j)}{\delta_K I_0(\gamma_j) - \delta_I K_0(\gamma_j)} \quad (3.3.27a)$$

and

$$B_j = \frac{+ \bar{P}_{wD} I_0(\gamma_j)}{\delta_K I_0(\gamma_j) - \delta_I K_0(\gamma_j)} \quad (3.3.27b)$$

Now substituting Eq. 3.3.27 in Eq. 3.3.24 and simplifying, an expression for the dimensionless wellbore pressure in Laplace space is obtained as:

$$\bar{P}_{wD}(l) = \left[ C_D l^2 + \sum_{j=1}^{NL} \frac{l}{\frac{s_j}{f_{2j}} + \frac{(a_{3j}b_{1j} - a_{1j}b_{3j})}{f_{2j}\sqrt{l}f_j (a_{3j}b_{2j} + a_{2j}b_{3j})}} \right]^{-1} \quad (3.3.28)$$

The various coefficients  $a$  and  $b$  in this equation are as follows:

$$a_{1j} = I_0(\beta_j), \quad b_{1j} = K_0(\beta_j)$$

$$a_{2j} = I_1(\beta_j), \quad b_{2j} = K_1(\beta_j)$$

$$a_{3j} = I_0(\gamma_j), \quad b_{3j} = K_0(\gamma_j)$$

As previously defined,  $\beta_j = \sqrt{l}f_j$ , and  $\gamma_j = r_{eD}\beta_j$ .

Numerical inversion of Eq. (3.3.28) was obtained using the Stehfest algorithm (Stehfest, 1970). The solution was verified against the single-layer constant pressure boundary type-curves presented by Kumar and Ramey (1974), an example comparison being given in Fig. 3.6. The maximum difference between the two solutions, with 8 terms in the Stehfest approximation formula, was less than 0.5%.

### 3.3.2. Drawdown Behavior

The drawdown response of hypothetical stratified systems is shown as graphs of dimensionless sandface pressure  $p_{wD}$  against dimensionless time  $t_D$ , where  $p_{wD}$  is:

$$p_{wD} = \frac{2\pi T_l}{q} [ p_i - p_{wf} ] \quad (3.3.29)$$

Since use of a pressure derivative graph has been shown to enhance the pressure response signal for a variety of conditions (e.g., Tiab and Kumar, 1978; Bourdet *et al.*, 1984), drawdown data is also shown in terms of the dimensionless pressure derivative group:

$$\frac{dp_{wD}}{d\ln(t_D)} = \frac{2\pi T_l}{q} \left[ \frac{d(p_i - p_{wf})}{d\ln(t)} \right] \quad (3.3.30)$$

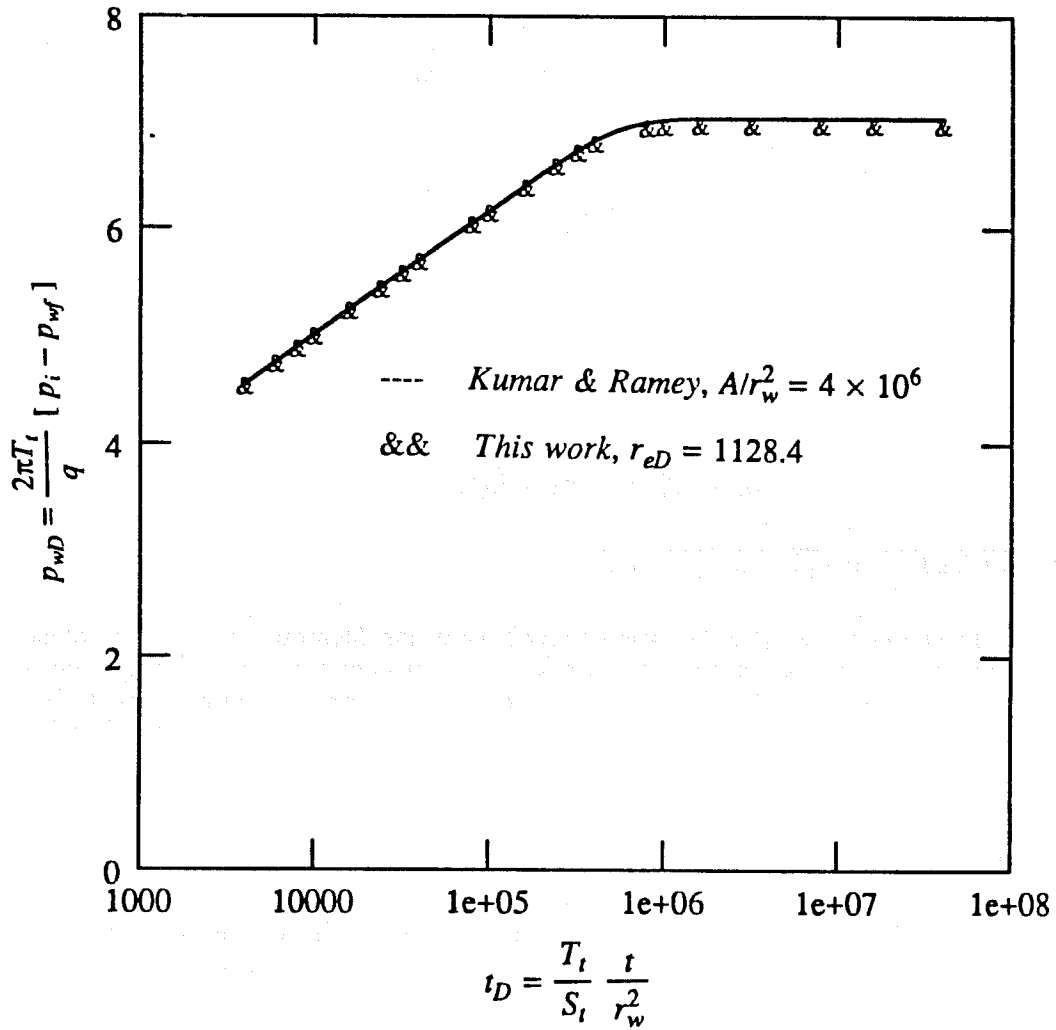


Fig. 3.6 Verification of model for generating pressure response.

Figures 3.7 and 3.8 are semi-log graphs showing the effect of layering and permeability contrast on drawdown behavior. Also graphed for comparison is the dimensionless pressure behavior of a homogeneous system. Three flow periods are evident in both multi- and single-layer responses: an infinite-acting period, a late-transient period and a steady-state period. During the infinite-acting period, multi-layer responses closely follow the homogeneous system curve. The effect of permeability contrast (Fig. 3.8) is clearly greater than that of layering (Fig. 3.7) in shifting the multi-layered system curve from the homogeneous response. This shift may also be interpreted as an apparent skin effect, the skin being proportional to the degree of permeability contrast. Usually, this apparent skin will be small.

Another important observation is that the slopes of the infinite-acting semi-log straight lines (corresponding to the layered systems) appear to be approximately equal to that of the homogeneous system. An examination of the derivative graphs (Figs. 3.9 and 3.10) shows a slight time dependence in the early-time data, which implies that the corresponding semi-log slopes may not be constant. However, regression results show a high degree of linearity ( $R^2 > 0.9999$ ) in slopes computed between  $t_D$  of 100 and 10000. Table 3.3 gives values of such slopes calculated for different hypothetical stratified systems. The maximum error (as compared with the theoretical value of 1.151) corresponds to the highest value of  $V_{DP}$ , but is less than 2%. It follows that during the infinite-acting period, a multi-layered system will behave like a single-layer reservoir for practical purposes. Since the definition of  $p_{wD}$  includes the total transmissivity,  $T_t$ , the slope of a semi-log drawdown graph will be inversely proportional to the total system transmissivity. However, because of the error in slope (which is always positive), total transmissivity will be slightly underestimated. These results are essentially similar to those reported in other studies of multi-layered system pressure response during the infinite-acting period (see the review by Raghavan, 1986).

A second interesting observation from the derivative graphs (Figs. 3.9 and 3.10) is that the transition from infinite-acting to steady-state is longer for a layered system with a constant pressure boundary, as compared to the equivalent homogeneous system. This is similar to the response of layered systems with a no-flow outer boundary, where the transition time from infinite-acting to pseudo steady-state is greater than that for the equivalent single-layer system. The steady-state behavior for multi-layered systems is identical to that of homogeneous media, although steady-state is attained later in the multi-layer case.

### 3.3.3. Buildup Behavior

The buildup response, which can be generated from the drawdown solution using the principle of superposition, is analyzed using the method of Horner (1951). Dimensionless shut-in Horner pressure  $p_{DHOR}$  is graphed against Horner time ratio  $[t_p + \Delta t] / \Delta t$ , where  $p_{DHOR}$  is defined as:

$$p_{DHOR} = \frac{2\pi T_t}{q} [p_i - p_{ws}] = p_{wD}(t_{pD} + \Delta t_D) - p_{wD}(\Delta t_D) \quad (3.3.31)$$

Here  $t_{pD}$  is the dimensionless producing time, and  $\Delta t_D$  the dimensionless shut-in time. Figure 3.11 is a dimensionless Horner graph showing the effect of permeability contrast and producing time on buildup behavior. As in the drawdown case, the homogeneous system response is also given for comparison. The early-time (infinite-acting) data produces a semi-log straight line with a slope approximately equal to 1.151. An examination of the corresponding derivative graph (Fig. 3.12), where the derivative of  $p_{DHOR}$  is taken with respect to the logarithm of the Horner time ratio, shows a slight time-dependance in these slopes. However,

**TABLE 3.3**

**DIMENSIONLESS SEMI-LOG SLOPES FROM INFINITE-ACTING PERIOD DATA**

**(a) Drawdown Data**

$V_{DP}$	$NL$	Slope	Error (%)
0.55	5	1.1595	0.71
0.55	10	1.1606	0.81
0.35	5	1.1555	0.37
0.75	5	1.1695	1.57

**(b) Buildup Data**

$V_{DP}$	$NL$	Slope	Error (%)
0.35	5	1.1553	0.35
0.55	5	1.1584	0.62
0.75	5	1.1634	1.05

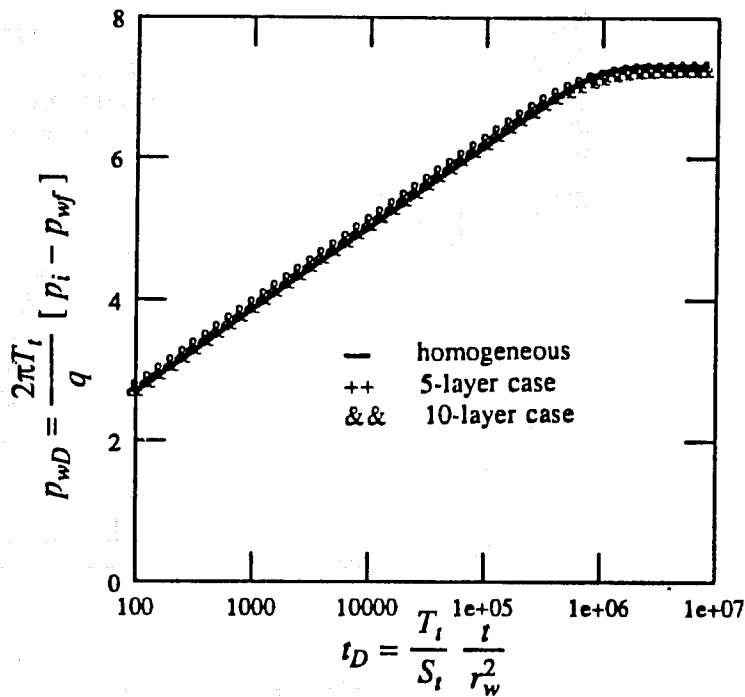


Fig. 3.7 Effect of layering on drawdown behavior,  $V_{DP} = 0.55$ , dimensionless pressure data.

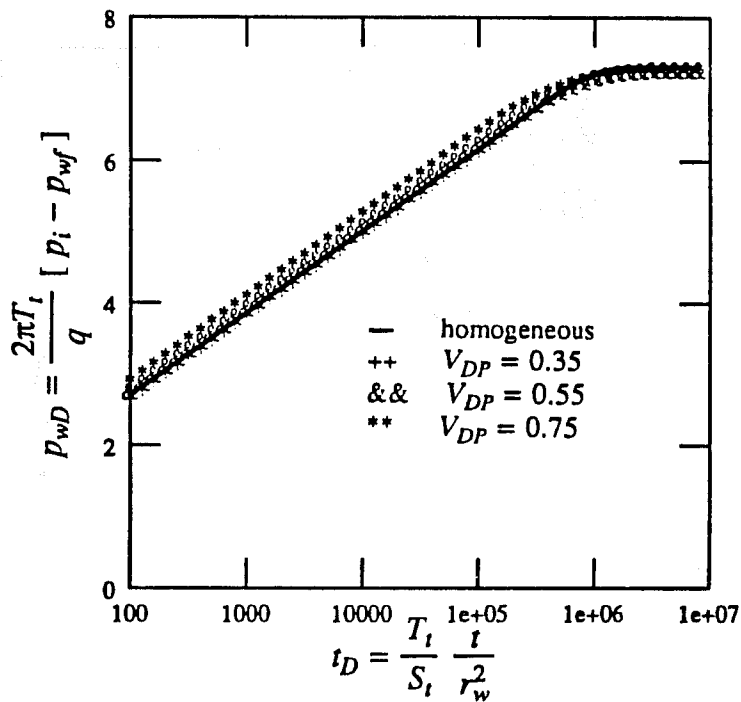


Fig. 3.8 Effect of permeability contrast on drawdown behavior, 5-layer case, dimensionless pressure data.

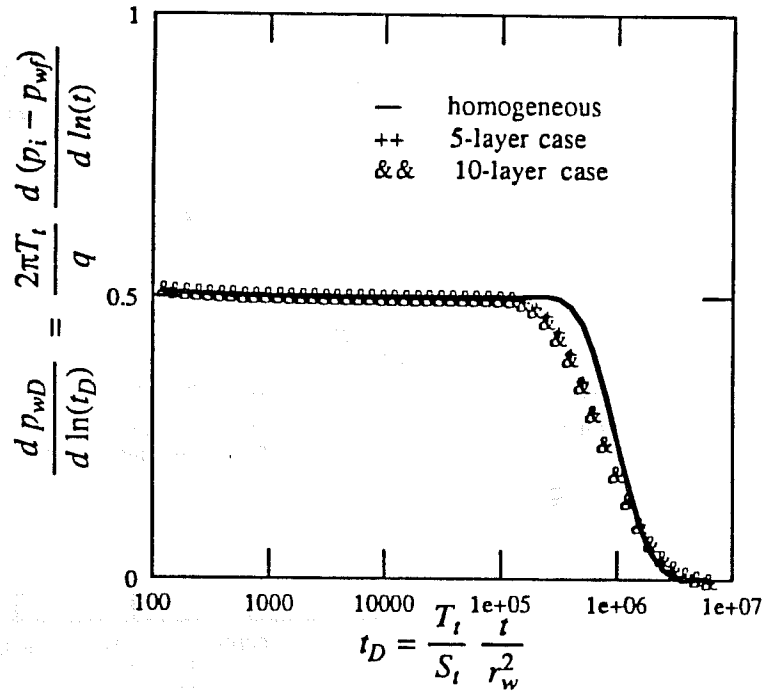


Fig. 3.9 Effect of layering on drawdown behavior,  $V_{DP} = 0.55$ , dimensionless pressure derivative data.

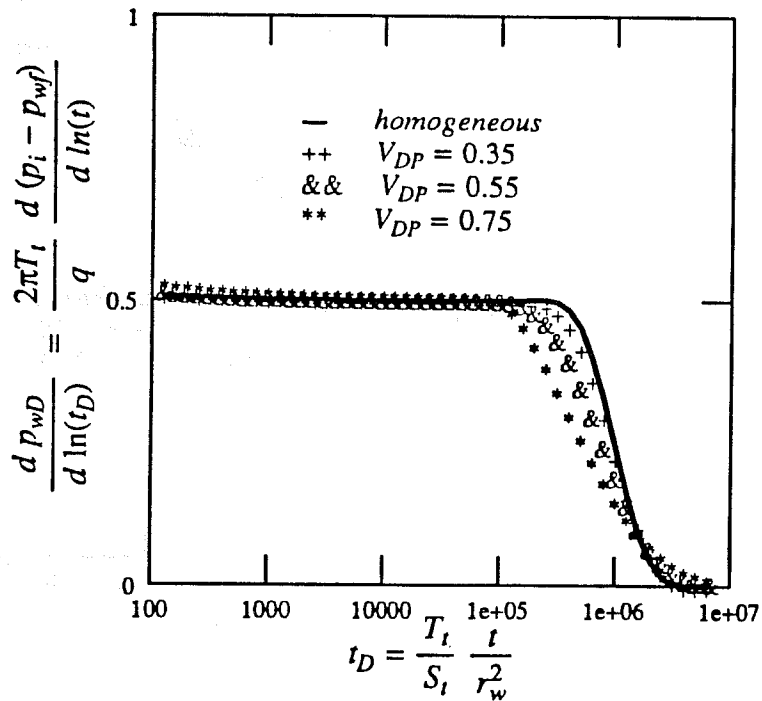


Fig. 3.10 Effect of permeability contrast on drawdown behavior, 5-layer case, dimensionless pressure derivative data.

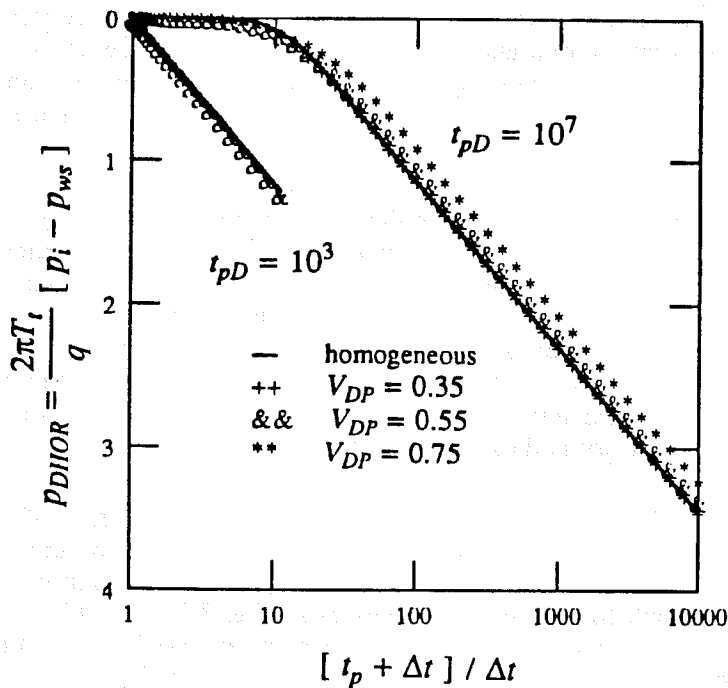


Fig. 3.11 Effect of permeability contrast on buildup behavior, 5-layer case, dimensionless Horner graph.

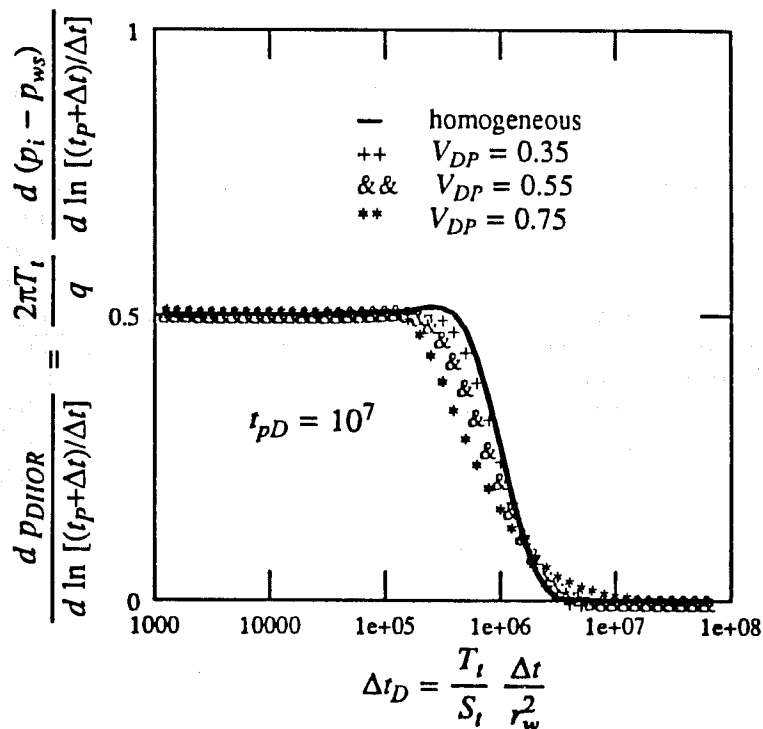


Fig. 3.12 Effect of permeability contrast on buildup behavior, 5-layer case, dimensionless pressure derivative graph.

regression calculated slopes of *apparent* semi-log straight lines, between  $\Delta t_D$  of 100 and 10000, show a maximum deviation of approximately 1% from the theoretical value of 1.151 (see also Table 3.3). As observed before, layered system responses are displaced from the homogeneous system curve and the degree of deviation increases with  $V_{DP}$ . In general then, the early-time buildup pressure behavior of a multi-layered system can be considered similar to that of a single-layer reservoir with an effective transmissivity equal to the total transmissivity,  $T_t$ .

Further examination of the buildup derivative graph (Fig. 3.12) indicates that the transition between infinite-acting and steady-state periods starts earlier and lasts longer for the layered system case, as compared to the homogeneous system response. However, the steady-state behavior is the same, i.e., initial pressure is attained so that  $p_{DHOR} = 0$ . The effect of producing time on layered system buildup behavior is also similar to that of single-layer systems, in that the dimensionless Horner graphs shift to the right before bending over as  $t_{pD}$  increases. The general trend of buildup behavior in a multi-layered system with a constant pressure outer boundary is thus similar to the equivalent homogeneous system.

This is an important observation with regard to the effect of the outer boundary. The classical buildup behavior of a closed-boundary layered system shows a hump due to differential depletion between layers (Lefkovits *et al.*, 1961). An example is Fig. 3.13, which is the Horner graph for the same systems as in Fig. 3.11, but with a no-flow outer boundary. The greater the permeability contrast, the more pronounced is the hump because of increased differential depletion. No such phenomenon is evident in Fig. 3.11 because fluid recharge has balanced fluid withdrawal, and hence differential depletion as well as the hump on the Horner graph are absent.

When the principle of superposition is used to generate the buildup response (as in Eq. 3.3.31), it is implicitly assumed that all wells in the pattern are shut-in at the same time. In reality, only one well (the production well of interest) is shut-in, while all others in the pattern continue to produce and/or inject. For such conditions, the appropriate buildup equation is:

$$P_{DHOR} = \frac{2\pi T_t}{q} [ p_i - p_{ws} ] = p_{wD}(t_{pD} + \Delta t_D, CPB) - p_{wD}(\Delta t_D, INF) \quad (3.3.32)$$

where the first term in the right hand side refers to the dimensionless pressure function for the constant pressure boundary case (injection-production pattern), and the second term refers to the dimensionless pressure function for a well in an infinite medium. In order to evaluate the difference between Eqs. (3.3.31) and (3.3.32), buildup responses were generated for the 5-layer case with  $V_{DP} = 0.75$ , and  $t_{pD} = 10^7$ . The response computed with Eq. (3.3.31), where all the wells are shut-in (i.e. the balanced system), and that with Eq. (3.3.32), where only the well of interest is shut-in (i.e. the unbalanced system), are graphed together in Fig. 3.14. During the infinite-acting period, both situations produce the same pressure-time behavior. However, once the effect of the outer boundary is felt, the two responses begin to differ. Pressure in the balanced system case approaches the initial pressure, whereas pressure in the unbalanced system continues to increase because of fluid influx from injectors. However, the infinite-acting period is really the segment of interest since it yields the semi-log straight line from which total transmissivity can be computed. Hence, for practical purposes, the actual buildup equation used is of little consequence.

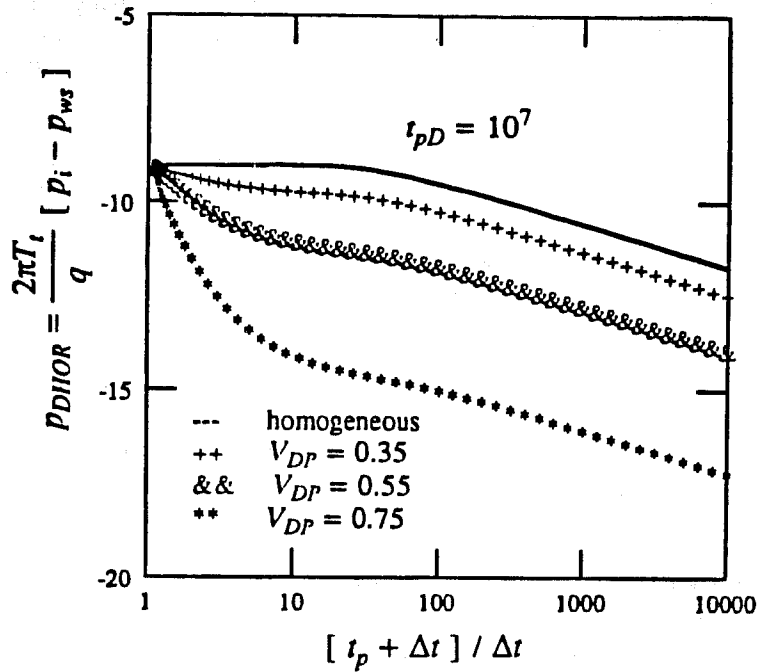


Fig. 3.13 Effect of permeability contrast on buildup behavior, 5-layer case, dimensionless Horner graph, no-flow outer boundary.

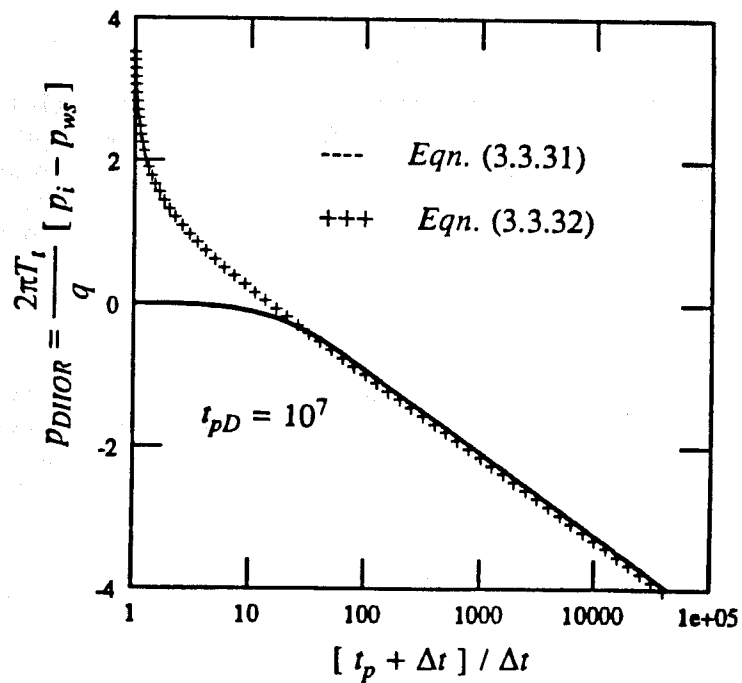


Fig. 3.14 Comparison of buildup responses, 5-layer case,  $V_{DP} = 0.75$ , dimensionless Horner graph.

### 3.4. TRACER TEST RESPONSE

The objectives here are to generate tracer test data using the model of Abbaszadeh-Dehghani and Brigham (1982) for systems whose pressure behavior was described in the previous section, and provide a comparison of the effect of stratification on pressure and tracer test responses.

#### 3.4.1. Mathematical Model

The theoretical treatment in this section closely follows that of Abbaszadeh-Dehghani and Brigham. The basic assumptions are :

1. Originally one mobile fluid in the system,
2. Completely miscible with resident and chase fluids,
3. Unit-mobility ratio displacement,
4. No tracer adsorption and/or reaction,
5. Small tracer slug compared to pattern volume, and
6. Steady-state flow conditions.

As shown by Brigham (1973), the approximate equation describing mixing in such situations for one-dimensional tracer transport is:

$$\frac{C}{C_{inj}} = \frac{1}{2} \operatorname{erfc} \left\{ \frac{s - \bar{s}}{\sqrt{2\sigma_m^2}} \right\} \quad (3.4.1)$$

where  $\sigma_m$  is a measure of the mixing zone length, and corresponds to the standard deviation of a normal (Gaussian) probability density function. Since the length of the mixed zone is a function of : (a) fluid movement through the porous medium (the longer the distance travelled, the greater the mixed zone), and (b) geometry of flow path (the wider the passage, the narrower the mixed zone), the total change in  $\sigma_m$  can be expressed by:

$$d\sigma_m = d\sigma_s + d\sigma_g \quad (3.4.2)$$

where the first term on the right hand side refers to change due to movement, and the second term refers to change due to geometry of the passage. For a system of arbitrary shape, integration of Eq. 3.4.2 with proper expressions for  $d\sigma_s$  and  $d\sigma_g$ , as derived by Abbaszadeh-Dehghani and Brigham, gives:

$$\sigma_m^2(\bar{s}) = 2\alpha v^2(\bar{s}) \int_0^{\bar{s}} \frac{ds}{v^2(s)} \quad (3.4.3)$$

where  $v$  is the velocity of the fluid along the streamline at location  $s$  or  $\bar{s}$ ,  $\alpha$  the dispersivity, and  $ds$  the incremental path along the streamline.

Consider now a repeated flooding pattern such as a 5-spot (Fig 3.15a), into which a tracer slug is injected followed by a chase fluid. The tracer is divided between the many streamtubes comprising the pattern volume, and mixes with both the resident fluid (at the leading edge,  $\bar{s}_1$ ) and the chase fluid (at the trailing edge,  $\bar{s}_2$ ). Using Eq. 3.4.1 to approximate mixing at both these edges, tracer concentration in a streamtube can be expressed as:

$$\frac{C}{C_{inj}} = \frac{1}{2} \operatorname{erfc} \left\{ \frac{s - \bar{s}_1}{\sqrt{2\sigma_{m1}^2}} \right\} - \frac{1}{2} \operatorname{erfc} \left\{ \frac{s - \bar{s}_2}{\sqrt{2\sigma_{m2}^2}} \right\} \quad (3.4.4)$$

Figure 3.15b illustrates the notations used in this equation. The size of the tracer slug in any streamtube is constant at all times (because of the conservative tracer assumption), but the undiluted width of the tracer ( $W = \bar{s}_1 - \bar{s}_2$ ) is a function of position, and hence a function of the width of the streamtube at that location. Assuming a small slug, Equation 3.4.4 can be rewritten in terms of the derivative of the error function as:

$$\frac{C}{C_{inj}} = \frac{W}{\sqrt{2\pi\sigma_m^2}} \exp \left[ -\frac{[s - \bar{s}]^2}{2\sigma_m^2} \right] \quad (3.4.5)$$

This equation expresses the concentration of the tracer at any location within the streamtube, in terms of the distance along the streamline. However, it is more convenient to express this in terms of volumes. As derived by Abbaszadeh-Dehghani and Brigham, this is given by the following expression:

$$\frac{C(\psi)}{C_{inj}} = \frac{0.453384}{\sqrt{Y(\psi)}} \sqrt{\frac{a}{\alpha}} F_r \exp \left[ -\frac{0.645776}{Y(\psi)} \frac{a}{\alpha} \left\{ V_{pDBT}(\psi) - V_{pD} \right\}^2 \right] \quad (3.4.6)$$

where  $V_{pDBT}(\psi)$  is the pore volumes of displacing fluid injected into the pattern to fill a streamtube under study,  $V_{pD}$  is the total pore volumes of displacing fluid injected, and  $F_r$  is the size of the tracer slug injected as a fraction of the pattern pore volume. The  $Y$  term is related to the line integral in Eq. 3.4.3, and is derived in their Appendix C by Abbaszadeh-Dehghani and Brigham.

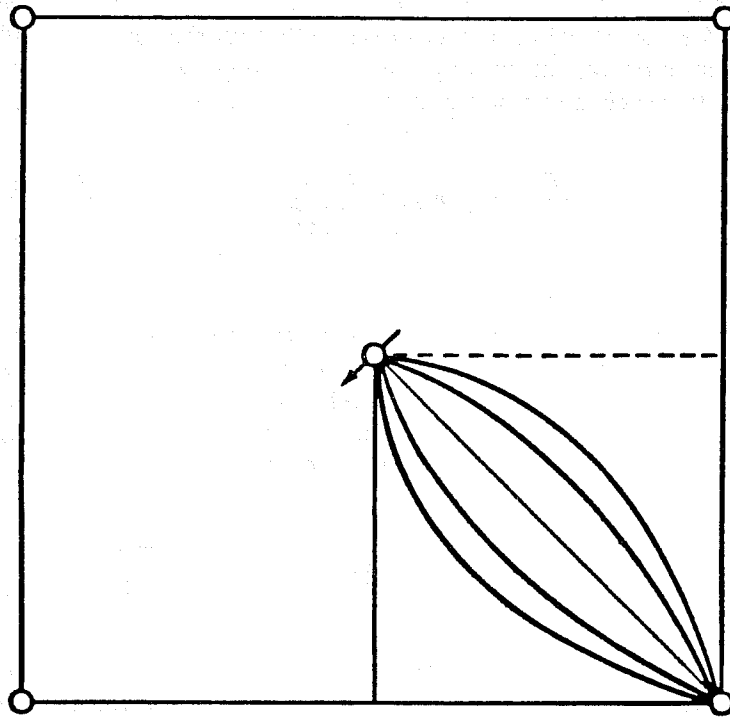
At any time, the composite breakthrough curve at the production well is due to tracer production from all streamtubes. By integrating over the symmetry element shown in Fig. 3.14, the following expression is obtained:

$$\bar{C}_D = 0.577266 \int_0^{\frac{\pi}{4}} \frac{\exp \left[ -\frac{0.645776}{Y(\psi)} \frac{a}{\alpha} \left\{ V_{pDBT}(\psi) - V_{pD} \right\}^2 \right] d\psi}{\sqrt{Y(\psi)}} \quad (3.4.7)$$

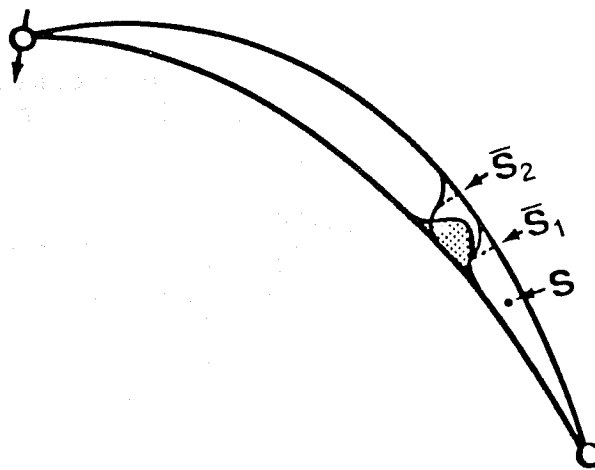
where the dimensionless tracer concentration  $\bar{C}_D$  is given by:

$$\bar{C}_D = \frac{\bar{C}}{C_{inj} F_r \sqrt{\frac{a}{\alpha}}} \quad (3.4.8)$$

and  $\bar{C}$  is the effluent tracer concentration at the production well.



3.15 (a) Repeated 5-spot pattern with symmetry element.



3.15 (b) Streamline geometry showing mixing of tracer slug.

Fig. 3.15 Mixing in a symmetry element of a repeated 5-spot.

This solution can be extended to the multi-layer case under unit-mobility ratio displacement conditions. The major assumptions required are : (a) layers are homogeneous with respect to  $k$ ,  $\phi$  and  $h$ , and (b) dispersivity,  $\alpha$ , and water saturation,  $S_w$ , are the same for all layers. Because of the unit-mobility ratio condition, any material injected is distributed among the layers in proportion to the layer transmissivities. If  $V_T(\tau)$  is the total volume of displacing fluid injected at time  $\tau$ , the pore volume injected into layer  $j$  is given by:

$$V_{pDj}(\tau) = \frac{T_j}{T_t} \frac{V_T(\tau)}{A S_w (\phi h)_j} \quad (3.4.9)$$

The effluent tracer concentration at a producing well is the volumetric sum of the tracer concentrations from individual layers:

$$\bar{C}_t(\tau) = C_{inj} \sqrt{\frac{a}{\alpha}} \sum_{j=1}^{NL} \frac{T_j}{T_t} F_{rj} \bar{C}_{Dj}(\tau) \quad (3.4.10)$$

where  $F_{rj}$  is the tracer slug size injected into layer  $j$ , in terms of the pore volume of layer  $j$ , and the total amount of tracer injected  $V_{Tr}$ :

$$F_{rj} = \frac{T_j}{T_t} \frac{V_{Tr}}{A S_w (\phi h)_j} \quad (3.4.11)$$

$\bar{C}_{Dj}(\tau)$  is the dimensionless concentration from layer  $j$ , calculated as a function of  $V_{pDj}(\tau)$  from Eq. (3.4.7).

### 3.4.2. Tracer Concentration-time Behavior

Figures 3.16 and 3.17 show tracer breakthrough curves for 5- and 10-layer systems with  $V_{DP} = 0.55$  with other data as listed in Table 3.1. In general, the number of peaks in each case is equal to the number of layers. This indicates that the presence of layering with permeability contrast between layers creates preferential flow paths for the tracer, and thus each layer produces a concentration peak. However, only nine of the ten layers have broken through in Fig. 3.17, because of the limited time-scale shown.

Figures 3.18 and 3.19 show tracer breakthrough curves for 5-layer systems with  $V_{DP} = 0.35$  and  $0.75$ . All 5 layers can be seen in the first case (Fig. 3.18), since the layer properties are fairly uniform, and the tracer slug is more evenly divided between the layers than in Fig. 3.19. As permeability contrast increases, more tracer is confined to the high permeability layers, which are the only ones apparent in the concentration-time data of Fig. 3.19. Another observation from these curves is that for a given number of layers, tracer breakthrough is accelerated for a higher  $V_{DP}$ . This implies that the degree of heterogeneity does affect the tracer flow behavior, unlike the transient pressure response.

Figures 3.20 and 3.21 show the effect of the level of dispersion (as characterized by dispersivity,  $\alpha$ ) on tracer concentration-time data. For small  $\alpha$  (i.e., Fig. 3.20), the flow is convection dominated and hence the concentration peaks are much sharper, reflecting the lack of spreading. Increasing  $\alpha$  tends to smooth out a front, although the influence of layering clearly persists in the multi-modal nature of the breakthrough curves (Fig. 3.21).

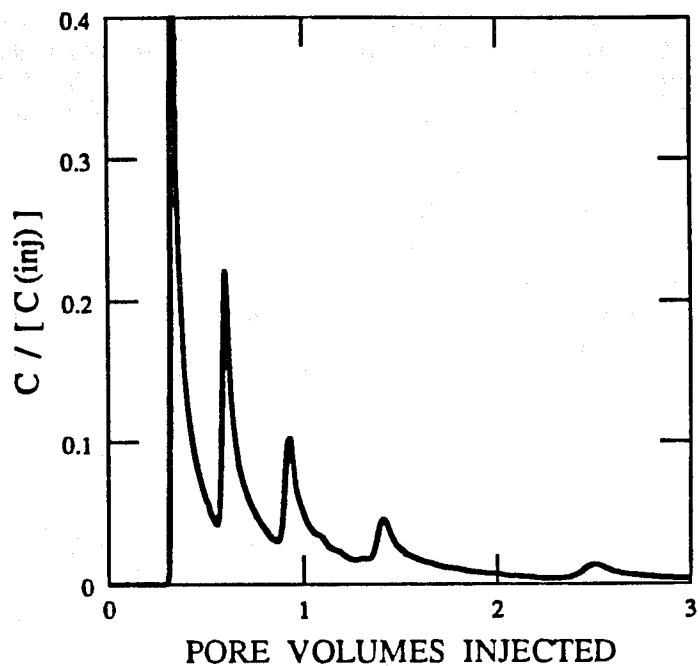


Fig. 3.16 Tracer breakthrough curve, 5-layer case,  $V_{DP} = 0.55$ .

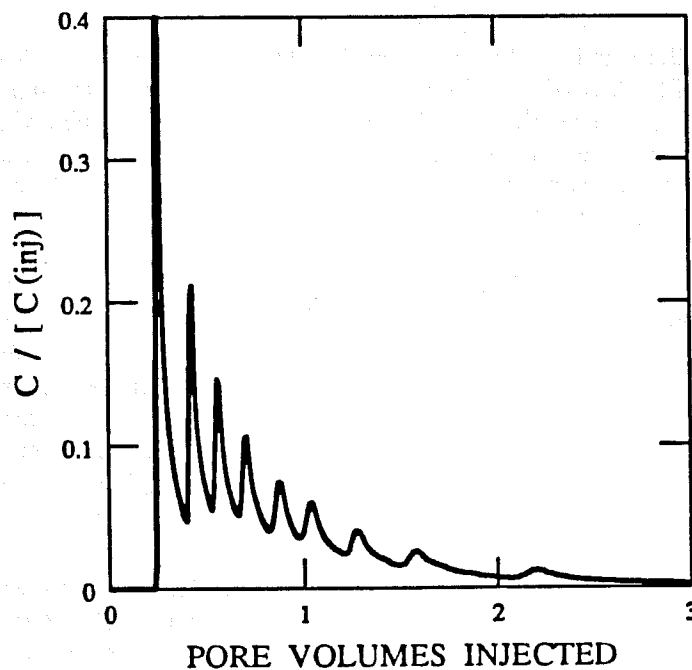


Fig. 3.17 Tracer breakthrough curve, 10-layer case,  $V_{DP} = 0.55$ .

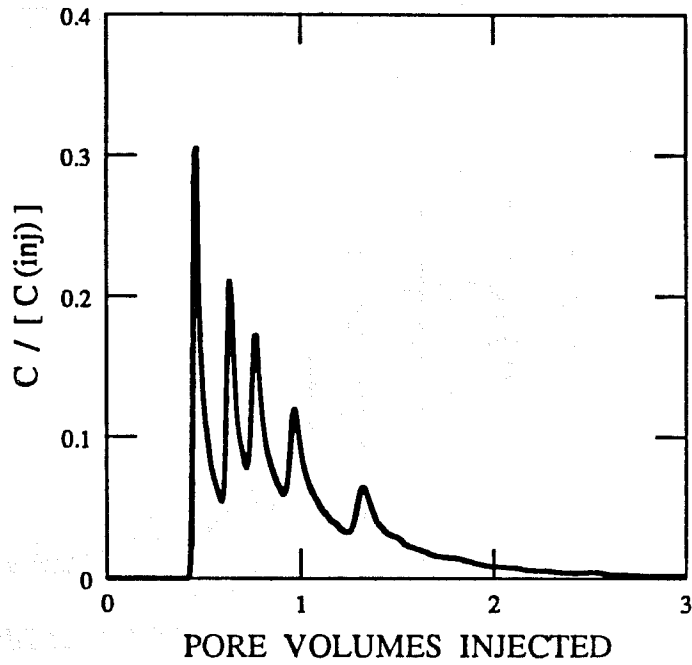


Fig. 3.18 Tracer breakthrough curve, 5-layer case,  $V_{DP} = 0.35$ .

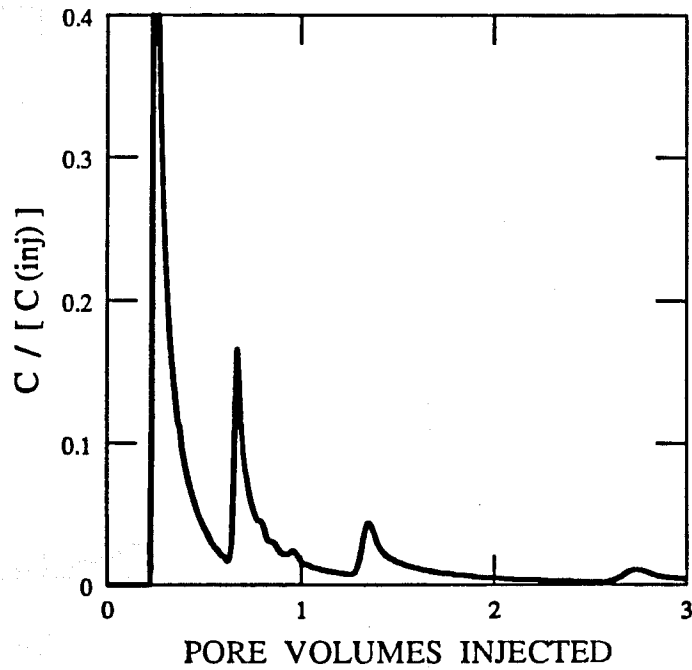


Fig. 3.19 Tracer breakthrough curve, 5-layer case,  $V_{DP} = 0.75$ .

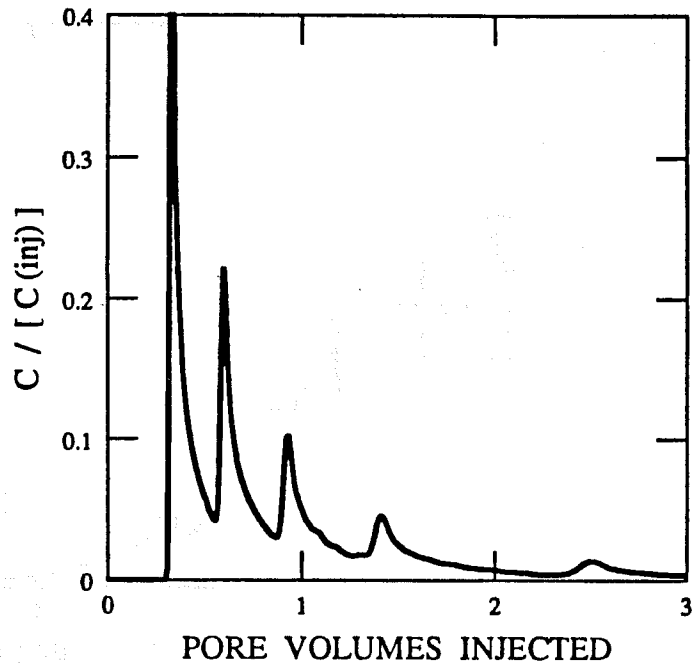


Fig. 3.20 Tracer breakthrough curve, 5-layer case,  $V_{DP} = 0.55$ ,  $\alpha = 0.1 \text{ ft.}$

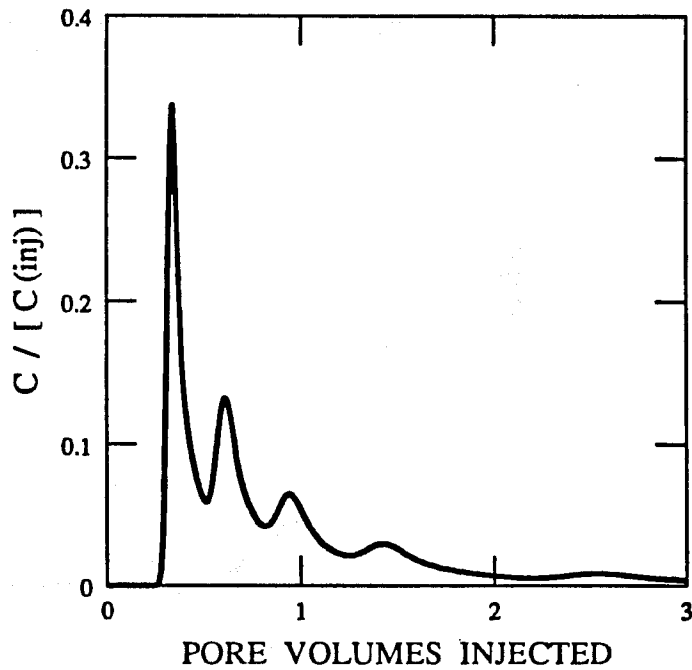


Fig. 3.21 Tracer breakthrough curve, 5-layer case,  $V_{DP} = 0.55$ ,  $\alpha = 1.0 \text{ ft.}$

Tracer breakthrough curves from multi-layered systems (such as those presented) can be analyzed to obtain individual layer properties. Because of the nonlinear nature of the interpretation model (Eqs. 3.4.9 - 3.4.11), it is necessary to use a nonlinear regression procedure for curve fitting. The objective is to minimize the function:

$$SSQ = \sum_{i=1}^{NPT} \left\{ C_{obs,i} - \bar{C}_{t,i} \right\}^2 \quad (3.4.12)$$

where  $SSQ$  is the residual sum of squares (the error criterion),  $C_{obs}$  is the observed concentration,  $\bar{C}_t$  the model computed overall concentration,  $i$  an observation point, and  $NPT$  the number of data points.

As shown by Abbaszadeh-Dehghani and Brigham, Eqs. 3.4.9 - 3.4.11 can be rewritten in the form:

$$\bar{C}_{t,i} = \sum_{j=1}^{NL} \frac{(kh)_j}{(\phi h)_j \sum kh} \frac{(kh)_j}{\sum kh} \Gamma \left[ \frac{(kh)_j}{(\phi h)_j \sum kh} \right] \quad (3.4.13)$$

where  $\Gamma$  is the functional form obtained from the preceding equations. Then, minimization of Eq. 3.4.12 with  $\bar{C}_{t,i}$  in the form of Eq. 3.4.13 can be achieved by a variable projection algorithm for nonlinear optimization, as implemented in the subroutine VARPRO (Golub and Pereyra, 1972). Abbaszadeh-Dehghani and Brigham have demonstrated the application of this algorithm for several hypothetical cases, as well as a field case.

### 3.5. DISCUSSION OF RESULTS

The results presented here indicate that conventional pressure testing of layered systems without interlayer crossflow produces an integrated response during the infinite-acting period, from which only total system properties can be calculated. Although the various systems examined show slightly different responses, these differences are not great enough to be used for diagnostic purposes. Moreover, if the outer boundary is at constant pressure (i.e., the fluid injection case, as in this study), typical layered system diagnostic features (e.g. humps) may not appear on the pressure buildup trace. This implies that at least under the conditions discussed here, effects of reservoir stratification may not appear in a pressure transient test. However, it may be possible to resolve this identification problem by a combined analysis of bottomhole pressure and layer flow rate data (Ehlig-Economides and Joseph, 1985).

On the other hand, tracer tests appear sensitive to reservoir heterogeneities. Qualitatively, the shape of the tracer breakthrough curve is indicative of the presence of stratification. The level of layering may be seen from the number of concentration peaks, the magnitude of permeability variation is reflected in the time to breakthrough, the dispersivity affects the height of the peaks, and the relative size of the individual layers influences the height and width of the peaks. Such behavior is significantly different from the integrated response obtained from a transient pressure test in the absence of individual layer flow rate data. Moreover, if the tracer test is run long enough, and the value of total transmissivity is available from a pressure test, it is possible to obtain layer properties from the tracer concentration-time data using the deconvolution method described previously.

As pointed out by Brigham and Abbaszadeh-Dehghani (1987), pressure and tracer tests are complementary and not competing methods. Information from both types of tests can be combined to better describe the reservoir. The results of this section suggest that the important difference between conventional pressure testing and well-to-well tracer testing is in the level

of detail regarding permeability variation present in test data. The resolution of each technique must therefore be kept in mind when constructing descriptions of a physical system based on well test analysis.

## 4. WELL TEST ANALYSIS FOR AREALLY HETEROGENEOUS SYSTEMS

*Numerical models for simulating pressure and tracer test response in areally heterogeneous systems are described. The effect of heterogeneities on well test data is analyzed, and the problem of quantifying spatial permeability variation is examined.*

### 4.1. INTRODUCTION

Sedimentary deposits are characterized by variability in material properties in both areal and vertical dimensions. Vertical variations manifest themselves as individual strata, such as discussed in the previous section. Within each layer, lateral variations in rock properties may be caused by decaying energy of the depositional process. An example would be a fan deposit, which is more homogeneous at its mouth than its tip (Richardson *et al.*, 1987).

In this section, the concern is with the effect of lateral changes in rock properties. The flow geometry of interest, Fig. 4.1, is one quadrant of a single-layer developed 5-spot pattern being flooded under balanced conditions. Heterogeneity is assumed to be only due to areal variations in permeability.

### 4.2. REPRESENTATION OF HETEROGENEOUS MEDIA

Field evidence indicates that properties of porous media such as permeability vary from point to point in a random manner, and also exhibit spatial correlation. In the petroleum literature, variation of permeability has been analyzed statistically by many investigators (e.g., Law, 1944; Warren *et al.*, 1961; Bennion and Griffiths, 1966; Jensen *et al.*, 1985). Measurements of spatial continuity have been undertaken only recently using geostatistical techniques (e.g., Da Costa e Silva, 1985; Goggin *et al.*, 1986; Stalkup and Ebanks, 1986). Hoeksema and Kitanidis (1985) provide an excellent analysis of the spatial variability and structure of material properties for several groundwater aquifers.

As it is difficult to describe heterogeneities in complete deterministic detail, a geostatistical (stochastic) approach is adopted. Permeability is assumed to be a random function with known mean, variance and spatial correlation structure. Furthermore statistical homogeneity (i.e., stationarity) is also assumed to be valid in the flow domain (Journel and Huijbregts, 1978), which implies: (a) the mean is independent of location:

$$E [ z(\mathbf{x}) - z(\mathbf{x}+\mathbf{h}) ] = 0 \quad (4.2.1)$$

and (b) spatial correlation between two samples depends only on their separation:

$$2 \gamma(\mathbf{h}) = E \left[ \left\{ z(\mathbf{x}) - z(\mathbf{x}+\mathbf{h}) \right\}^2 \right] \quad (4.2.2)$$

The notion of stationarity in this case is appropriate only for an infinite domain, of which only a finite sub-space is considered. Here  $E$  is the statistical expectation (i.e., the average value),  $\mathbf{x}$  the spatial coordinate vector and  $\mathbf{h}$  the lag vector. The quantity  $\gamma$  is called the semi-variance, and the function relating  $\gamma$  to  $\mathbf{h}$  is known as the semi-variogram. Because of the

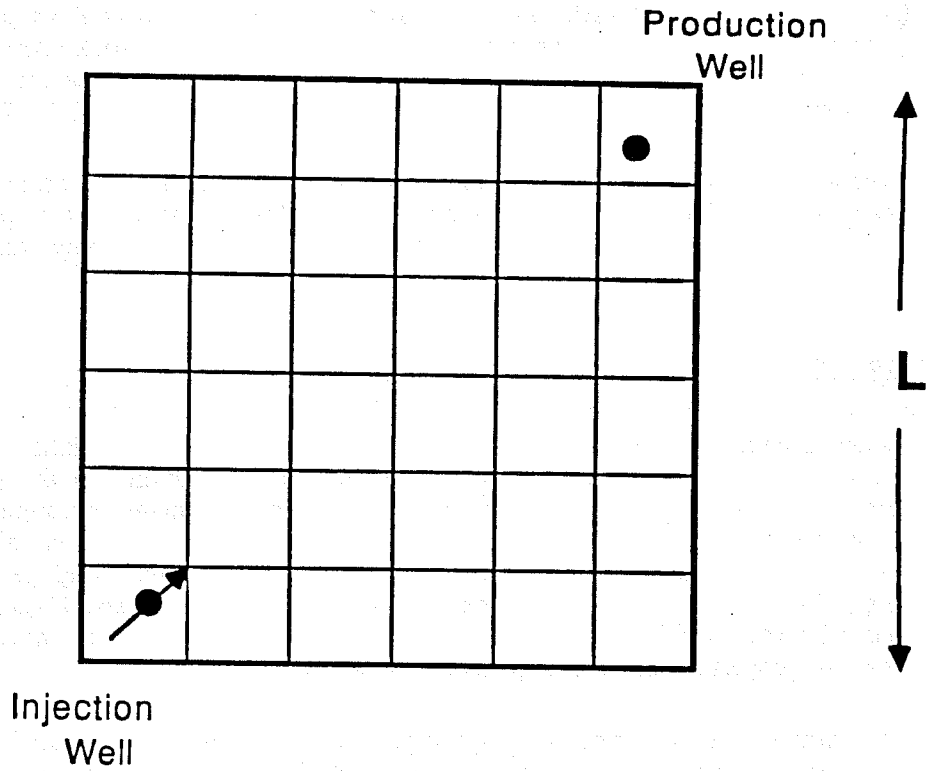


Fig. 4.1 System schematic, showing a quadrant from a repeated 5-spot.

assumptions of Eqs. 4.2.1 and 4.2.2, it is possible to estimate semi-variances for a one-dimensional process from the expression:

$$\gamma(h) = \frac{1}{2n(h)} \sum_{i=1}^{n(h)} [z(x_i) - z(x_i+h)]^2 \quad (4.2.3)$$

where  $n(h)$  is the number of pairs of observations separated by  $h$ .

Usually, the semi-variance,  $\gamma$ , is observed to increase with increasing lag,  $h$ , to some maximum, beyond which it remains unchanged (Fig. 4.2). This maximum variance is the *sill* of the semi-variogram, and is also equal to the variance,  $\sigma_z^2$ . The lag at which the sill is reached is referred to as the *range* of the semi-variogram. The range,  $\lambda$ , marks the limit of spatial continuity in the property concerned. In this work, the term *correlation length scale* is used in preference to range. A dimensionless correlation length scale can then be defined by normalizing  $\lambda$  with some characteristic flow length,  $L$  (Fig. 4.1). Such semi-variograms (with a finite variance or sill) describe the spatial correlation structure of properties which become more dissimilar on the average with increasing separation, and are characterized by a finite lag within which all variation is encountered. Some typical functional forms for semi-variograms of this type are given in Table 4.1.

Alternatively, one might encounter properties which appear to vary increasingly without limit with sampling area/volume, and which never seem to reach the origin when variations over successively smaller distances are examined. There is always some finite variance, no matter how small the sampling unit. Such behavior can be described by a semi-variogram of the following form:

$$\gamma(h) = \kappa h^\theta \quad (4.2.4a)$$

Here  $\kappa$  is a constant and  $\theta$  a positive number greater than 0 and less than 2 (McBratney and Webster, 1986). Eq. 4.2.4a also implies statistical self-similarity, because variations over any scale  $bh$  can be related to variations over a scale  $h$  by:

$$\gamma(bh) = b^\theta \gamma(h) \quad (4.2.4b)$$

This representation is identical to the idea of fractals developed by Mandelbrot (1982), and is also referred to as fractional Brownian motion. Ordinary Brownian motion corresponds to the value  $\theta = 1$ . Mandelbrot has shown that when  $\theta$  ranges from 1 to 2, a family of trails smoother than those of Brownian motion are obtained. Conversely, for  $\theta$  values between 1 and 0, traces are noisier than Brownian motion. Some typical semivariograms of this type are shown in Fig. 4.3. Recently, Hewett (1986) argued that reservoir rock properties may also exhibit fractal characteristics.

However, for the purposes of this study, permeability is assumed to be isotropic in two-dimensions, and the transformed variable  $z = \ln(k)$  is assumed to follow a circular semi-variogram model. This simple model can be visualized as that occurring in the middle of a large geologic deposit, such that an isotropic circular zone of influence prevails. Furthermore,  $z$  is taken to be log-normally distributed, so that its variability can be characterized by the Dykstra-Parsons coefficient (Dykstra and Parsons, 1950):

$$V_{DP} = \frac{\bar{k} - k_\sigma}{\bar{k}} = 1 - \exp(-\sigma_{\ln(k)}) \quad (4.2.5)$$

TABLE 4.1

SOME COMMON FUNCTIONAL FORMS FOR SEMI-VARIOGRAMS

MODEL	EQUATION	COMMENT
Linear	$\gamma(h) = \sigma^2 \left[ \frac{h}{\lambda} \right]$ $= \sigma^2$	$0 < h < \lambda$  $h \geq \lambda$
Circular	$\gamma(h) = \sigma^2 \left\{ 1 - \frac{2}{\pi} \cos^{-1} \left[ \frac{h}{\lambda} \right] + \frac{2h}{\pi\lambda} \sqrt{1 - \frac{h^2}{\lambda^2}} \right\}$ $= \sigma^2$	$0 < h < \lambda$  $h \geq \lambda$
Spherical	$\gamma(h) = \sigma^2 \left\{ \frac{3h}{2\lambda} - \frac{1}{2} \left[ \frac{h}{\lambda} \right]^3 \right\}$ $= \sigma^2$	$0 < h < \lambda$  $h \geq \lambda$
Exponential	$\gamma(h) = \sigma^2 \left\{ 1 - \exp \left[ \frac{-h}{\lambda_e} \right] \right\}$	

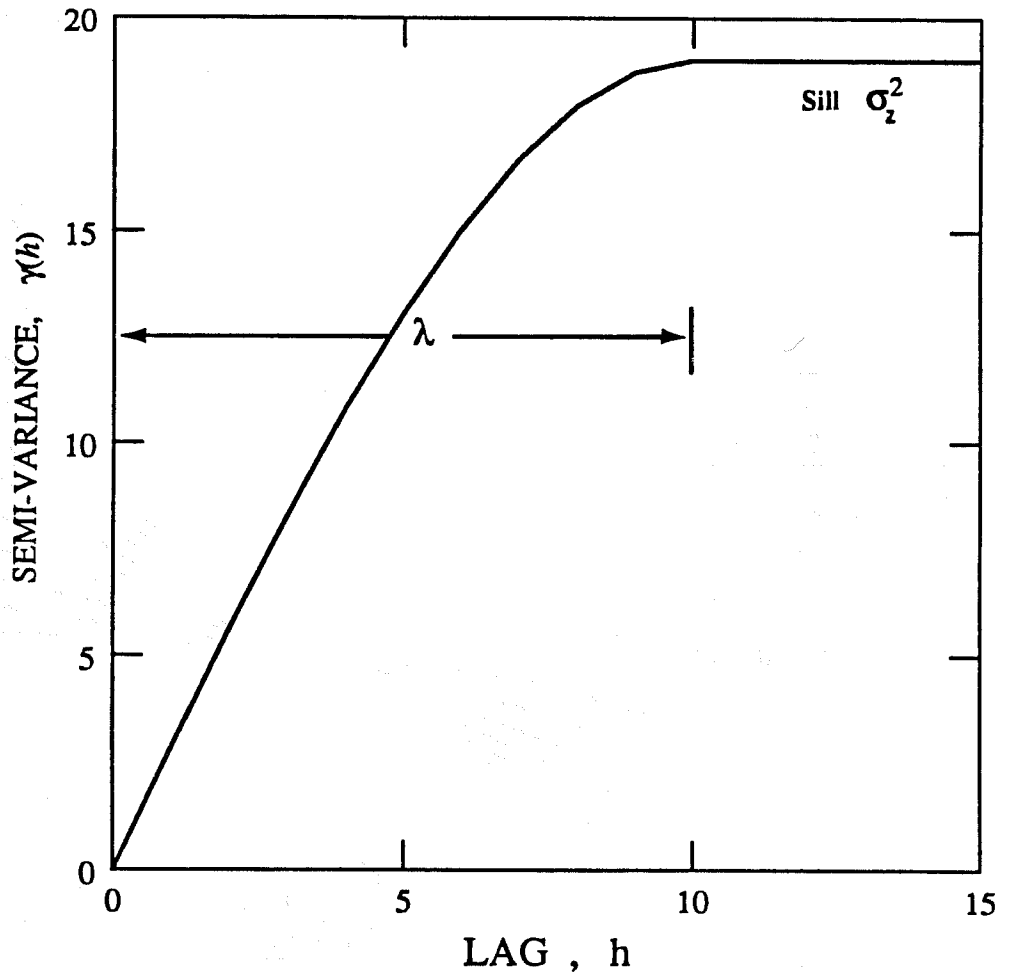


Fig. 4.2 Hypothetical semi-variogram with a finite range.

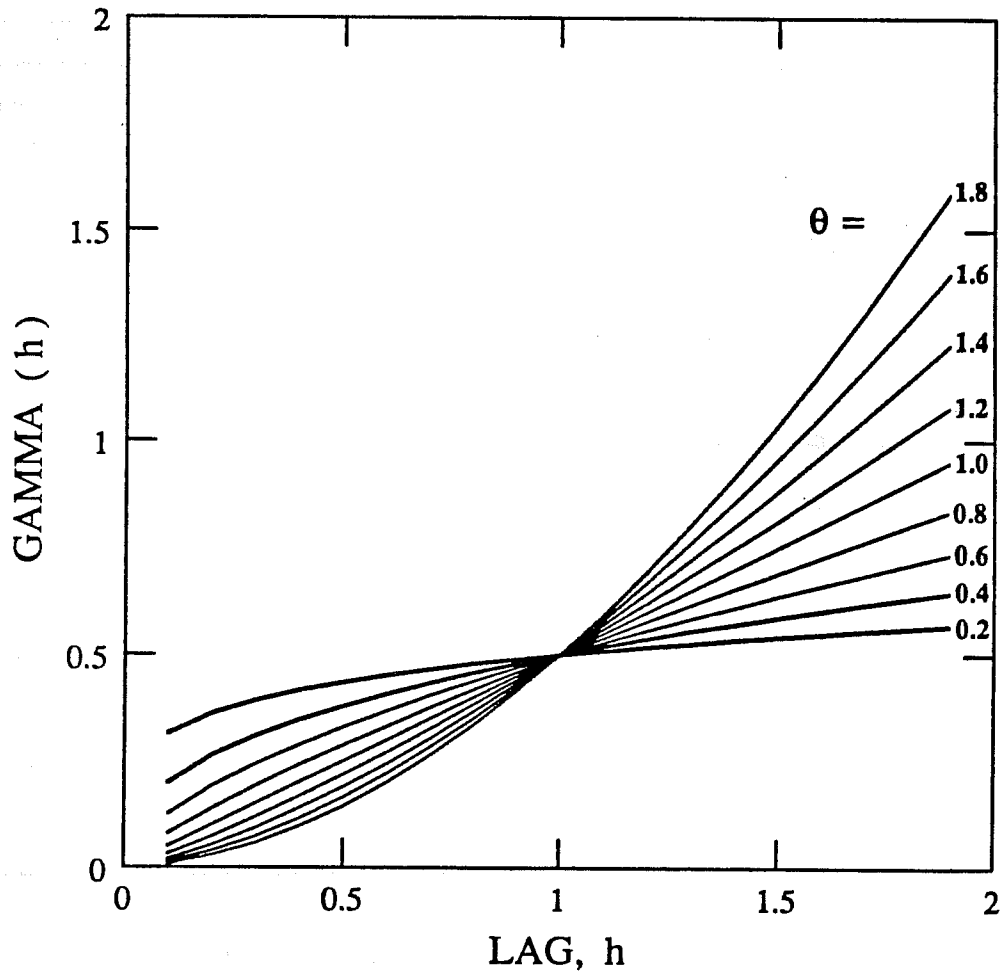


Fig. 4.3 Hypothetical semi-variogram showing fractal behavior.

where  $\bar{k}$  is the median permeability (i.e., the 50 percent value),  $k_{\sigma}$  is the permeability at one standard deviation (i.e., the 84.1 percent value) on a log-permeability cumulative distribution function (CDF), and  $\sigma_{\ln(k)}^2$  is the variance. An idealized log-permeability cumulative distribution function was shown in Fig. 3.4.

Several methods are available for generating spatially correlated parameter fields when the mean, variance and correlation length scales are known (Luster, 1985). The moving average method was used in this research, since it is conceptually simple and produces an isotropic log-permeability field with a circular semi-variogram in two dimensions. Briefly, this technique can be described as follows.

1. Extend the simulation grid in each dimension by  $\lambda$ , and generate a set of uniform random numbers,  $r(u)$ , ranging from zero to one, over the entire augmented grid.
2. Attribute to each node,  $s$ , in the simulation grid a value,  $y(s)$ , equal to the sum of all  $r(u)$  located inside a circle of diameter,  $\lambda$ , and centered at  $s$ .
3. Standardize the resulting realization,  $y(s)$ , to mean zero, and variance one, and then rescale so that the mean equals  $\ln(\bar{k})$ , and variance equals  $\sigma_{\ln(k)}^2$ . This produces a normally distributed log-permeability field,  $z(s)$ .
4. Exponentiate these values of  $z(s)$  to obtain permeability values over the required simulation grid.

A computer program for generating autocorrelated permeability fields with the moving average method is given in Appendix C. Figure 4.4 shows the perspective of a typical permeability data set generated using this procedure, where the permeability surface represents the variation of  $z = \ln(k)$ . Actual permeability values vary rather widely, from 1.3 md to 52.7 md. The semivariogram corresponding to this permeability field is shown in Fig. 4.5, and is obtained by weighting equally the  $x$ - and  $y$ -directional semivariograms calculated with Eq. 4.2.3. The semivariances are first computed along the rows (i.e., the  $x$ -direction), and then along the columns (i.e. the  $y$ -direction). The global semivariogram is finally estimated as the average of the two directional semivariograms, which is consistent with the assumption of isotropy. As seen from Fig. 4.5, the moving average procedure reproduces the input variance ( $\sigma_{\ln(k)}^2 = 0.48$ ) and correlation length ( $\lambda_D = 6/15$ ) reasonably. Table 4.2 presents other rock and fluid property data, which will subsequently be used as input to pressure and tracer test simulation codes. All of the results presented in the following sections are for a  $15 \times 15$  grid. The effect of grid refinement on pressure and tracer test responses is discussed in Appendix B.

### 4.3. PRESSURE TEST RESPONSE

As indicated by the literature review in Section 2.2.2, most studies have attempted to estimate effective permeabilities under steady-state conditions. Detailed analysis of averaging effects during transient flow conditions (e.g. buildup or drawdown testing) has been dealt with only briefly (Warren and Price, 1961). Moreover, the problem of obtaining some measure of permeability variation from single or multi-well pressure data does not appear to have been addressed. These aspects will be the focus of this segment of the research.

TABLE 4.2

SYSTEM DATA FOR MODELING PRESSURE AND TRACER RESPONSE

Area, $A$	20 acres
Grid size ( $NX * NY$ )	15 * 15
Thickness, $h$	10 ft
Porosity, $\phi$	0.10
Median perm, $\bar{k}$	10 md
Injection rate, $q_{inj}$	106.3 bbl/day (0.50 pore volumes/year)
Production rate, $q_{prd}$	106.3 bbl/day (0.50 pore volumes/year)
Tracer Slug size, $V_{TR}$	0.10 pore volumes
$V_{DP} [\sigma_{in(k)}^2]$	0.35 (0.18), 0.50 (0.48), 0.65 (1.10)
$\lambda_D$	1/15, 6/15, 16/15

V DP = 0.50 , LAMBDA D = 6/15

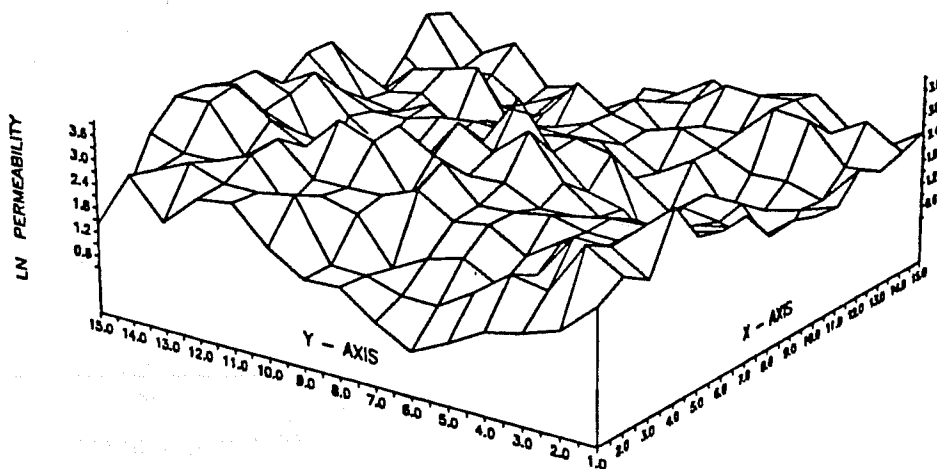


Fig. 4.4 Perspective of simulated permeability field.

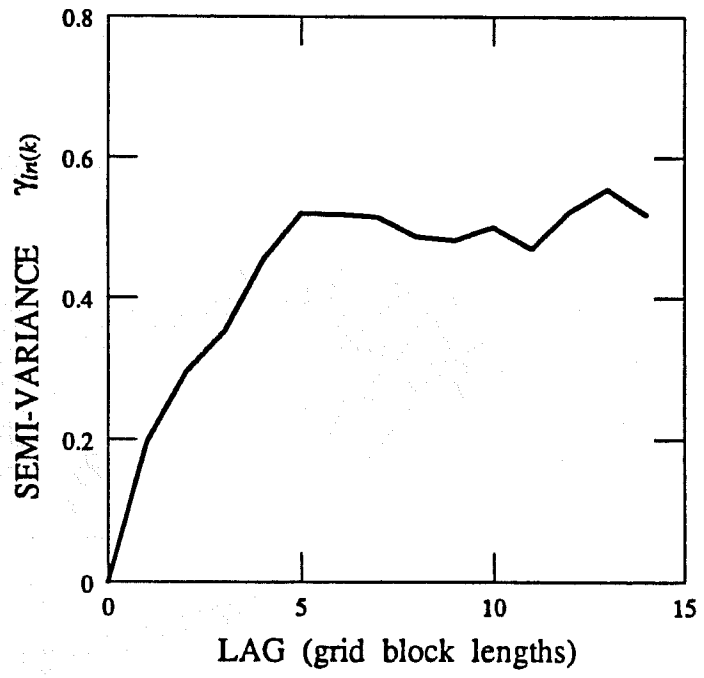


Fig. 4.5 Experimental semi-variogram.

### 4.3.1. Simulation of Pressure Behavior

The flow geometry of interest (Fig. 4.1) is a quadrant of a 5-spot from a repeated, balanced flooding pattern. The system is discretized into a set of grid-blocks, each of which is assigned a permeability according to the procedure described in Section 4.2. The other assumptions of importance are: (a) single-phase flow in two areal dimensions, (b) constant  $\phi$  and  $h$ , (c) slightly compressible fluid with constant  $\mu$  and  $c_p$ , and (d) production and injection rates constant over time, and equal to each other.

For these conditions, the depth-averaged pressure-diffusion equation is given by:

$$h\phi c_t \frac{\partial p}{\partial t} - qh = \frac{\partial}{\partial x} \left[ \frac{k_x h}{\mu} \frac{\partial p}{\partial x} \right] + \frac{\partial}{\partial y} \left[ \frac{k_y h}{\mu} \frac{\partial p}{\partial y} \right] \quad (4.3.1)$$

This equation was discretized using a forward-in-time, central-in-space (FTCS) finite difference formulation (Aziz and Settari, 1979), which leads to:

$$\begin{aligned} & \frac{\left[ h\phi c_t \right]_{ij}}{\Delta t} \left[ p_{ij}^{n+1} - p_{ij}^n \right] - \left\{ qh \right\}_{ij} \\ &= \frac{\left[ \frac{k_x h}{\mu} \right]_{i+1/2,j} \frac{2 \left[ p_{i+1,j}^{n+1} - p_{i,j}^{n+1} \right]}{\Delta x_{i+1,j} + \Delta x_{i,j}} - \left[ \frac{k_x h}{\mu} \right]_{i-1/2,j} \frac{2 \left[ p_{i,j}^{n+1} - p_{i-1,j}^{n+1} \right]}{\Delta x_{i,j} + \Delta x_{i-1,j}}}{\Delta x_{ij}} \\ &+ \frac{\left[ \frac{k_y h}{\mu} \right]_{i,j+1/2} \frac{2 \left[ p_{i,j+1}^{n+1} - p_{i,j}^{n+1} \right]}{\Delta y_{i,j+1} + \Delta y_{i,j}} - \left[ \frac{k_y h}{\mu} \right]_{i,j-1/2} \frac{2 \left[ p_{i,j}^{n+1} - p_{i,j-1}^{n+1} \right]}{\Delta y_{i,j} + \Delta y_{i,j-1}}}{\Delta y_{ij}} \end{aligned} \quad (4.3.2)$$

Here  $i$  and  $j$  denote the two space indices, and  $n$  denotes the time index. The interblock transmissibilities are evaluated by a harmonic average of grid-block transmissibilities as:

$$\left\{ \frac{k_x h}{\mu} \right\}_{i+1/2,j} = \frac{\Delta x_{i+1,j} + \Delta x_{i,j}}{\left\{ \frac{\mu \Delta x}{k_x h} \right\}_{ij} + \left\{ \frac{\mu \Delta x}{k_x h} \right\}_{i+1,j}} \quad (4.3.3)$$

with the y-directional transmissibility evaluated in a similar manner. Now multiplying both sides of Eq. (4.3.2) by  $\Delta x_{ij} \Delta y_{ij}$  and using the following grouping of terms:

$$\left\{ \tau_x \right\}_{i+1/2,j} = \frac{2 \Delta y_{ij}}{\left\{ \frac{\mu \Delta x}{k_x h} \right\}_{ij} + \left\{ \frac{\mu \Delta x}{k_x h} \right\}_{i+1,j}} \quad (4.3.4a)$$

$$\left\{ \tau_y \right\}_{i,j+1/2} = \frac{2 \Delta x_{ij}}{\left\{ \frac{\mu \Delta y}{k_y h} \right\}_{ij} + \left\{ \frac{\mu \Delta y}{k_y h} \right\}_{i,j+1}} \quad (4.3.4b)$$

one obtains after some manipulations:

$$\begin{aligned}
 & - \left[ \tau_x \right]_{i+1/2,j} \left[ p_{i+1,j}^{n+1} \right] - \left[ \tau_y \right]_{i,j+1/2} \left[ p_{i,j+1}^{n+1} \right] - \left[ \tau_x \right]_{i-1/2,j} \left[ p_{i-1,j}^{n+1} \right] - \left[ \tau_y \right]_{i,j-1/2} \left[ p_{i,j-1}^{n+1} \right] \\
 & + \left[ \left[ \tau_x \right]_{i+1/2,j} + \left[ \tau_y \right]_{i,j+1/2} + \left[ \tau_x \right]_{i-1/2,j} + \left[ \tau_y \right]_{i,j-1/2} + \frac{S_{ij}}{\Delta t} \right] \left[ p_{ij}^{n+1} \right] \\
 & = \frac{S_{ij}}{\Delta t} p_{ij}^n + Q_{ij}
 \end{aligned} \tag{4.3.5}$$

where  $S = h\phi c_i \Delta x \Delta y$  and  $Q = qh \Delta x \Delta y$ . Equation (4.3.5) may also be written as:

$$\mathbf{A} \mathbf{P}^{n+1} = \mathbf{B} \tag{4.3.6}$$

where  $\mathbf{A}$  is a sparse pentadiagonal matrix of coefficients,  $\mathbf{B}$  is a vector acting as the driving function, and  $\mathbf{P}$  is a vector of unknown pressures to be evaluated. The matrix,  $\mathbf{A}$ , is time-invariant as long as the viscosity of the injected fluid is the same as that of the fluid in-situ, but not time-step invariant. Thus it is updated only if the time-step size is changed. The vector,  $\mathbf{B}$ , contains well flow rate terms as well as pressures from the previous time step. This system of equations, Eq. (4.3.6), which is implicit in pressure, can be solved using direct solution methods. The matrix-solver used was a band-solve algorithm based on a modified Gaussian elimination procedure.

The simulator also uses an automatic time-step selection process, with logarithmic time incrementing suitable for conventional pressure analysis. Several test runs were made for a homogeneous system to select initial and maximum time step sizes. Initial time step sizes ranging from 0.001 days to 0.01 days were tested, and a value of 0.005 days was finally selected as a compromise between accuracy and stability. The maximum time step size was fixed such that no more than a preset fraction of a grid block pore volume could be injected or produced during a time step. This fraction was selected as 0.1, again as a compromise between accuracy in result and stability of the numerical algorithm. A flow chart for the simulator is given in Fig. 4.6.

### 4.3.2. Interpretation Methodology

Since a balanced injection-production pattern is being considered, the system will reach steady-state some time after the onset of injection and withdrawal. The transient pressure decline at the production well, and the transient pressure rise at the injection well, can be analyzed to estimate effective permeabilities around these wells. Assuming infinite-acting radial flow, permeability,  $k_j$ , can be related to the slope,  $m_j$ , of the linear portion on a semi-log pressure-time graph (Earlougher, 1977):

$$k_j = \frac{q\mu}{4\pi m_j h} \tag{4.3.7}$$

where the subscript  $j$  denotes injection (*inj*) or production (*prd*) as the case may be. In oil-field units, when  $q$  is in bbl/day,  $\mu$  in cp,  $h$  in ft,  $m$  in psi/log-cycle, and  $k$  in md, the numerical constant becomes 162.6 instead of  $1/4\pi$ . The effective permeability calculated with Eq. (4.3.7) measures some average property in a finite zone of influence around the well

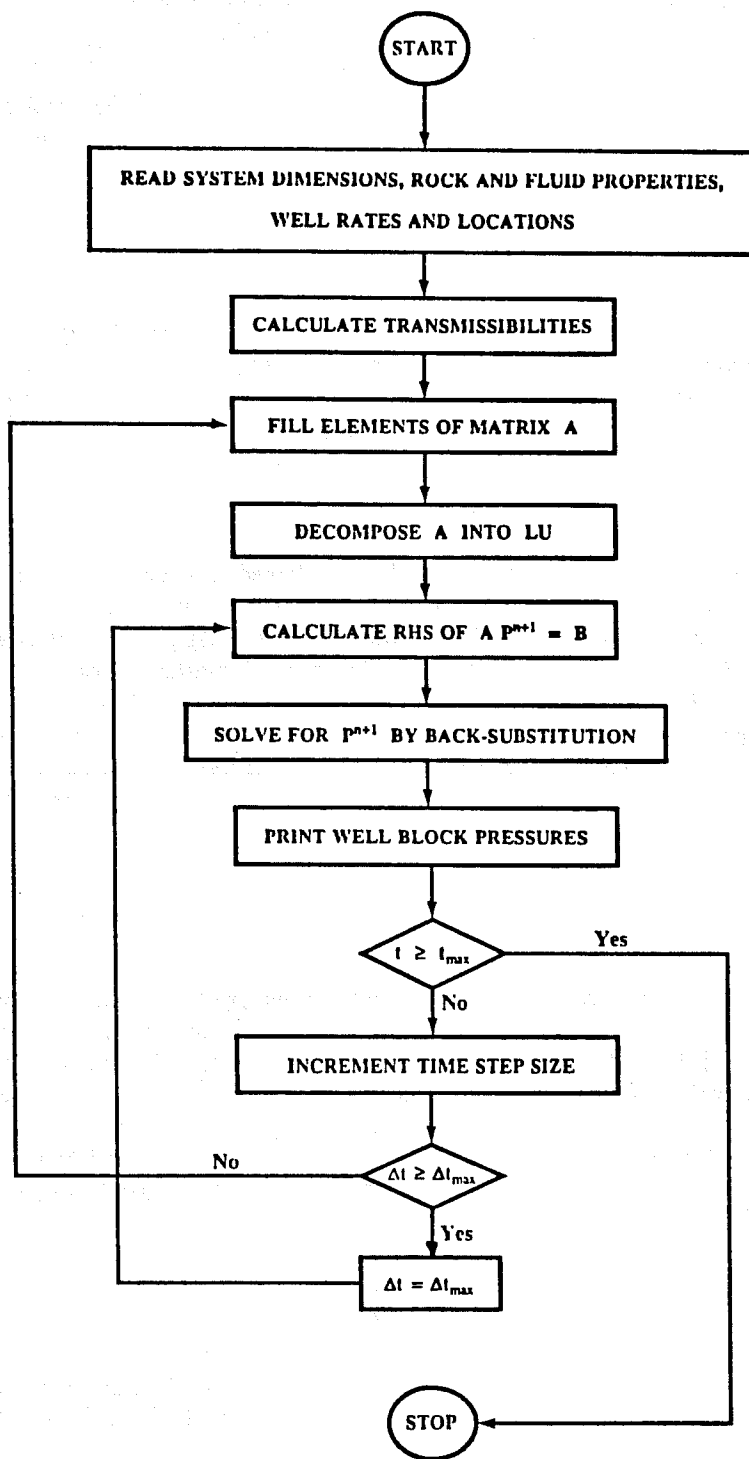


Fig. 4.6 Flow chart of numerical model simulating pressure behavior.

block. This value, referred to as the injection (or production) well permeability, is not necessarily the permeability of the grid-block containing the well.

The steady-state pressure drop between the wells,  $\Delta p_{ss}$ , can also be used to calculate a steady-state interwell permeability,  $k_{ss}$ . The appropriate interpretive equation, based on the injectivity equation for a repeated 5-spot, is (Craig, 1971):

$$k_{ss} = \frac{q\mu F}{\pi h \Delta p_{ss}} \quad (4.3.8)$$

In oil-field units, when  $\Delta p_{ss}$  is in psi, and the rest are in the units mentioned previously, the numerical constant becomes 282.4 instead of  $1/\pi$ . The geometric factor,  $F$ , which is a function of the interwell distance,  $d$ , and effective well radius,  $r_o$ , is defined as:

$$F = \ln \left\{ \frac{d}{r_o} \right\} - 0.619 \quad (4.3.9)$$

and is calculated in two ways. The first method is based on calibrating a steady-state simulation of a homogeneous system with known permeability. Using the data listed in Table 4.2, and a homogeneous system with  $k = 10$  md, the simulated  $\Delta p_{ss}$  is obtained as 3333 psi, which corresponds to  $F = 2.775$  and  $r_o = 44.3$  ft. The second method is based on calculating  $r_o$  analytically from the formula given by Abou-Kassem and Aziz (1985). For a repeated 5-spot quadrant with corner wells, simulated with a 5-point block-centered finite-difference formulation, their Table 1 gives a geometric factor of 0.63888, which corresponds to  $r_o = 44.84$  ft and  $F = 2.763$ . Both these values agree well with those computed by the first method.

### 4.3.3. Analysis of Pressure Test Data

In order to illustrate the general nature of simulated pressure-time graphs, a homogeneous system simulation with  $k = 10$  md is shown in Fig. 4.7. The early-time data resembles the early-time response of a finite radius well (which is expected as the effective wellbore radius is large compared to the grid block size), the middle-time data appears to correspond to the infinite-acting radial flow period, and the late-time data corresponds to steady-state. The slope of the semi-log straight line from the middle-time (infinite-acting) period yields the correct permeability value when used with Eq. (4.3.7). The duration of this period, shown in Fig. 4.7, can be converted to a dimensionless time based on the formula:

$$t_{Do} = \frac{kt}{\phi\mu c_i r_o^2} \quad (4.3.10)$$

In oil-field units, when  $t$  is in days,  $c_i$  in  $\text{psi}^{-1}$ , and  $r_o$  in ft, the numerical constant becomes  $6.33 \times 10^{-3}$  instead of 1. The limits shown in Fig. 4.7, i.e.  $t_{begin} = 0.03$  days, and  $t_{end} = 0.50$  days, correspond to dimensionless times of  $3 \leq t_{Do} \leq 50$  for the beginning and end of the semi-log straight line. Other simulations for homogeneous systems, with permeabilities ranging from 2.5 to 25 md, gave similar dimensionless time bounds for the semi-log straight line.

For each combination of  $V_{DP}$  and  $\lambda_D$ , pressure responses were simulated for 20 different realizations of the permeability field. Only two different pressure responses are graphed from each set of  $V_{DP}$  and  $\lambda_D$  for the sake of brevity. These are shown in Figs. 4.8

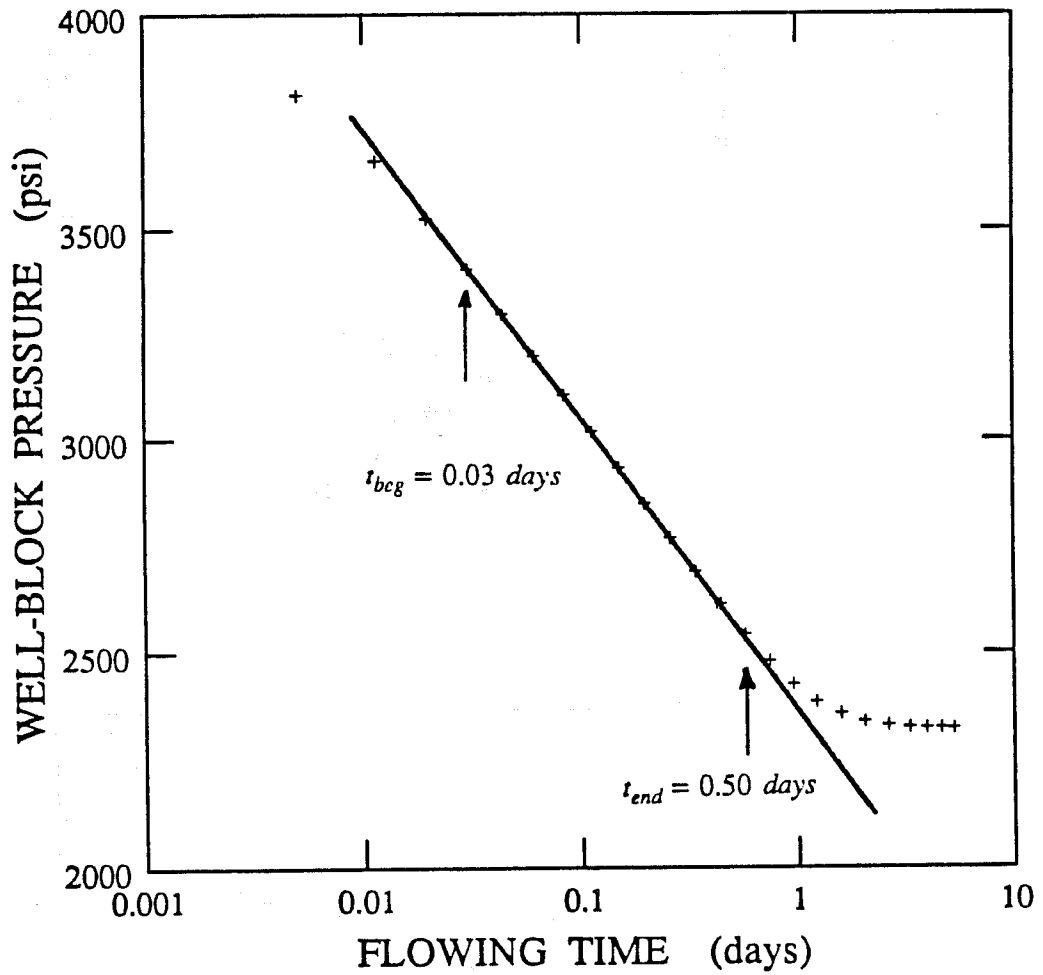
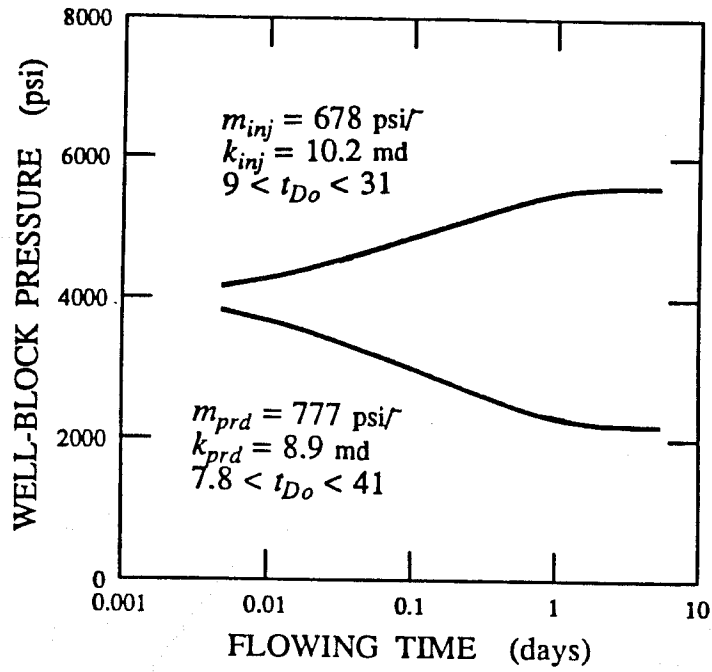
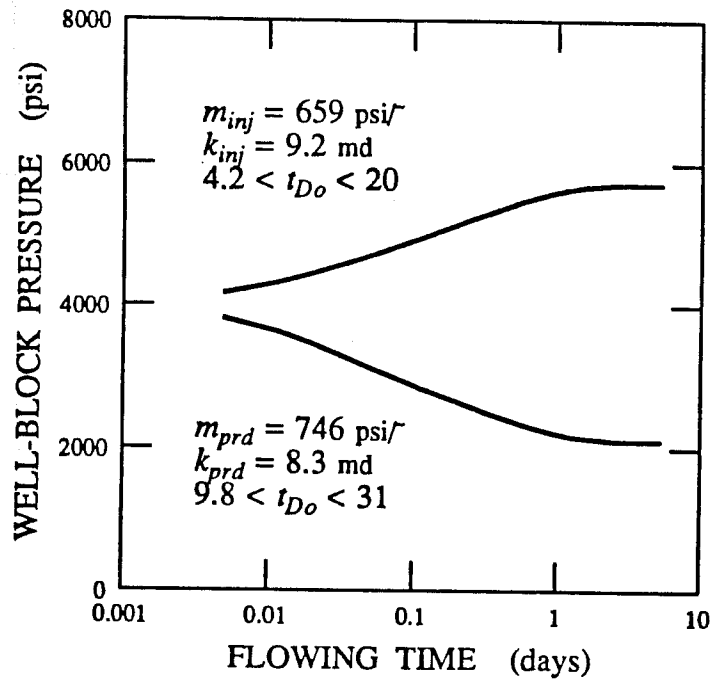


Fig. 4.7 - Well pressure history, homogeneous case,  $k = 10$  md.



4.8 (a) Run 2



4.8 (b) Run 9

Fig. 4.8 Simulated pressure response,  $V_{DP} = 0.35$ ,  $\lambda_D = 1/15$ .

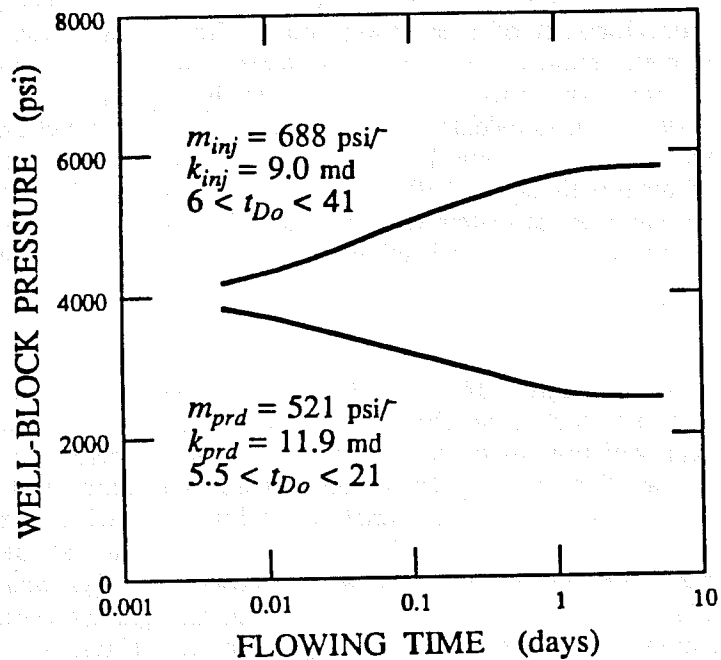
through 4.16. In general, heterogeneous system responses were seen to be similar to homogeneous system behavior. Use of Eq. (4.3.7) for computing transient permeabilities requires the development of a semi-log straight line on a pressure-time graph. Acceptable straight lines were found in most cases. In other cases, the smoothly varying data from the middle-time period was fitted with apparent straight lines. The slopes of these semi-log straight lines were used to calculate effective injection and production well permeabilities. The beginning and end of the semi-log straight lines were also determined, and converted to dimensionless form with Eq. (4.3.10). These were then checked against the dimensionless time bounds from homogeneous system data for internal consistency. Details of the fitting procedure are given in Appendix A. For each of the figures presented in this section, the semi-log slope, the effective permeability, and the dimensionless time limit of the semi-log straight line are indicated.

Figures 4.8 through 4.16 also show the probabilistic nature of these Monte-Carlo simulations. Because each permeability field is the outcome of a random generation procedure, some statistical variation is to be expected in pressure responses from one realization to another. Such variations also appear as differences in injection and production well pressure responses. When  $V_{DP}$  and  $\lambda_D$  are small (as in Figs. 4.8 and 4.9), the permeability fields are quite uniform, leading to almost similar injection/production well behavior as well as similar overall pressure responses in both realizations shown. As  $V_{DP}$  and  $\lambda_D$  increase (e.g. Figs. 4.12 and 4.13), systems become more nonuniform, and greater variability can be seen in the pressure responses. For larger values of  $V_{DP}$  and  $\lambda_D$  (Figs. 4.15 and 4.16), injection and production well responses are distinctly different from each other, and statistical variability between realizations is also distinct. It is clear that as  $V_{DP}$  and  $\lambda_D$  increase, there is a greater probability of clustering of like-permeability blocks, and thus the nonuniformity in well pressure responses will be more pronounced.

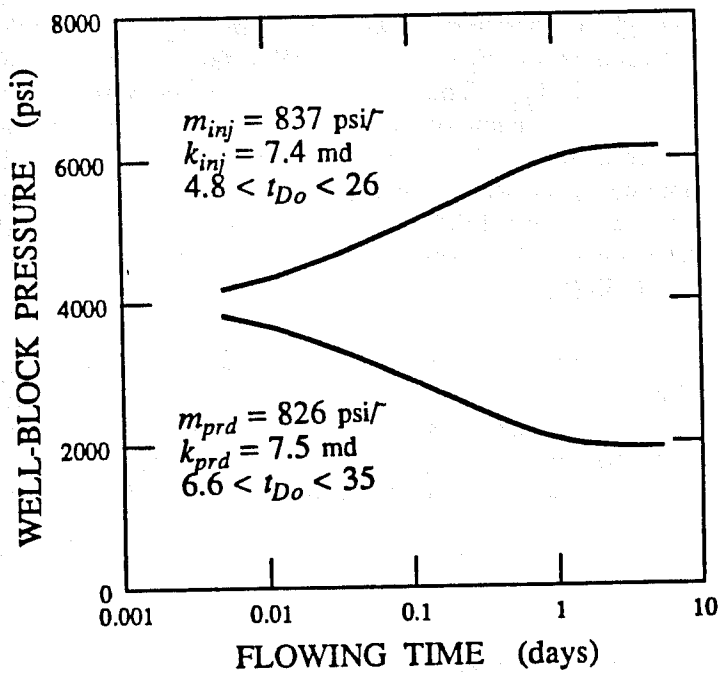
The computation of transient effective permeabilities, described previously, reflects averaging over scales localized around the wells. Another measurement, over a different scale, can be obtained by calculating a steady-state interwell permeability  $k_{ss}$  from Eq. (4.3.8). Tables 4.3 through 4.5 summarize  $k_{inj}$ ,  $k_{prd}$  and  $k_{ss}$  values calculated for each of the 20 realizations for each set of  $V_{DP}$  and  $\lambda_D$ . With few exceptions, values of  $k_{ss}$  were found to lie between  $k_{inj}$  and  $k_{prd}$ . This suggested that some weighted average of  $k_{inj}$  and  $k_{prd}$  could be used as an estimator of  $k_{ss}$ . The geometric mean was tested for this purpose and found to yield good results. The agreement between  $k_{ss}$  values calculated from Eq. (4.3.8) and those computed from the geometric mean approximation is shown in Figs. 4.17 through 4.19. The root mean squared difference was used as a measure of the goodness of fit between calculated and estimated  $k_{ss}$  values, and was calculated to be 5% for  $V_{DP} = 0.35$  (Fig. 4.17), 12% for  $V_{DP} = 0.50$  (Fig. 4.18), and 17% for  $V_{DP} = 0.65$  (Fig. 4.19).

The geometric mean relationship described above is not unexpected in view of the fact that permeability is assumed to be log-normally distributed. Warren and Price (1961) have shown that for random variations in permeability with a log-normal distribution, the steady-state effective permeability is the geometric average of the distribution. When the flow domain is effectively divided into injection and production well drainage areas, the transient effective permeability in each zone is essentially the geometric average of permeabilities within that area. Thus the geometric average of the two well permeabilities should approximately equal the steady-state interwell permeability.

Conditions under which  $k_{ss}$  might not be bounded by  $k_{inj}$  and  $k_{prd}$  are: (a) the presence of a high permeability streak along the diagonal joining the injection and production wells, which would cause  $k_{ss}$  to be higher than both well permeabilities, and (b) the presence of a low permeability streak in the transverse direction, which would result in  $k_{ss}$  being lower.

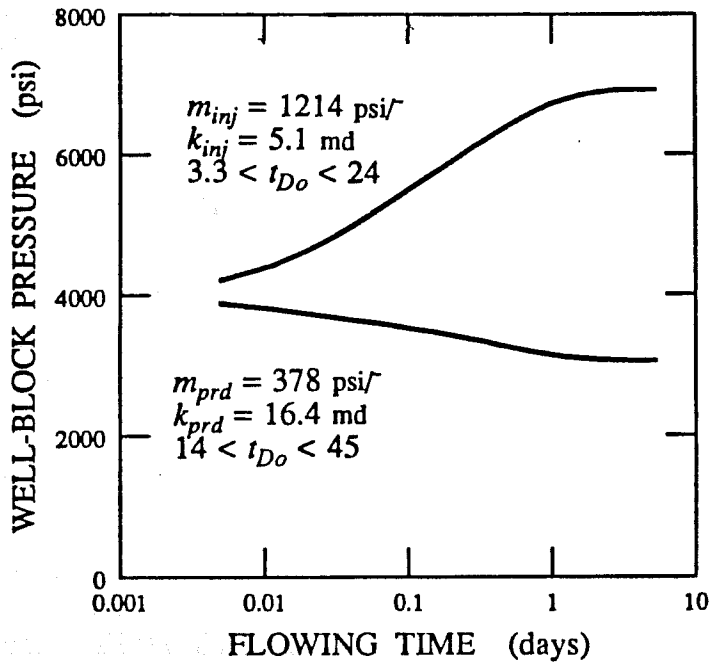


4.9 (a) Run 1

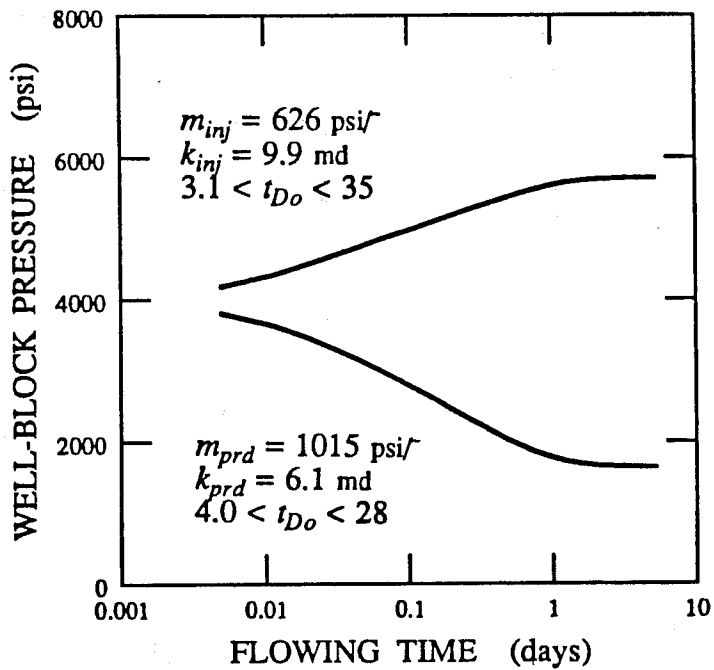


4.9 (b) Run 5

Fig. 4.9 Simulated pressure response,  $V_{DP} = 0.35$ ,  $\lambda_D = 6/15$ .

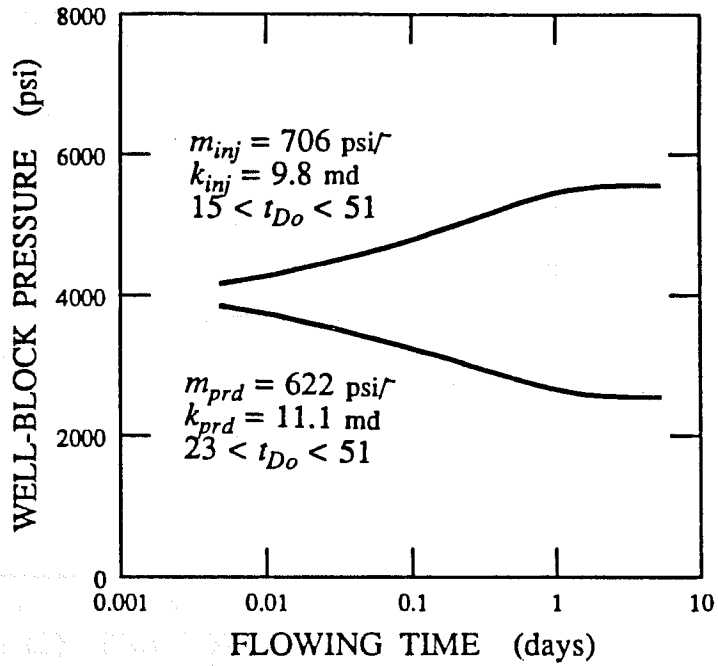


4.10 (a) Run 3

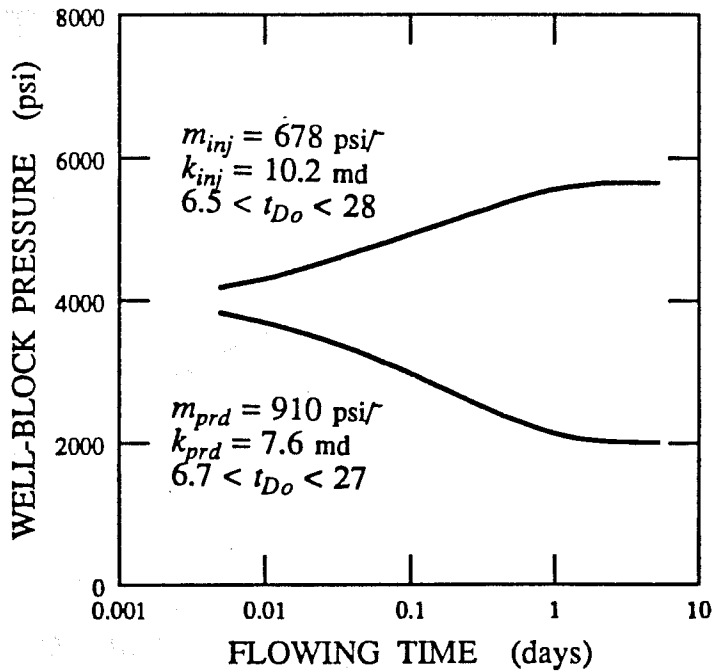


4.10 (b) Run 7

Fig. 4.10 Simulated pressure response,  $V_{DP} = 0.35$ ,  $\lambda_D = 16/15$ .

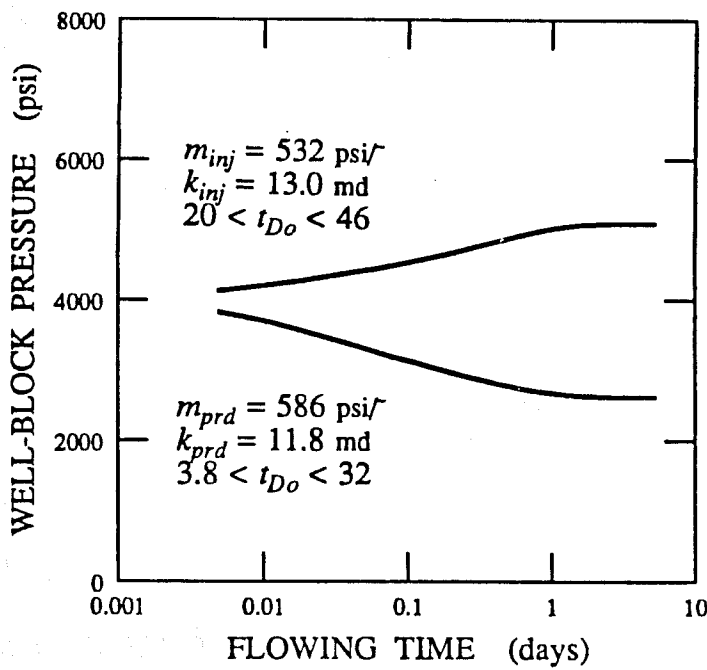


4.11 (a) Run 4

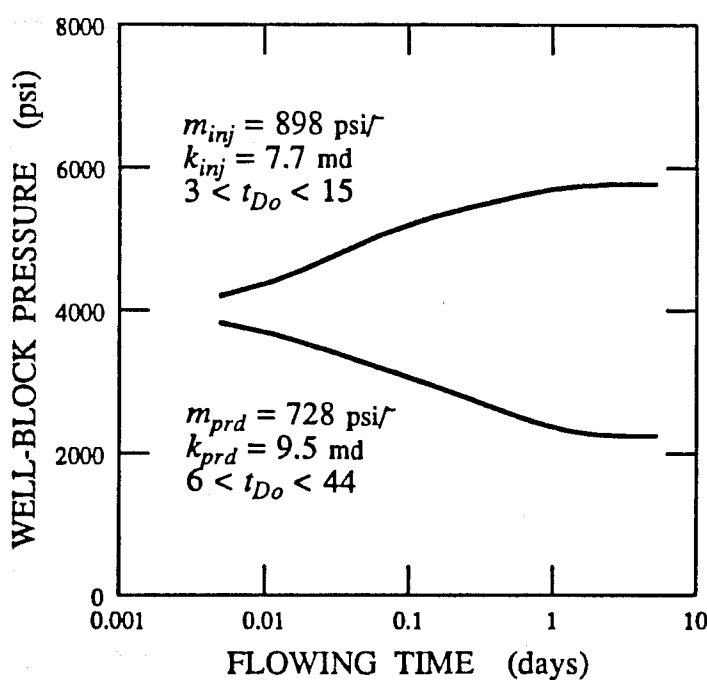


4.11 (b) Run 7

Fig. 4.11 Simulated pressure response,  $V_{DP} = 0.50$ ,  $\lambda_D = 1/15$ .

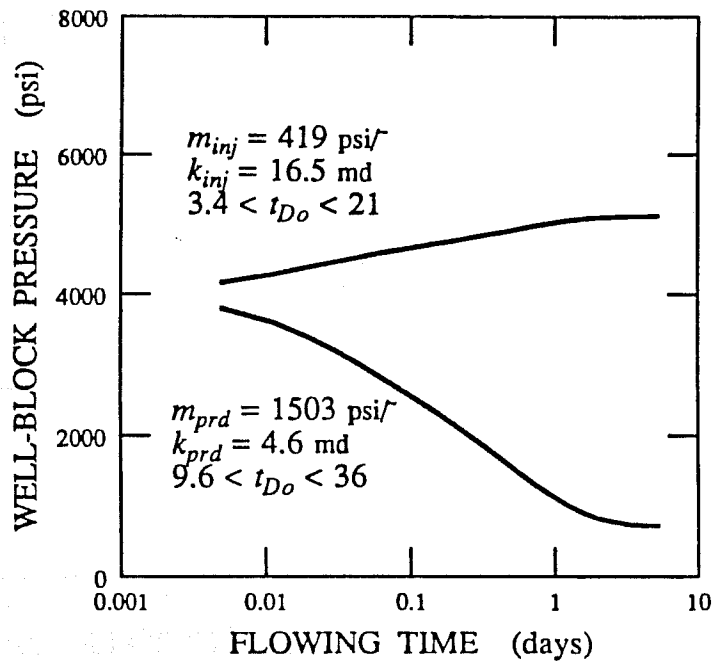


4.12 (a) Run 2

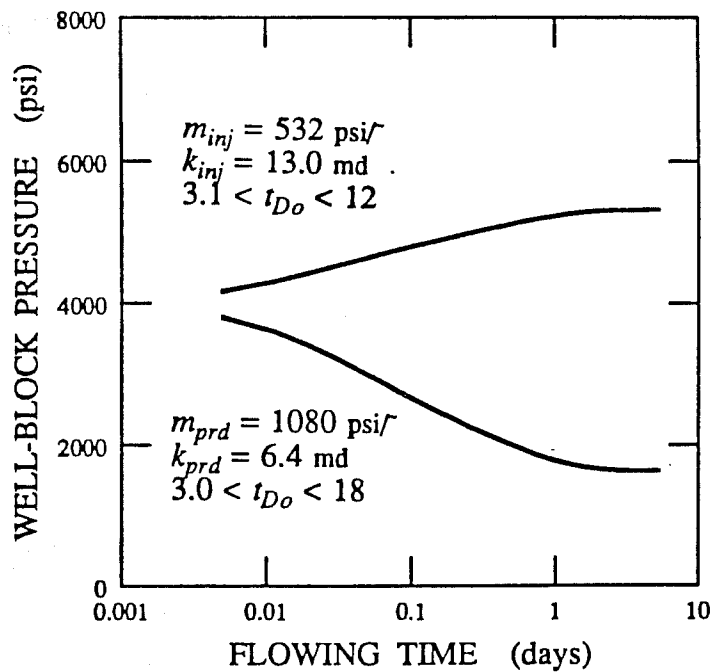


4.12 (b) Run 4

Fig. 4.12 Simulated pressure response,  $V_{DP} = 0.50$ ,  $\lambda_D = 6/15$ .

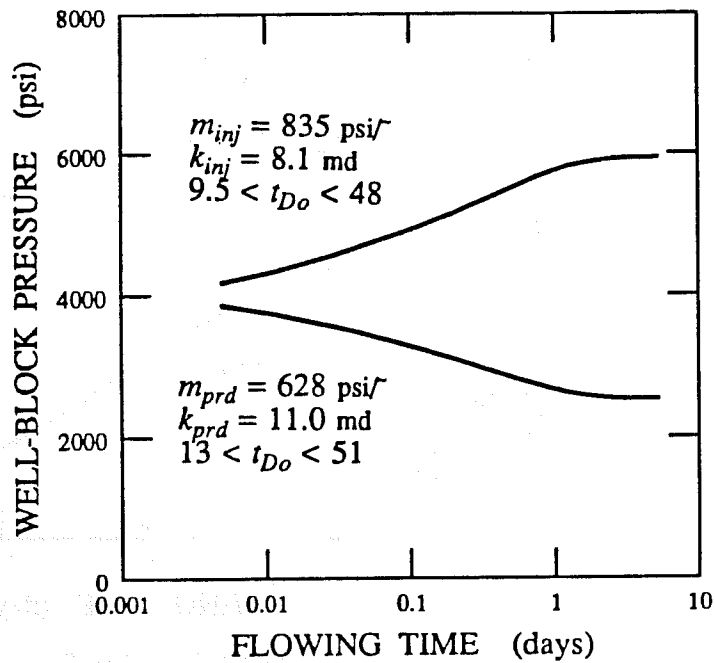


4.13 (a) Run 1

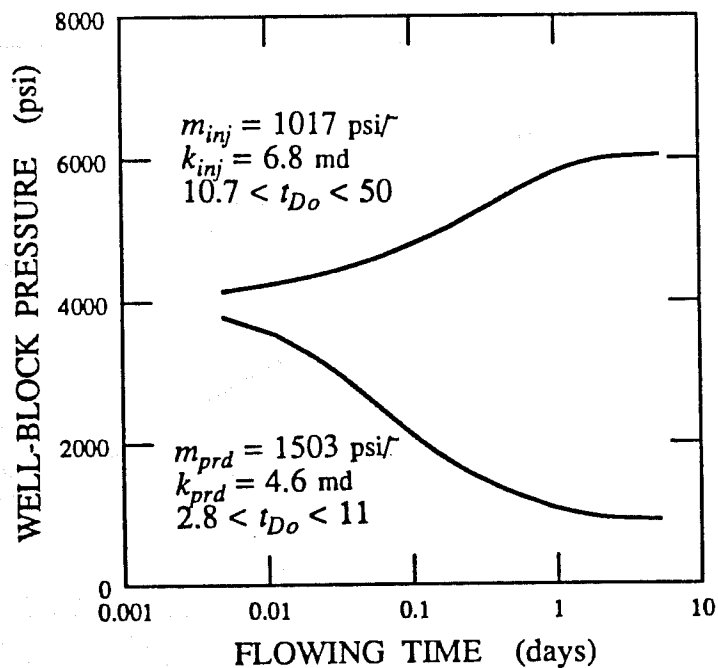


4.13 (b) Run 8

Fig. 4.13 Simulated pressure response,  $V_{DP} = 0.50$ ,  $\lambda_D = 16/15$ .

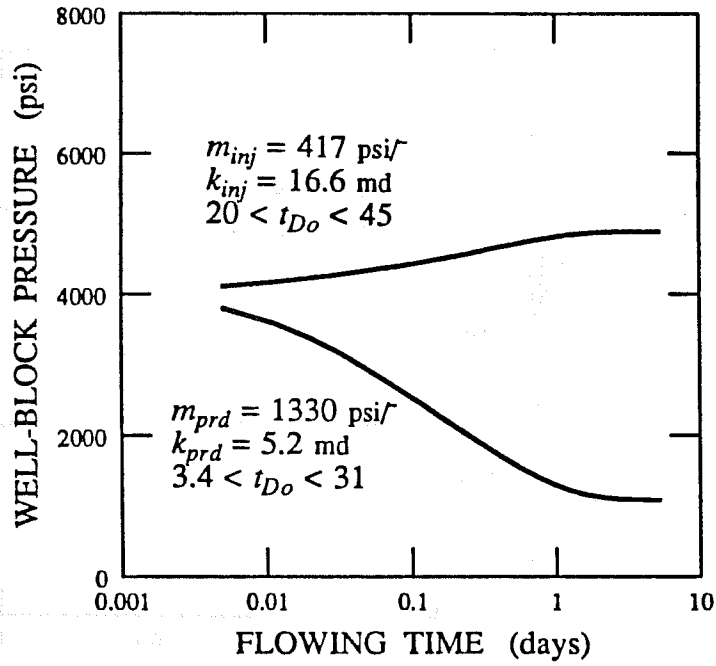


4.14 (a) Run 12

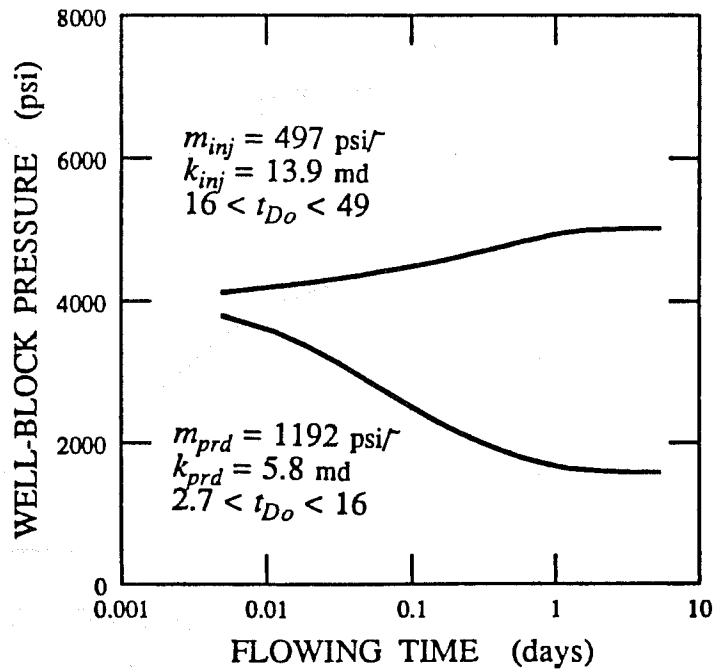


4.14 (b) Run 16

Fig. 4.14 Simulated pressure response,  $V_{DP} = 0.65$ ,  $\lambda_D = 1/15$ .

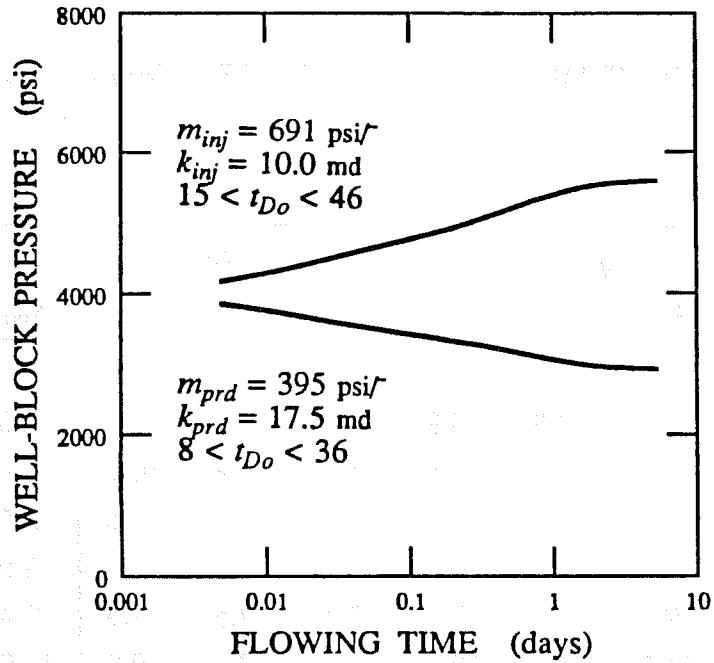


4.15 (a) Run 2

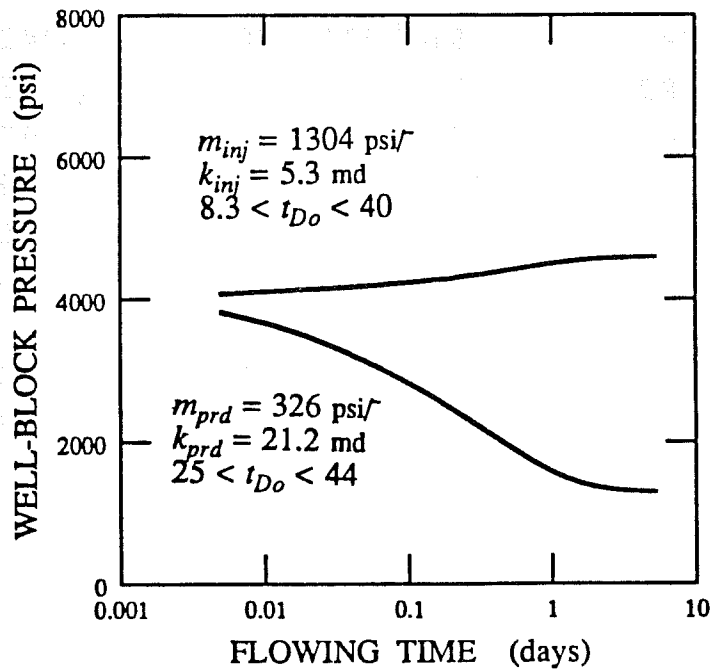


4.15 (b) Run 7

Fig. 4.15 Simulated pressure response,  $V_{DP} = 0.65$ ,  $\lambda_D = 6/15$ .



4.16 (a) Run 1



4.16 (b) Run 8

Fig. 4.16 Simulated pressure response,  $V_{DP} = 0.65$ ,  $\lambda_D = 16/15$ .

TABLE 4.3

PERMEABILITIES CALCULATED FROM SIMULATED  
PRESSURE DATA,  $V_{DP} = 0.35$

Run	$\lambda_D = 1/15$			$\lambda_D = 6/15$			$\lambda_D = 16/15$		
	$k_{inj}$	$k_{prd}$	$k_{ss}$	$k_{inj}$	$k_{prd}$	$k_{ss}$	$k_{inj}$	$k_{prd}$	$k_{ss}$
1	6.9	9.8	8.9	9.0	11.9	10.2	8.0	5.3	7.1
2	10.2	8.9	9.8	8.9	11.8	10.2	6.4	5.8	7.0
3	8.5	9.9	9.1	12.1	7.4	9.5	5.1	16.4	8.6
4	8.5	9.3	9.0	12.3	9.1	10.5	8.0	14.6	11.0
5	9.6	8.8	9.6	7.4	7.5	7.9	7.4	7.6	8.1
6	11.2	10.2	10.7	12.0	7.3	9.3	11.0	7.7	9.5
7	9.9	9.8	10.1	9.1	11.4	10.5	9.9	6.1	8.2
8	8.6	10.9	9.5	6.6	8.2	8.1	5.6	5.7	6.6
9	9.2	8.3	9.2	8.2	11.2	10.0	10.6	12.8	11.1
10	10.2	9.9	10.6	13.7	11.6	12.6	4.4	11.4	7.0
11	8.1	8.5	8.4	9.3	14.0	11.0	5.6	5.8	6.3
12	9.4	10.1	9.6	12.5	10.0	11.6	14.2	8.3	10.5
13	8.2	10.4	9.2	11.2	5.1	7.6	12.3	9.2	10.5
14	9.5	8.6	9.1	7.0	6.0	7.0	6.7	6.1	7.3
15	11.3	11.2	11.2	8.8	7.8	9.0	4.2	14.8	7.2
16	10.0	10.3	10.2	8.8	13.2	11.1	8.0	4.6	6.4
17	11.2	7.3	9.2	6.8	6.0	6.7	10.4	8.0	9.4
18	10.8	9.3	9.9	8.1	11.0	9.4	9.0	12.6	10.3
19	8.7	9.8	9.3	11.0	12.0	11.6	9.4	8.1	9.3
20	8.3	7.7	8.3	4.1	11.2	6.7	12.4	12.0	12.2

TABLE 4.4

PERMEABILITIES CALCULATED FROM SIMULATED  
PRESSURE DATA,  $V_{DP} = 0.50$

Run	$\lambda_D = 1/15$			$\lambda_D = 6/15$			$\lambda_D = 16/15$		
	$k_{inj}$	$k_{prd}$	$k_{ss}$	$k_{inj}$	$k_{prd}$	$k_{ss}$	$k_{inj}$	$k_{prd}$	$k_{ss}$
1	7.5	9.8	8.9	2.8	11.2	5.1	16.5	4.6	7.6
2	7.5	8.7	8.5	13.0	11.8	13.5	7.4	15.5	10.5
3	10.1	8.7	9.3	14.1	6.4	9.9	17.8	3.1	6.8
4	9.8	11.1	11.0	7.7	9.5	9.4	12.3	4.5	6.9
5	9.5	7.1	8.2	5.3	9.7	7.7	14.2	6.3	9.5
6	8.5	6.2	7.9	16.7	4.2	7.9	8.7	4.2	5.9
7	10.2	7.6	9.1	12.5	4.3	7.7	4.1	17.3	8.2
8	7.2	10.2	8.9	12.8	8.6	11.4	13.0	6.4	9.1
9	6.3	9.3	7.7	8.4	12.8	10.9	2.6	17.2	5.5
10	7.8	10.2	9.2	3.8	13.6	6.6	10.4	7.7	9.2
11	8.8	9.1	8.9	13.9	8.8	11.7	17.2	5.2	5.4
12	7.2	11.1	8.6	12.9	11.5	11.8	13.8	14.2	14.0
13	10.0	6.2	8.4	14.0	6.4	9.1	8.0	13.3	10.2
14	11.8	8.2	9.3	13.1	12.5	11.3	5.1	16.0	8.2
15	10.0	7.8	8.7	12.2	8.2	10.8	14.5	5.2	7.9
16	9.6	10.1	9.6	12.7	14.7	13.7	13.9	12.9	13.4
17	10.1	7.1	8.9	4.8	4.9	5.3	10.0	10.9	10.6
18	8.6	6.4	8.1	15.6	8.6	11.2	3.6	4.7	4.4
19	8.9	5.8	7.4	14.7	12.6	13.0	16.5	8.8	11.6
20	8.9	9.4	9.3	5.3	17.0	9.4	12.7	9.1	10.7

TABLE 4.5

PERMEABILITIES CALCULATED FROM SIMULATED  
PRESSURE DATA,  $V_{DP} = 0.65$

Run	$\lambda_D = 1/15$			$\lambda_D = 6/15$			$\lambda_D = 16/15$		
	$k_{inj}$	$k_{prd}$	$k_{ss}$	$k_{inj}$	$k_{prd}$	$k_{ss}$	$k_{inj}$	$k_{prd}$	$k_{ss}$
1	3.4	10.0	5.9	12.7	2.0	4.2	10.0	17.5	12.6
2	8.4	6.1	8.0	16.6	5.2	8.8	3.3	3.7	4.2
3	5.1	5.4	6.2	7.4	8.1	8.9	2.1	15.8	3.9
4	11.8	6.0	8.4	6.9	11.9	8.1	16.1	1.6	3.6
5	6.4	9.8	8.1	4.3	11.2	7.5	18.1	9.4	12.6
6	8.4	8.8	9.5	7.0	12.9	9.6	10.9	15.1	13.1
7	6.5	8.3	7.5	13.9	5.8	9.7	9.7	20.1	13.2
8	10.9	9.2	9.6	1.7	7.4	3.7	21.2	5.3	10.1
9	9.5	10.2	9.9	9.4	15.0	12.6	3.4	16.6	6.2
10	8.7	11.8	10.2	2.7	3.9	3.8	2.2	19.0	4.8
11	10.5	8.0	9.8	2.6	7.1	4.5	19.2	9.8	14.0
12	8.1	11.0	9.8	5.7	11.5	7.7	6.5	12.5	9.2
13	8.2	10.5	10.2	8.1	12.7	10.8	21.0	4.7	8.3
14	6.2	7.5	7.0	18.7	9.2	13.8	11.2	10.5	11.0
15	7.9	5.0	7.0	16.0	11.8	13.4	7.2	12.1	10.3
16	6.8	4.6	6.5	11.4	8.6	9.8	2.2	24.0	5.3
17	7.2	5.8	6.7	4.1	4.3	4.7	19.0	15.9	17.1
18	6.6	8.9	8.3	12.0	10.2	11.9	15.2	16.8	16.5
19	6.1	9.0	7.5	3.4	8.2	5.1	1.0	12.2	2.3
20	10.0	5.1	7.2	4.4	12.7	7.4	1.2	17.0	2.8

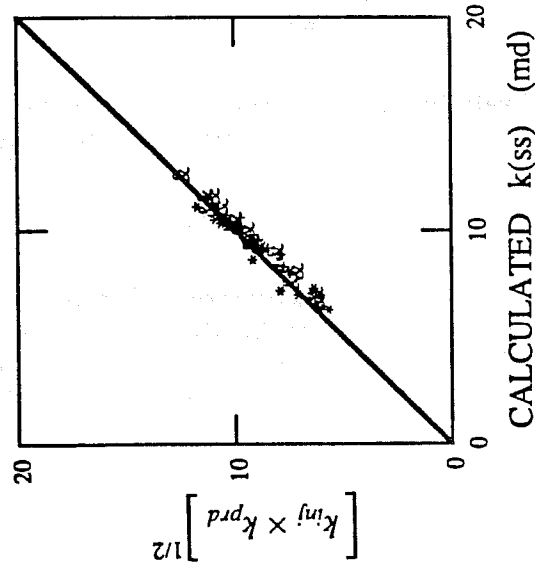


Fig. 4.17 Comparison between calculated and estimated  $k_{ss}$ ,  $V_{DP} = 0.35$ .

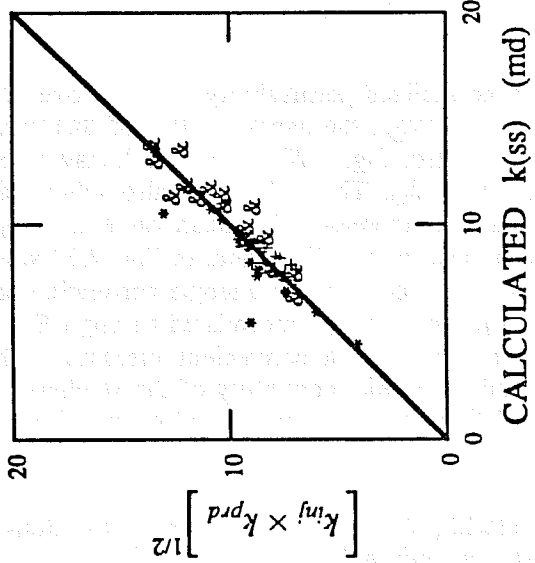


Fig. 4.18 Comparison between calculated and estimated  $k_{ss}$ ,  $V_{DP} = 0.50$ .

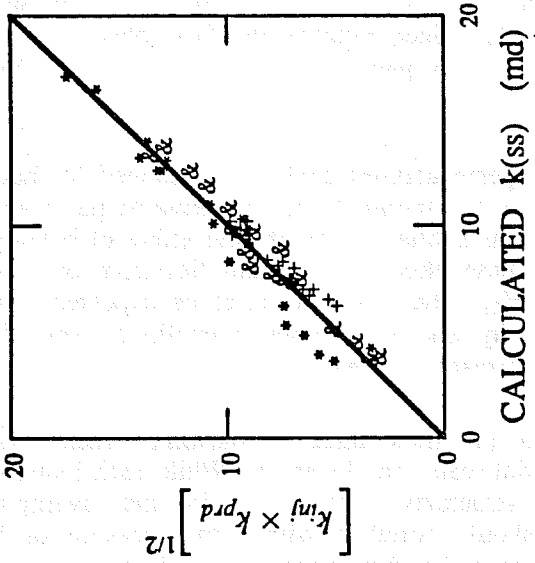


Fig. 4.19 Comparison between calculated and estimated  $k_{ss}$ ,  $V_{DP} = 0.65$ .

— Line of perfect agreement  
 ++  $\lambda_D = 1/15$   
 &&  $\lambda_D = 6/15$   
 \*\*  $\lambda_D = 16/15$

However, only a few high permeability blocks along the main diagonal of flow can increase  $k_{ss}$ , while more low permeability blocks are needed in the transverse direction to divert flow significantly and thus reduce  $k_{ss}$ . Such behavior has been observed in the simulations reported here,  $k_{ss}$  being higher than both well permeabilities on 17 cases, and lower than both on only 2 cases (see Tables 4.3-4.5).

The fact that effective permeabilities could be calculated for heterogeneous permeability fields suggests that the pressure response is not sensitive to permeability variations. In other words, the pressure test acts as a filter to smooth the effect of heterogeneous elements in the system. The variability of these effective permeabilities from one simulation run to another was seen to increase with  $V_{DP}$  and  $\lambda_D$ . This is to be expected, because greater  $V_{DP}$  and  $\lambda_D$  imply greater heterogeneity, and hence more variability between the response produced by different realizations of the permeability field.

Thus each simulation produces three permeability measurements, which represent averaging over different spatial scales and locations. While each individual measurement cannot distinguish heterogeneous structures present within the averaging area/volume, some combination of the three should correlate with some measure of heterogeneity. For this purpose, a dimensionless permeability difference is defined as:

$$\Delta k_D = \frac{|k_{inj} - k_{prd}|}{k_{ss}} \quad (4.3.11)$$

which can be interpreted as a normalized permeability variance over the scale of the problem. For each combination of  $V_{DP}$  and  $\lambda_D$ , the average value of this parameter as obtained from all 20 simulation runs was calculated. Fig. 4.20 shows the behavior of the averaged value of  $\Delta k_D$  as a function of  $V_{DP}$  and  $\lambda_D$ . These data are also tabulated in Table 4.6. As the dimensionless correlation length  $\lambda_D$  increases, the mean value of  $\Delta k_D$  also increases, and the increase is larger when  $V_{DP}$  is also large. The trend in Fig. 4.20 suggests that some suitable combination of  $V_{DP}$  and  $\lambda_D$  might prove to be a single correlating parameter. One possible grouping is  $\sigma_{ln(k)}^2 \lambda_D$ , since  $V_{DP}$  and  $\sigma_{ln(k)}^2$  are related through Eq. (4.2.5). This parameter group, termed the *heterogeneity index*, is a convenient measure of heterogeneity because it captures both the variability and the spatial continuity of the stochastic permeability field. The choice of  $\sigma_{ln(k)}^2 \lambda_D$  as a correlating parameter was based on two lines of reasoning, which are described next.

As shown by Taylor (1920), the variance of spatial locations of a swarm of tracer particles moving in a stochastic velocity field is:

$$\sigma_x^2 = \frac{2\sigma_v^2}{\bar{v}^2} \int_0^{\bar{x}} \int_0^x \rho(h) dh dx \quad (4.3.12)$$

where  $\sigma_v^2$  is the variance of velocity,  $\bar{v}$  is the mean velocity,  $\bar{x}$  the mean distance of travel, and  $\rho(h)$  the autocorrelation function, which is related to the semi-variogram by the following expression:

$$\gamma(h) = \sigma^2 \left[ 1 - \rho(h) \right] \quad (4.3.13)$$

Dispersivity,  $\alpha = \sigma_x^2 / 2\bar{x}$ , can be used as another measure of spreading instead of the variance, and can be computed from Eq. (4.3.12) if the form of the autocorrelation function (or the semi-variogram) is known. For semi-variogram models with a finite sill (Table 4.1), characterized by the correlation length scale,  $\lambda$ , and for the case when the mean distance of

TABLE 4.6

STATISTICS OF DIMENSIONLESS PERMEABILITY DIFFERENCE  $\Delta k_D$

$V_{DP}$	$\lambda_D$	$\sigma_{ln(k)}^2 \lambda_D$	$\langle \Delta k_D \rangle$	$\sigma_{\Delta k_D}$	95% Confidence Interval
0.35	1/15	0.0124	0.154	0.149	$\pm 0.065$
0.35	6/15	0.0740	0.276	0.280	$\pm 0.123$
0.35	16/15	0.1984	0.433	0.391	$\pm 0.171$
0.50	1/15	0.0320	0.268	0.139	$\pm 0.061$
0.50	6/15	0.1920	0.607	0.540	$\pm 0.237$
0.50	16/15	0.5120	0.954	0.740	$\pm 0.324$
0.65	1/15	0.0735	0.336	0.246	$\pm 0.108$
0.65	6/15	0.441	0.726	0.494	$\pm 0.217$
0.54	16/15	1.176	1.813	1.774	$\pm 0.777$

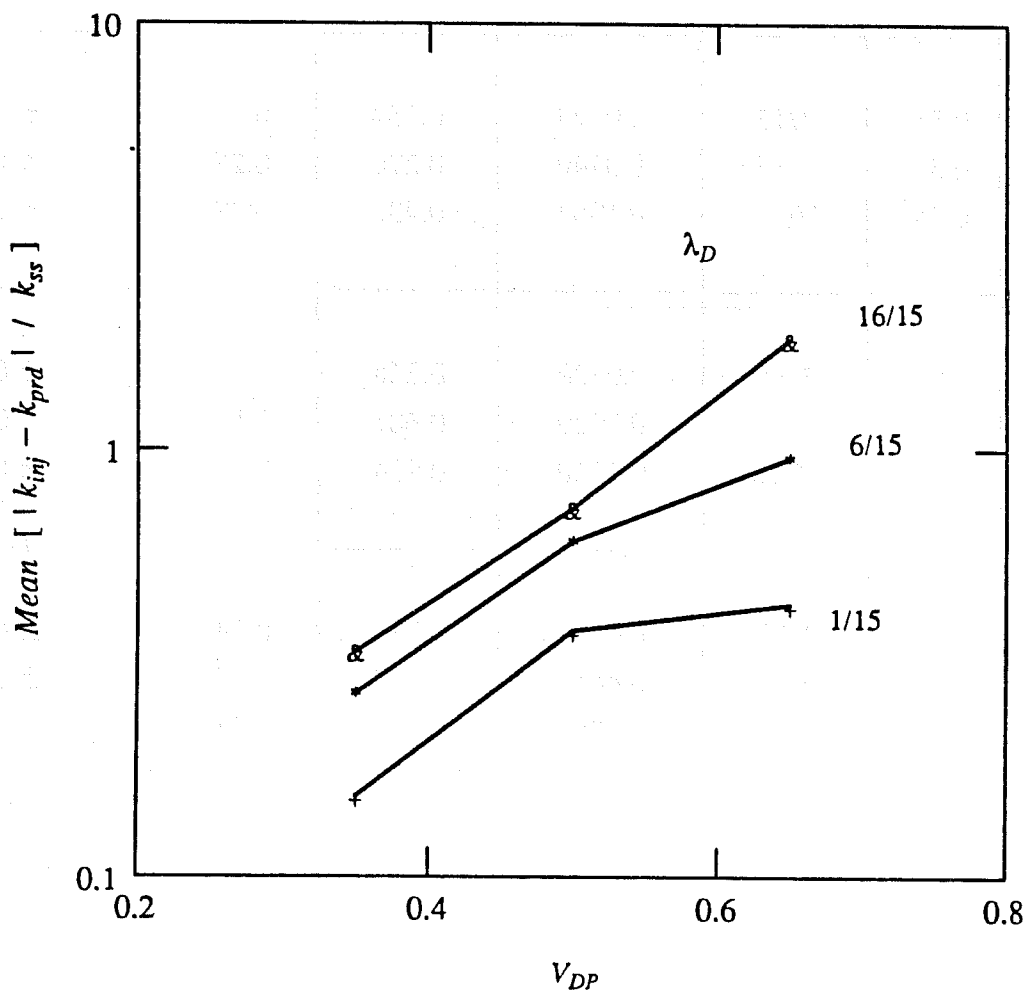


Fig. 4.20 Dimensionless permeability difference  $\Delta k_D$  as a function of  $V_{DP}$  and  $\lambda_D$ .

travel,  $\bar{x}$ , is much greater than  $\lambda$ , it can be shown that:

$$\alpha = \frac{\sigma_v^2}{\bar{v}^2} \lambda \quad (4.3.14)$$

For one-dimensional flow in heterogeneous media, where variations in permeability are directly responsible for velocity fluctuations of the tracer particles, it is reasonable to assume that  $\sigma_v / \bar{v} \approx \sigma_k / \bar{k} \approx \sigma_{ln(k)}$ . A normalized dispersivity, scaled with the characteristic length,  $L$ , is then obtained as:

$$\frac{\alpha}{L} = \sigma_{ln(k)}^2 \frac{\lambda}{L} = \sigma_{ln(k)}^2 \lambda_D \quad (4.3.15)$$

Thus, a relationship between dispersivity due to convective effects and the parameter group  $\sigma_{ln(k)}^2 \lambda_D$  can be derived. Gelhar and Axness (1983) have developed a similar relationship for multi-dimensional transport using spectral analysis. Since a major objective of this work is to compare pressure and tracer responses, it is useful to establish the way in which permeability variability (as obtained from pressure test analysis) can be linked to this group.

The second argument, which is more heuristic in nature, is as follows. The dimensionless parameter  $\Delta k_D$ , which is a measure of the difference in mean effective permeability at the two wells, quantifies the significance of the trend in the permeability distribution over the scale of the problem. When trends are significant, i.e.  $\lambda_D$  is of the order of unity, the probability of clustering of like-permeability blocks is high. Thus, if the average permeability around the injection well is higher than the median, the average permeability around the production well would be lower than the median. The difference between these two values would then be proportional to  $\sigma_k$ . Since the steady-state interwell permeability is related to  $\bar{k}$ , this implies that  $\Delta k_D \approx \sigma_k / \bar{k} \approx \sigma_{ln(k)}$ . It follows that the group  $\sigma_{ln(k)}^2 \lambda_D$  is a suitable correlating parameter, at least over some range of  $\Delta k_D$ . Fig. 4.21 is a graph of the expected value of  $\Delta k_D$  against  $\sigma_{ln(k)}^2 \lambda_D$  on log-log coordinates. Also shown are 95% confidence intervals around the data points. A least-squares fit of this data set yields the following power law relationship:

$$\Delta k_D = 1.3 \left[ \sigma_{ln(k)}^2 \lambda_D \right]^{1/2} \quad (4.3.16)$$

This simple relation provides a way of quantifying in-situ permeability variation from pressure transient data alone.

#### 4.4. TRACER TEST RESPONSE

As indicated in the review of literature in Section 2.2.2, the convection-diffusion equation may be an inappropriate model for field-scale tracer dispersion in spatially correlated permeability fields. Therefore, it is necessary to investigate whether the solutions of Abbazadeh-Dehghani and Brigham (1982), derived for homogeneous systems, can be used to analyze tracer breakthrough curves for heterogeneous media and yield effective dispersivities. Associated objectives are to examine the range and conditions over which the convection-diffusion equation is valid, and to relate field-scale dispersivity to some measure of permeability variation.

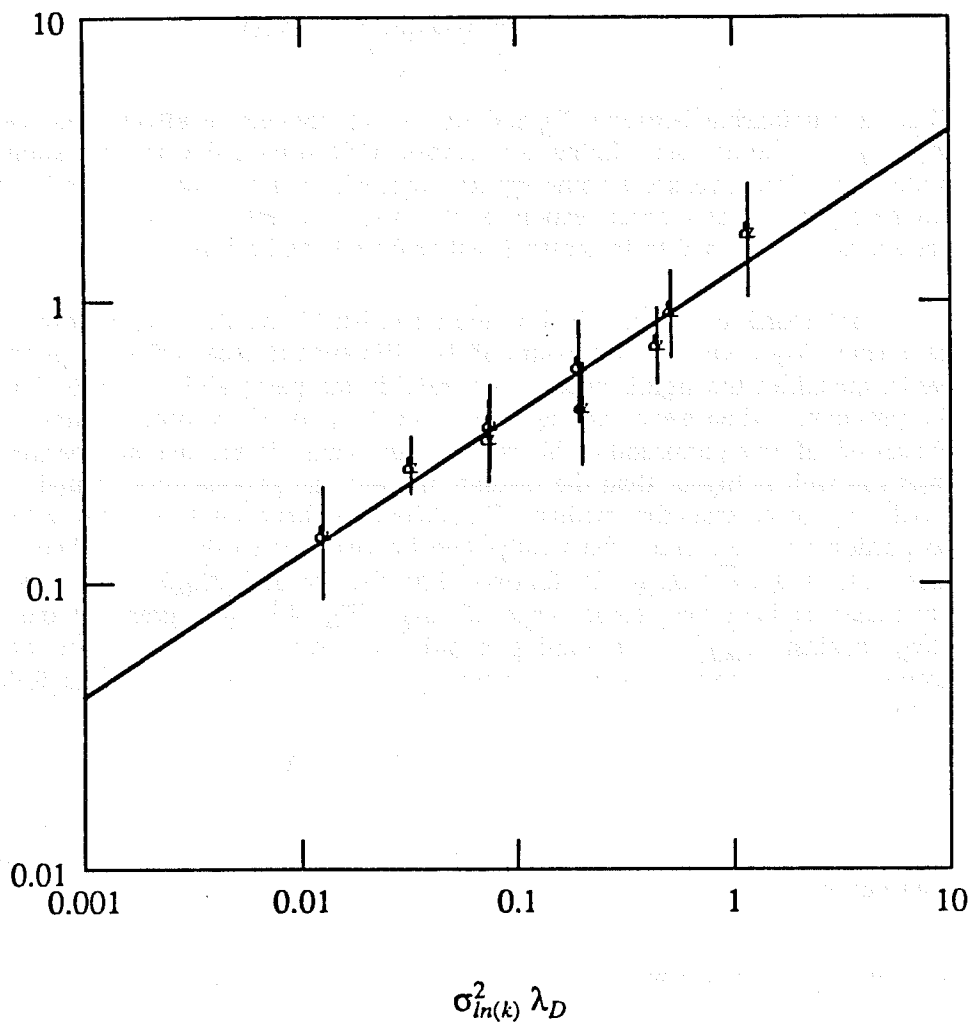


Fig. 4.21 Relationship between  $\Delta k_D$  and heterogeneity index  $\sigma_{ln(k)}^2 \lambda_D$ .

#### 4.4.1. Simulation of Tracer Flow

The numerical tool used in modeling tracer flow under steady-state unit mobility ratio miscible displacement conditions was the USGS Solute Transport simulator (Konikow and Bredehoeft, 1978), which is based on a method of characteristics scheme first proposed by Garder *et al.* (1964) to simulate miscible displacement processes. Details of the model and the computer code can be found in the USGS report by Konikow and Bredehoeft. A brief review is given in the following. The nomenclature of Konikow and Bredehoeft is modified slightly to conform to that of this dissertation.

The basic assumptions in the development of the simulator equations are :

- (a) Unit-mobility ratio miscible displacement;
- (b) Constant porosity;
- (c) No chemical reactions;
- (d) Negligible molecular diffusion; and
- (e) Density, viscosity and temperature gradients do not affect velocity distribution.

For two-dimensional transport, the convection-diffusion equation is:

$$\begin{aligned} \frac{\partial C}{\partial t} = & \frac{\partial}{\partial x} \left[ D_{xx} \frac{\partial C}{\partial x} \right] + \frac{\partial}{\partial y} \left[ D_{yy} \frac{\partial C}{\partial y} \right] + \frac{\partial}{\partial x} \left[ D_{xy} \frac{\partial C}{\partial y} \right] \\ & + \frac{\partial}{\partial y} \left[ D_{yx} \frac{\partial C}{\partial x} \right] - \frac{\partial}{\partial x} [CV_x] - \frac{\partial}{\partial y} [CV_y] - \frac{C'q}{\phi h} \end{aligned} \quad (4.4.1)$$

where  $D_{ij}$  are the components of the hydrodynamic dispersion tensor,  $C'$  is the solute concentration of the source/sink fluid, and  $q$  the rate of injection and/or withdrawal expressed as volume flux per unit area. For steady-state conditions, the equation of continuity gives:

$$\frac{\partial V_x}{\partial x} + \frac{\partial V_y}{\partial y} = - \frac{q}{\phi} \quad (4.4.2a)$$

where  $V_x$  and  $V_y$  are the interstitial velocities:

$$V_x = - \frac{k_x}{\phi\mu} \frac{\partial p}{\partial x} \quad ; \quad V_y = - \frac{k_y}{\phi\mu} \frac{\partial p}{\partial y} \quad (4.4.2b)$$

Substitution of Eq. (4.4.2a) in (4.4.1) results in:

$$\begin{aligned} \frac{\partial C}{\partial t} = & \frac{\partial}{\partial x} \left[ D_{xx} \frac{\partial C}{\partial x} \right] + \frac{\partial}{\partial y} \left[ D_{yy} \frac{\partial C}{\partial y} \right] + \frac{\partial}{\partial x} \left[ D_{xy} \frac{\partial C}{\partial y} \right] \\ & + \frac{\partial}{\partial y} \left[ D_{yx} \frac{\partial C}{\partial x} \right] - V_x \frac{\partial C}{\partial x} - V_y \frac{\partial C}{\partial y} + \frac{q [C - C']}{\phi h} \end{aligned} \quad (4.4.3)$$

At this point, it is useful to introduce the concept of material derivative:

$$\frac{dC}{dt} = \frac{\partial C}{\partial t} + \frac{\partial C}{\partial x} \frac{dx}{dt} + \frac{\partial C}{\partial y} \frac{dy}{dt} \quad (4.4.4)$$

which is the rate of change of concentration observed when moving with the fluid particle. The more common derivative,  $\partial C/\partial t$ , is the rate of change of concentration observed from a fixed point. Now:

$$\frac{dx}{dt} = V_x \quad (4.4.5a)$$

$$\frac{dy}{dt} = V_y \quad (4.4.5b)$$

Thus, combining Eqs. (4.4.3) through (4.4.5) yields:

$$\begin{aligned} \frac{dC}{dt} = \frac{\partial}{\partial x} \left[ D_{xx} \frac{\partial C}{\partial x} \right] + \frac{\partial}{\partial y} \left[ D_{yy} \frac{\partial C}{\partial y} \right] + \frac{\partial}{\partial x} \left[ D_{xy} \frac{\partial C}{\partial y} \right] \\ + \frac{\partial}{\partial y} \left[ D_{yx} \frac{\partial C}{\partial x} \right] + \frac{q [ C - C' ]}{\phi h} \end{aligned} \quad (4.4.6)$$

The solutions of Eqs. (4.4.5) and (4.4.6) can be given as:

$$x = x(t) \quad ; \quad y = y(t) \quad ; \quad C = C(t) \quad (4.4.7)$$

and are called the characteristic curves of Eq. (4.4.3), the solutions to which may be obtained by following the characteristic curves. In other words, the solution is represented as the trajectory in the composition space, and is obtained numerically by introducing a set of reference particles that can be traced within the stationary coordinates of the finite-difference grid. Each point has a concentration and position associated with it, and is moved through the flow field in proportion to the flow velocity at its location.

The first step in this particle-tracking procedure (which simulates convective transport) is placing points uniformly over the entire grid. The model allows either 4, 9 or 16 points to be specified. A few trial simulations were run with 16 points per grid, but the increased resolution in tracking the concentration front was offset by the significant increase in computation time. Hence, all simulations performed in this study used 9 points per grid. After the particles have been placed, the position of each particle is specified by its x- and y-coordinates. The initial concentration assigned to each point is the initial concentration of the grid containing the point. During a time step, the displacement of each particle is computed as follows:

$$x_{p,n} = x_{p,n-1} + \Delta t V_x [ x_{p,n}, y_{p,n} ] \quad (4.4.9)$$

$$y_{p,n} = y_{p,n-1} + \Delta t V_y [ x_{p,n}, y_{p,n} ] \quad (4.4.10)$$

Here  $p$  refers to the index number for particle identification, and  $n$  the current time step. The x- and y-velocities at the position of any point  $p$  are calculated using bilinear interpolation over the area of half a grid using the velocities at adjacent grids and block boundaries. After all the points have been moved, the concentration at each node is temporarily assigned the average of the concentrations of all points located within the grid-block. This is denoted by  $C_{i,j,n^*}$ , where  $n^*$  is the new time level only with respect to convective transport.

Changes in concentration due to hydrodynamic dispersion and fluid sources/sinks are calculated using a finite-difference approximation to Eq. (4.4.6), which is given by:

$$\Delta t \left[ \frac{\partial}{\partial x} \left\{ D_{xx} \frac{\partial C}{\partial x} + D_{xy} \frac{\partial C}{\partial y} \right\} + \frac{\partial}{\partial y} \left\{ D_{yy} \frac{\partial C}{\partial y} + D_{yx} \frac{\partial C}{\partial x} \right\} \right] + \frac{\Delta t q [C - C']}{\phi h} = \Delta C_{ij,n} \quad (4.4.11)$$

This equation can also be written in the form:

$$\Delta C_{ij,n} = \left[ \Delta C_{ij,n} \right]_I + \left[ \Delta C_{ij,n} \right]_{II} \quad (4.4.12)$$

where the first term on the right-hand side (also the first term on the left-hand side of Eq. 4.4.11) refers to concentration changes due to hydrodynamic dispersion, and the second term to concentration changes caused by mixing at sources and sinks.

The major interest in this segment of the research is the evaluation of tracer dispersion (i.e. spreading of the tracer slug) due to convective effects in a heterogeneous flow field, and hence hydrodynamic dispersion will be neglected in the simulations. The method of handling changes in concentration due to hydrodynamic dispersion is derived in detail by Konikow and Bredehoeft (their Eqs. 29-38), and will not be presented here. Briefly, an explicit finite-difference approximation is used in which all concentrations and their gradients are evaluated at the old time level.

For practical purposes, only the change in concentration due to fluid sources/sinks (in addition to that already attributed to convective transport) must be evaluated. This term is calculated using an explicit finite-difference approximation and is given by:

$$\left[ \Delta C_{ij,n} \right]_{II} = \frac{\Delta t}{\phi h} q_{ij,n} \left\{ C_{ij,n-1} - C'_{ij,n} \right\} \quad (4.4.13)$$

Even though this procedure defines a method for solving the characteristic equations, there is a problem of consistency. Proper representation of solute transport requires that Eqs. (4.4.5) and (4.4.6) be solved simultaneously. However, Eq. (4.4.5) is solved by particle movement using implicitly computed velocities, while Eq. (4.4.6) is solved explicitly with respect to concentrations, i.e. nodal concentrations and concentration gradients are evaluated at the old time level. The remedy is to use a two-step explicit procedure, where Eq. (4.4.11) is solved at each node by giving equal weight to concentration gradients computed from time level  $(n-1)$ , and those computed from time level  $n^*$ , where  $n^*$  is the new time level with respect to convective transport. This procedure can be expressed as:

$$\left[ \Delta C_{ij,n} \right]_{II} = \frac{\Delta t}{\phi h} q_{ij,n} \left[ \frac{\left\{ C_{ij,n-1} - C'_{ij,n} \right\}}{2} + \frac{\left\{ C_{ij,n^*} - C'_{ij,n} \right\}}{2} \right] \quad (4.4.14)$$

By ignoring concentration changes due to hydrodynamic dispersion, the new nodal concentrations at the end of time level  $n$  can be computed as:

$$C_{ij,n} = C_{ij,n^*} + \left[ \Delta C_{ij,n} \right]_{II} \quad (4.4.15)$$

A flow chart for the USGS simulator is given in Fig. 4.22. Other details of the computer model, such as stability criteria of the explicit finite-difference formulation, treatment of boundary conditions, handling of sources and sinks, have been discussed in detail by Konikow and Bredehoeft and will not be repeated here.

The computer program was verified by matching simulated tracer breakthrough curves for homogeneous systems with the analytical solutions of Abbaszadeh-Dehghani and Brigham. Two test cases were simulated, a continuous injection case with purely convective flow ( $\alpha = 0 \text{ ft}$ ), and a slug-injection case with convective-dispersive flow ( $\alpha = 10 \text{ ft}$ ). Comparisons between analytical and numerical model results are graphically shown in Fig. 4.23. These results indicate that use of the method of characteristics effectively eliminates the problem of numerical dispersion, which is a major drawback of conventional finite difference or finite element modeling of the convection-diffusion equation. The fluctuations in tracer concentration as seen in Fig. 4.23 simply reflect the fact that the number of tracer particles used in the simulations is finite.

#### 4.4.2. Interpretation Methodology

The basis for interpreting simulated tracer test data in heterogeneous media is the analytical solution of Abbaszadeh-Dehghani and Brigham, which has been discussed in detail in Section 3.4. When possible, the objective is to use this solution to calculate effective dispersivities by a least-squares minimization procedure. The function to be minimized is the residual sum of squares,  $SSQ$ , defined by:

$$SSQ = \sum_{i=1}^{NPT} \left\{ C_{obs,i} - C_{calc,i} \right\}^2 \quad (4.4.16)$$

where  $NPT$  is the number of data points to be fitted,  $C_{obs}$  the observed concentration, and  $C_{calc}$  the calculated concentration, which is a function of : (a) volume injected,  $V$ , and (b) dispersivity,  $\alpha$ . Minimization is achieved by a modified Levenberg-Marquardt algorithm, as implemented in the IMSL subroutine ZXSSQ. A description of this algorithm (and several others for nonlinear parameter estimation) can be found in Beck and Arnold (1977), and will not be presented here.

Tracer flow simulations were carried out in three stages. First, injection and production was initiated under balanced conditions till 0.25 years, at which time steady-state had been attained. Then a tracer slug of 0.1 pore volumes (7758 bbl) was injected over a period of 0.2 years. Finally, the tracer slug was displaced for 3.8 years (1.9 pore volumes or 147400 bbl). The output was reduced to a data set of 200 points using cubic splines with information on volume injected (bbl) and the corresponding effluent concentration (ppm). In each of these simulations, the dispersivity was set to zero, so that dispersion (spreading) only due to convective effects could be analyzed.

#### 4.4.3. Analysis of Tracer Test Data

Tracer responses were generated for each of the 20 simulated permeability fields corresponding to each set of  $V_{DP}$  and  $\lambda_D$ , of which only a few are presented here. Figures 4.24 through 4.32 show tracer breakthrough curves for the same physical systems whose pressure responses were graphed in Figs. 4.8-4.16. In these figures, simulated tracer test data are shown as solid lines, while the model fits are indicated as dashed lines. The basis for the interpretation models, and the fitting procedure, are described in a later section. As expected,

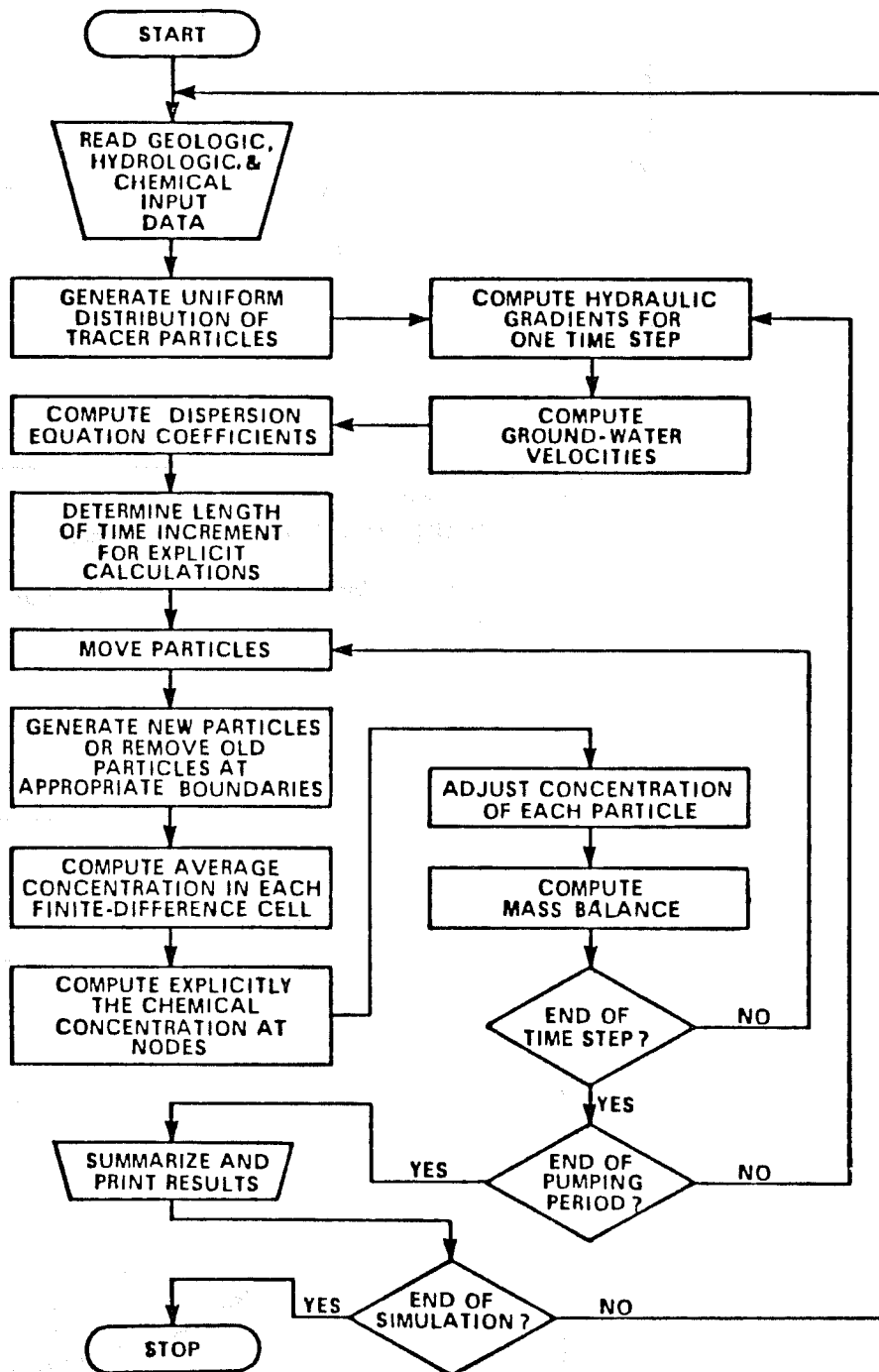
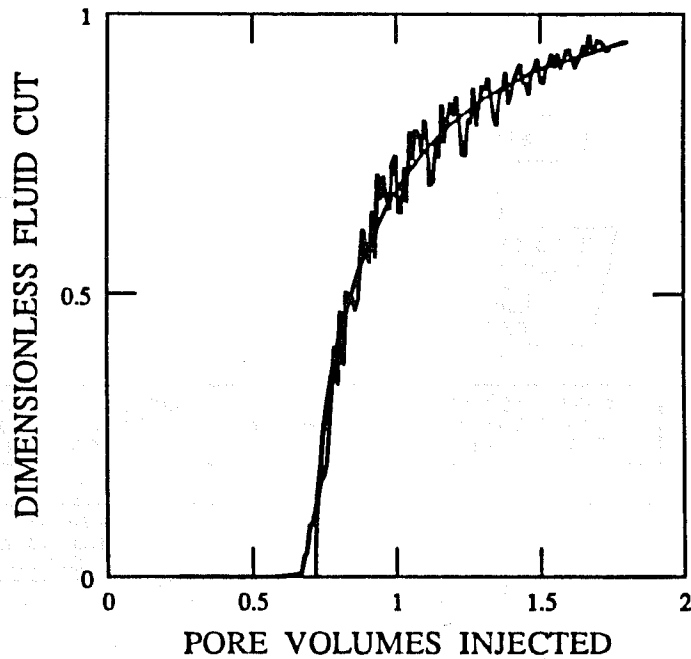
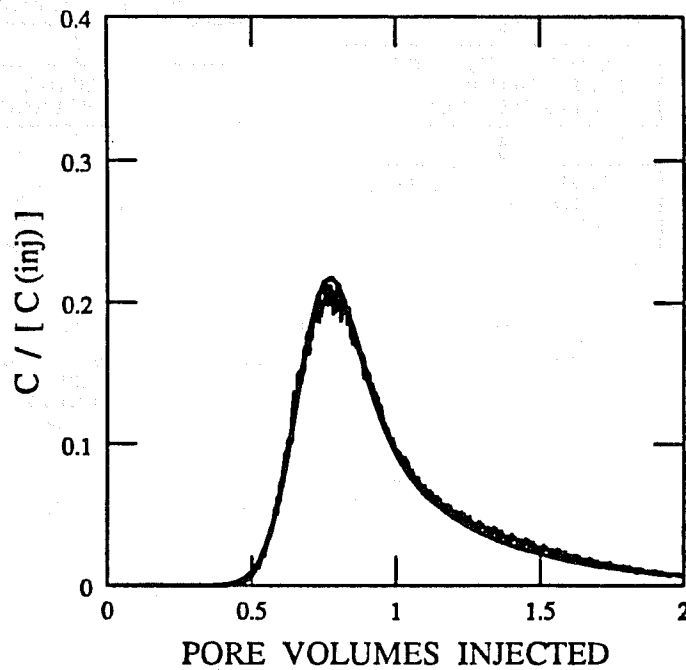


Fig. 4.22 Flow chart of USGS solute transport simulator.

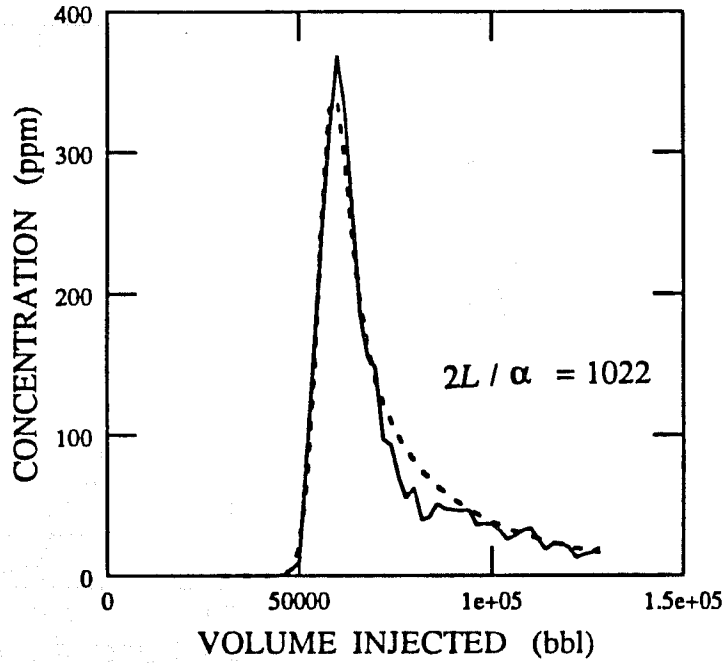


4.23 (a) Continuous injection,  $\alpha = 0$  ft.

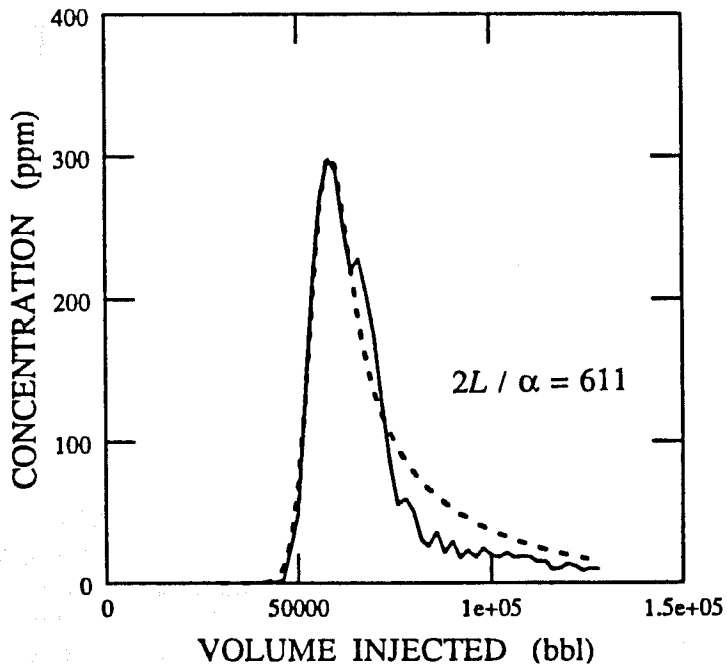


4.23 (b) Slug injection,  $\alpha = 20$  ft.

Fig. 4.23 Tracer flow simulator verification.

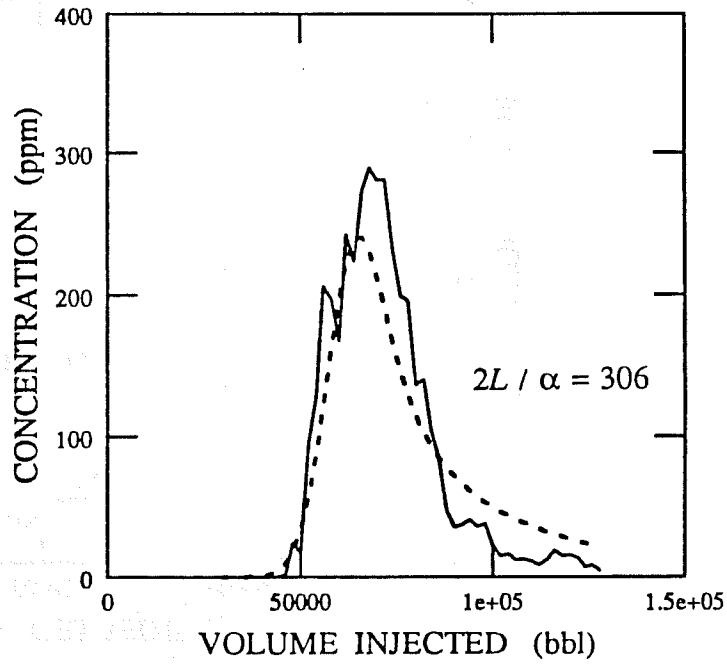


4.24 (a) Run 2

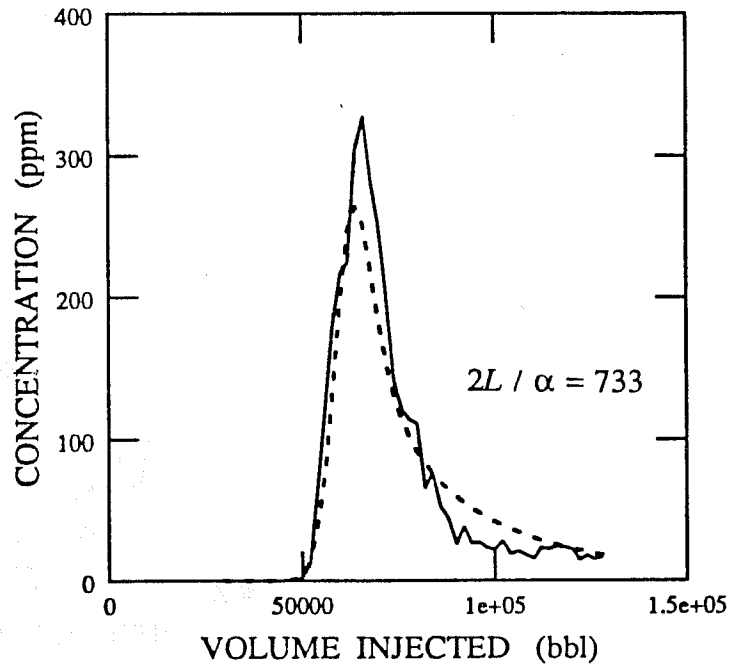


4.24 (b) Run 9

Fig. 4.24 Tracer breakthrough curve,  $V_{DP} = 0.35$ ,  $\lambda_D = 1/15$ .

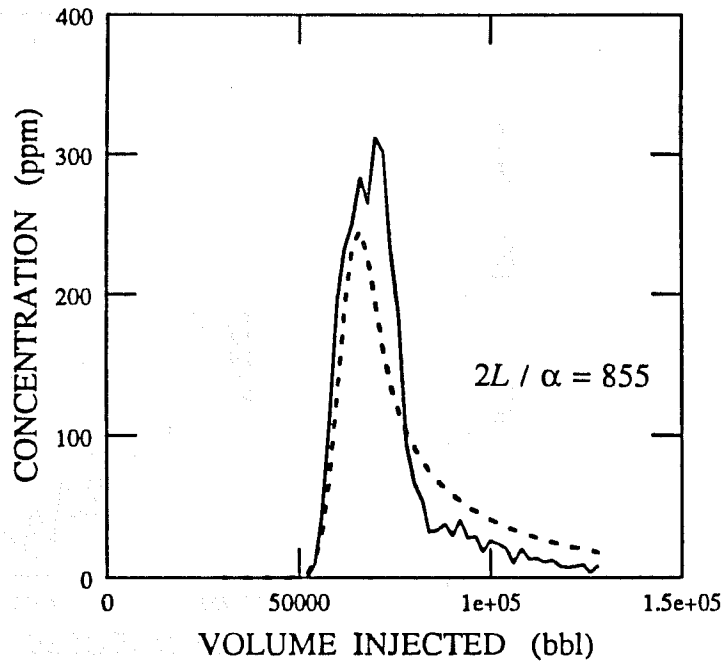


4.25 (a) Run 1

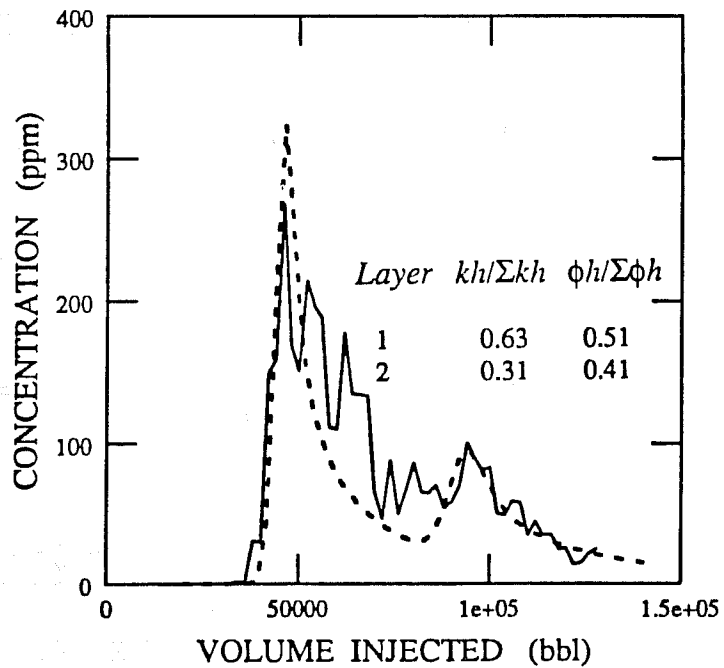


4.25 (b) Run 5

Fig. 4.25 Tracer breakthrough curve,  $V_{DP} = 0.35$ ,  $\lambda_D = 6/15$ .

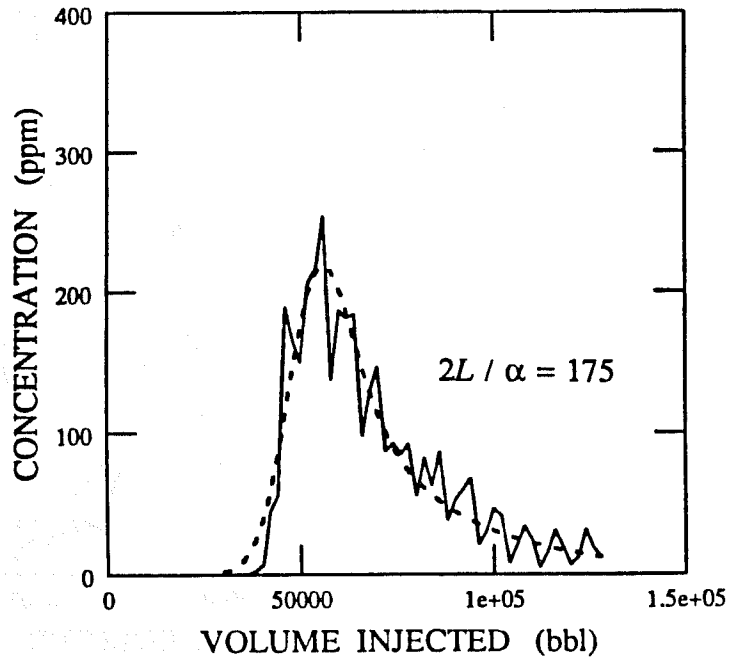


4.26 (a) Run 3

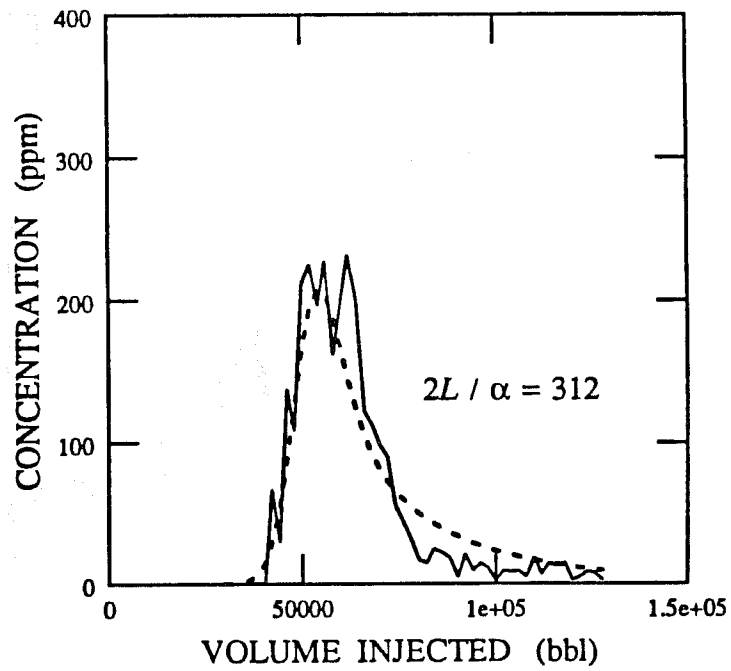


4.26 (b) Run 7

Fig. 4.26 Tracer breakthrough curve,  $V_{DP} = 0.35$ ,  $\lambda_D = 16/15$ .

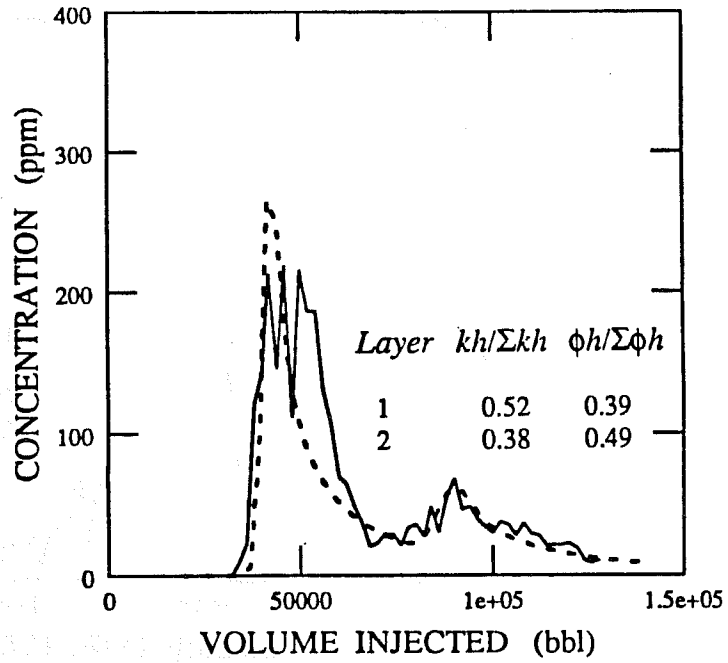


4.27 (a) Run 4

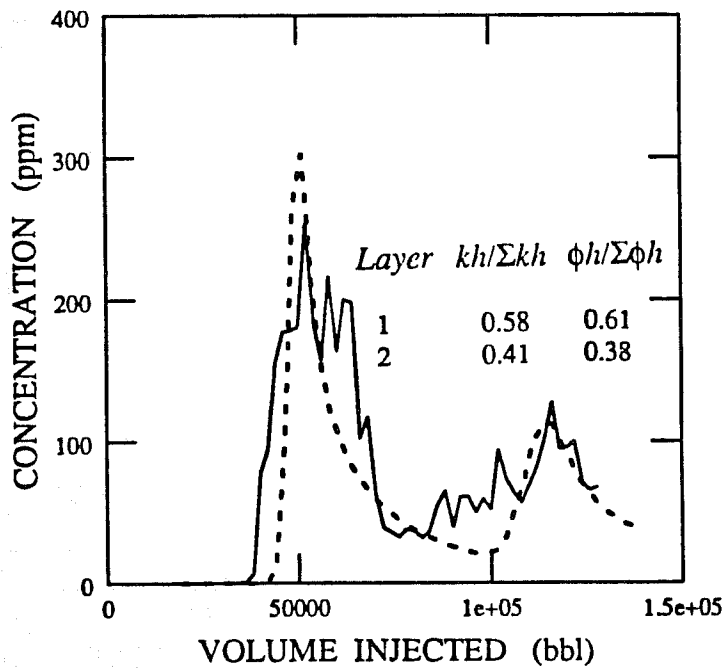


4.27 (b) Run 7

Fig. 4.27 Tracer breakthrough curve,  $V_{DP} = 0.50$ ,  $\lambda_D = 1/15$ .

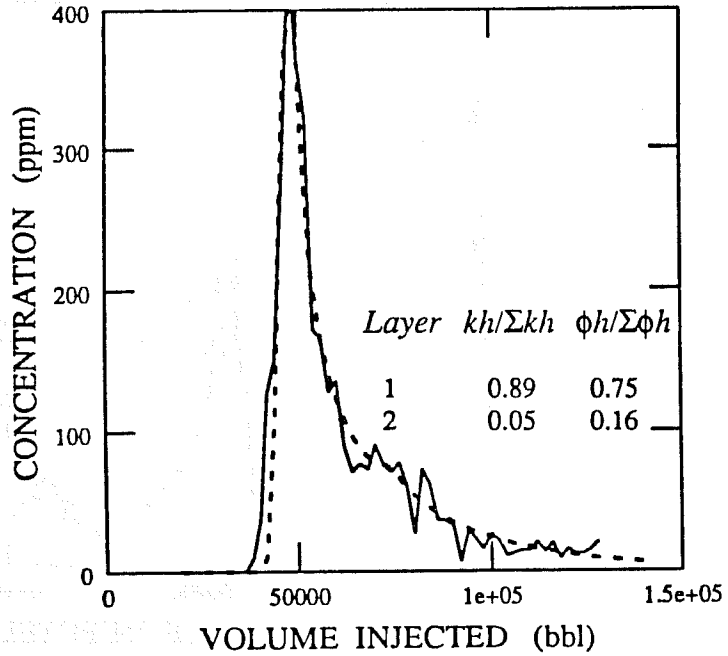


4.28 (a) Run 2

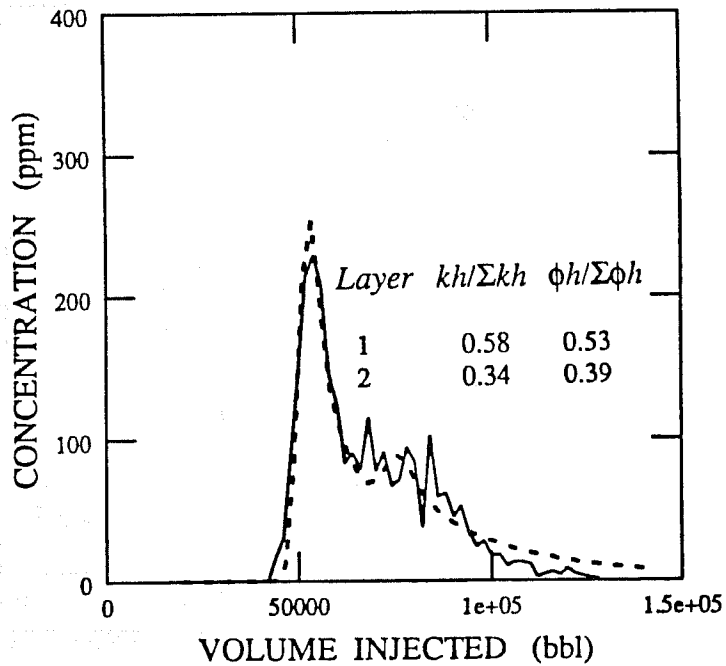


4.28 (b) Run 4

Fig. 4.28 Tracer breakthrough curve,  $V_{DP} = 0.50$ ,  $\lambda_D = 6/15$ .

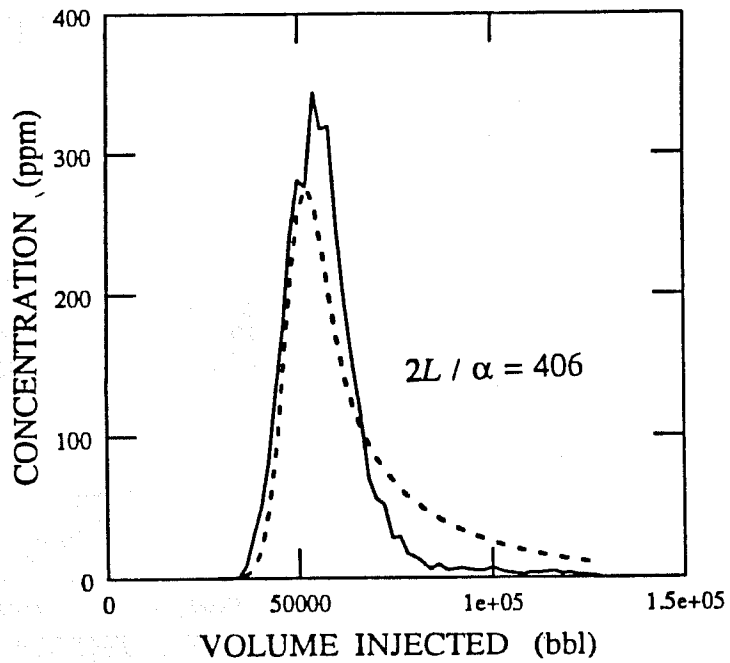


4.29 (a) Run 1

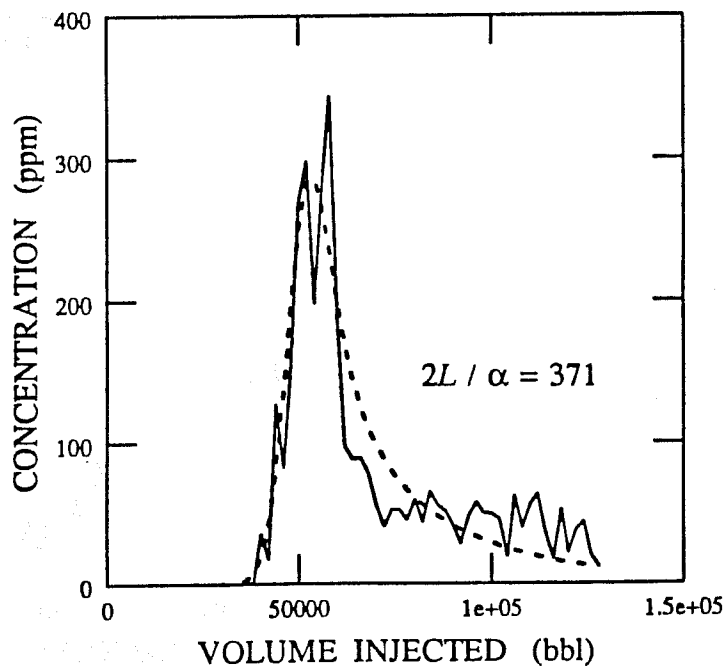


4.29 (b) Run 8

Fig. 4.29 Tracer breakthrough curve,  $V_{DP} = 0.50$ ,  $\lambda_D = 16/15$ .

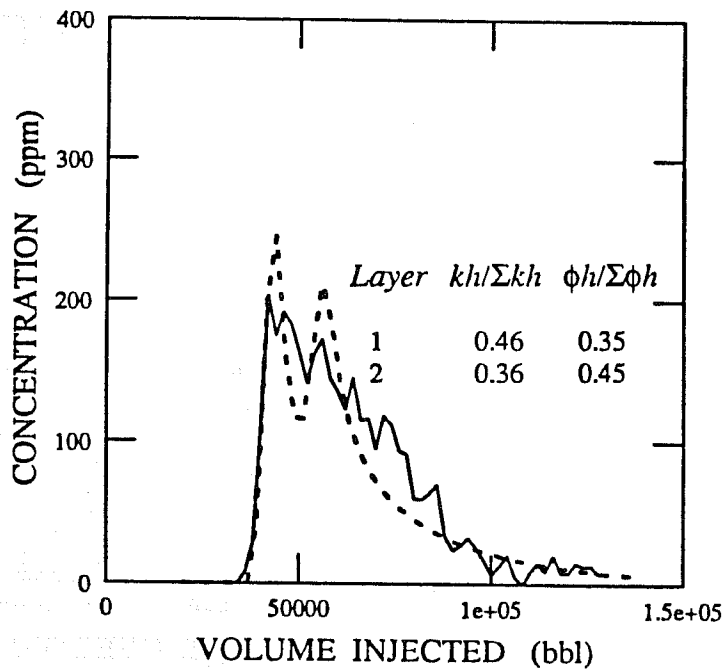


4.30 (a) Run 12

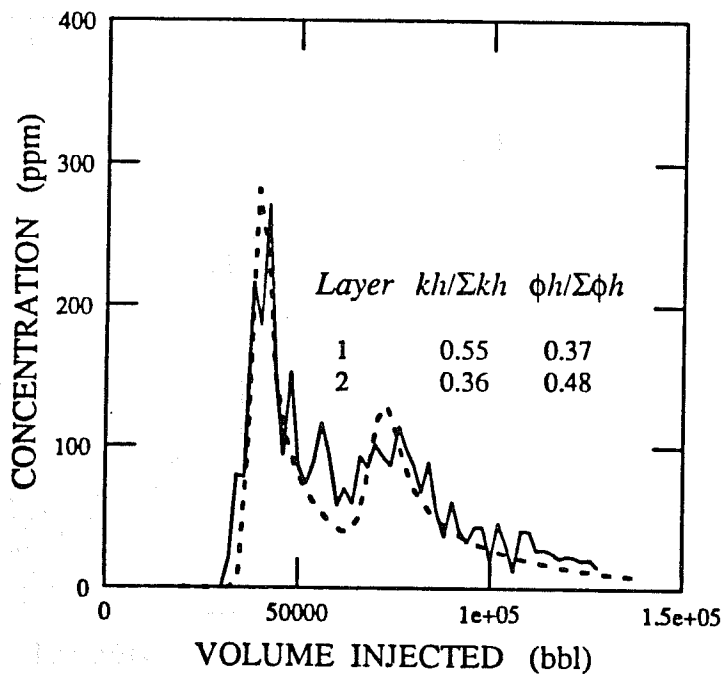


4.30 (b) Run 16

Fig. 4.30 Tracer breakthrough curve,  $V_{DP} = 0.65$ ,  $\lambda_D = 1/15$ .

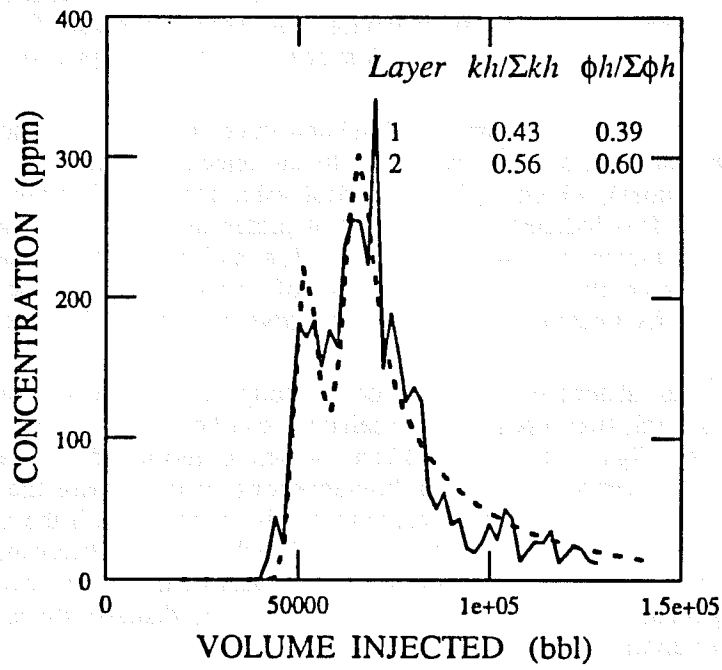


4.31 (a) Run 2

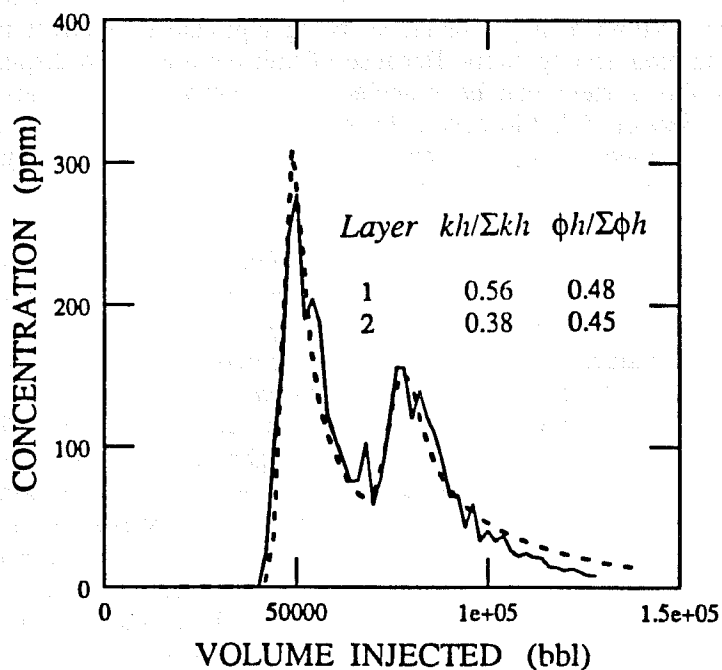


4.31 (b) Run 7

Fig. 4.31 Tracer breakthrough curve,  $V_{DP} = 0.65$ ,  $\lambda_D = 6/15$ .



4.32 (a) Run 1



4.32 (b) Run 8

Fig. 4.32 Tracer breakthrough curve,  $V_{DP} = 0.65$ ,  $\lambda_D = 16/15$ .

tracer concentration-time data show greater sensitivity to permeability variation than do transient pressure data. Similar behavior has been observed for layered reservoirs with noncommunicating strata in a repeated 5-spot pattern, as discussed in the previous section.

The first observation from the simulated tracer tests is that tracer breakthrough occurred much earlier than a time corresponding to an injected volume of approximately 56000 bbl (0.72 pore volumes), which is the theoretical value for breakthrough in a homogeneous 5-spot (Craig, 1971). This indicates the presence of preferential flow paths and/or fluid mixing. Since the simulation model considered no dispersion and numerical dispersion effects have been minimized through the use of the method of characteristics, these effects must have been caused by velocity fluctuations in a spatially varying permeability field.

The overall shapes of the tracer breakthrough curve also indicate the nature of the flow system. In general, two types of flow behavior can be distinguished, at least qualitatively. The first kind (e.g., Figs. 4.24, 4.25a, 4.26a), which is termed diffusive, or Fickian, produces a tracer response resembling that of a homogeneous system where the slug has been dissipated by mixing. In this case, the tracer response can be matched with the appropriate solution of the convection-diffusion equation (Abbaszadeh-Dehghani and Brigham, 1982) to calculate an effective dispersivity. Since slug dilution is attributable only to velocity/permeability variations in a heterogeneous flow field, the computed effective dispersivity is essentially a measure of permeability variation.

The second kind of flow behavior (as exhibited by the rest of the examples), is termed convective, or non-Fickian, and is characterized by multiple peaks in the tracer breakthrough curve, indicating the presence of more than one discrete channel for fluid flow. Responses such as these, which provide a verification for the qualitative speculation on *pseudo*-layering by Brigham and Abbaszadeh-Dehghani (1987) (see their Fig. 13), cannot be matched with a one-parameter solution of the convection-diffusion equation using a single layer with a single value of dispersivity. However, it is useful to picture such a geometry, consisting of multiple discrete flow channels within a single layer, as being equivalent in effect to a layered system with several noncommunicating strata. Because of unit-mobility ratio displacement conditions, tracer response in this system can be modeled by superposition of individual layer solutions, as presented in Section 3.4. Moreover, the nonlinear optimization procedure using the subroutine VARPRO, discussed previously, can be used to deconvolve the integrated tracer breakthrough curve for estimating *pseudo*-layer properties.

Figures. 4.24-4.32 also demonstrate the influence of the statistics of permeability variation (as represented by  $V_{DP}$  and  $\lambda_D$ ) on tracer breakthrough behavior. In general, Fickian behavior can be seen when both  $V_{DP}$  and  $\lambda_D$  are small, and non-Fickian behavior can be seen for larger values of these parameters. Moreover, the difference between breakthrough curves from one realization to another is small when  $V_{DP}$  and  $\lambda_D$  are small (i.e. Fig. 4.24). As  $\lambda_D$  increases (i.e. Figs. 4.25 and 4.26), one realization shows Fickian and the other non-Fickian behavior. Fig. 4.27, where  $V_{DP}$  is higher but  $\lambda_D$  smaller as compared with Fig. 4.26, is similar to Fig. 4.24 in that both breakthrough curves are monomodal, even though the level of spreading is higher. As  $\lambda_D$  increases, the variability between the output from different realizations increases, but now both Figs. 4.28 and 4.29 show non-Fickian behavior because of a higher  $V_{DP}$ . The trend in Figs. 4.30-4.32 is similar, in that all breakthrough curves show non-Fickian behaviour because both  $V_{DP}$  and  $\lambda_D$  are large. Such qualitative behavior was observed in all of the simulated tracer test responses.

#### 4.5. VALIDITY OF THE CONVECTION-DIFFUSION EQUATION

The Fickian model for field-scale dispersion has been shown to be appropriate (i.e. the convection-diffusion equation is valid) only for large time and length scales (Gelhar, 1986). When the dimensions of the flow field are fixed, as in this study, this implies that Fickian behavior can be expected only if permeability variation and correlation lengths are small enough to permit sufficient spatial velocity averaging during tracer transport. This was found to be qualitatively true in these simulations, Fickian behavior being observed for small  $V_{DP}$  and  $\lambda_D$ . For larger values of  $V_{DP}$  and  $\lambda_D$  preferential flow paths were generated to cause a non-Fickian (multi-modal) tracer response, and the convection-diffusion equation with a single value of dispersivity could no longer be used to match the tracer concentration data.

It seemed reasonable to test whether these observations could be quantified using the heterogeneity index ( $\sigma_{ln(k)}^2 \lambda_D$ ) defined previously. This group contains information on the degree of permeability variation, as well as the spatial scale over which such variations persist. In Fig. 4.33, the percentage of simulation runs showing non-Fickian behavior is graphed as a function of  $\sigma_{ln(k)}^2 \lambda_D$ . As expected, the relationship is monotonically increasing, and asymptotically approaches Fickian and non-Fickian limits at the two extremes. The dashed portions show extrapolation beyond the range of the actual data. Figure 4.33 establishes the uncertainty associated with Monte-Carlo simulation results of convective flow processes. However, it is possible to deduce approximate conditions under which Fickian or non-Fickian behavior will be dominant. Figure 4.33 suggests that Fickian behavior is restricted to values of  $\sigma_{ln(k)}^2 \lambda_D$  less than  $4 \times 10^{-2}$ , and non-Fickian behavior is to be expected when the value of  $\sigma_{ln(k)}^2 \lambda_D$  is greater than  $4 \times 10^{-1}$ .

Smith and Brown (1984) computed effective dispersivities in a two-dimensional heterogeneous medium by fitting space-averaged concentration-time data to a Fickian model. The maximum value of  $\sigma_{ln(k)}^2 \lambda_D$  considered by them was about  $8 \times 10^{-2}$  (see their Fig. 6a), which is slightly higher than the limiting criterion for diffusive behavior derived in this work. This also explains the general success of the Fickian model in matching their simulated data.

Arya *et al.* (1985) followed a similar procedure for matching concentration-time data in two-dimensional randomly heterogeneous media, and found that the Fickian model may not be appropriate when permeability variation and correlation length scale are large. Their results suggest that diffusive behavior is limited to cases when  $\lambda_e$  is less than  $0.1 - 0.2 L$ , where  $\lambda_e$  is the integral range of an exponential semi-variogram of log-permeability values, and is approximately equal to  $0.32 \lambda$ . Arya *et al.* used a  $V_{DP}$  value of 0.6 (Arya, A., personal communication), for which case their criterion becomes equivalent to  $\sigma_{ln(k)}^2 \lambda_D < 3 - 6 \times 10^{-2}$ , and is consistent with the criterion of Fig. 4.33.

#### 4.6. SIGNIFICANCE OF EFFECTIVE PARAMETERS

At this stage, it is useful to ask if the effective parameters calculated from tracer test data (i.e. dispersivities and *pseudo*-layer properties) can be correlated with some measure of permeability variation such as the heterogeneity index. Based on the criteria derived from Fig. 4.33, it was inferred that Fickian behavior was more probable for: (a)  $V_{DP} = 0.35$ ,  $\lambda_D = 1/15$ , and (b)  $V_{DP} = 0.50$ ,  $\lambda_D = 1/15$ . For these two cases, effective dispersivities were computed for all simulation runs qualitatively exhibiting Fickian behavior (i.e. with unimodal tracer breakthrough curves). The average value of dispersivity,  $\alpha$ , for each of these two data sets, normalized by the characteristic flow length,  $L$ , is tabulated in Table 4.7, and is graphed in Fig. 4.34 as a function of  $\sigma_{ln(k)}^2 \lambda_D$ . The straight line shown is the

TABLE 4.7

**EFFECTIVE DISPERSIVITIES FROM SIMULATED TRACER TEST DATA  
SHOWING FICKIAN BEHAVIOR**

Run	$V_{DP} = 0.35, \lambda_D = 1/15$ $2L/\alpha$	$V_{DP} = 0.50, \lambda_D = 1/15$ $2L/\alpha$
1	560	922
2	1022	Non-Fickian
3	No convergence*	No convergence*
4	Non-Fickian	175
5	596	No convergence*
6	No convergence*	257
7	1060	312
8	188	No convergence*
9	611	249
10	536	176
11	Non-Fickian	129
12	1021	371
13	334	705
14	380	Non-Fickian
15	Non-Fickian	164
16	247	151
17	362	Non-Fickian
18	658	Non-Fickian
19	550	425
20	485	320

\*The regression program developed by Abbaszadeh-Dehghani and Brigham (1982) did not converge to an answer.

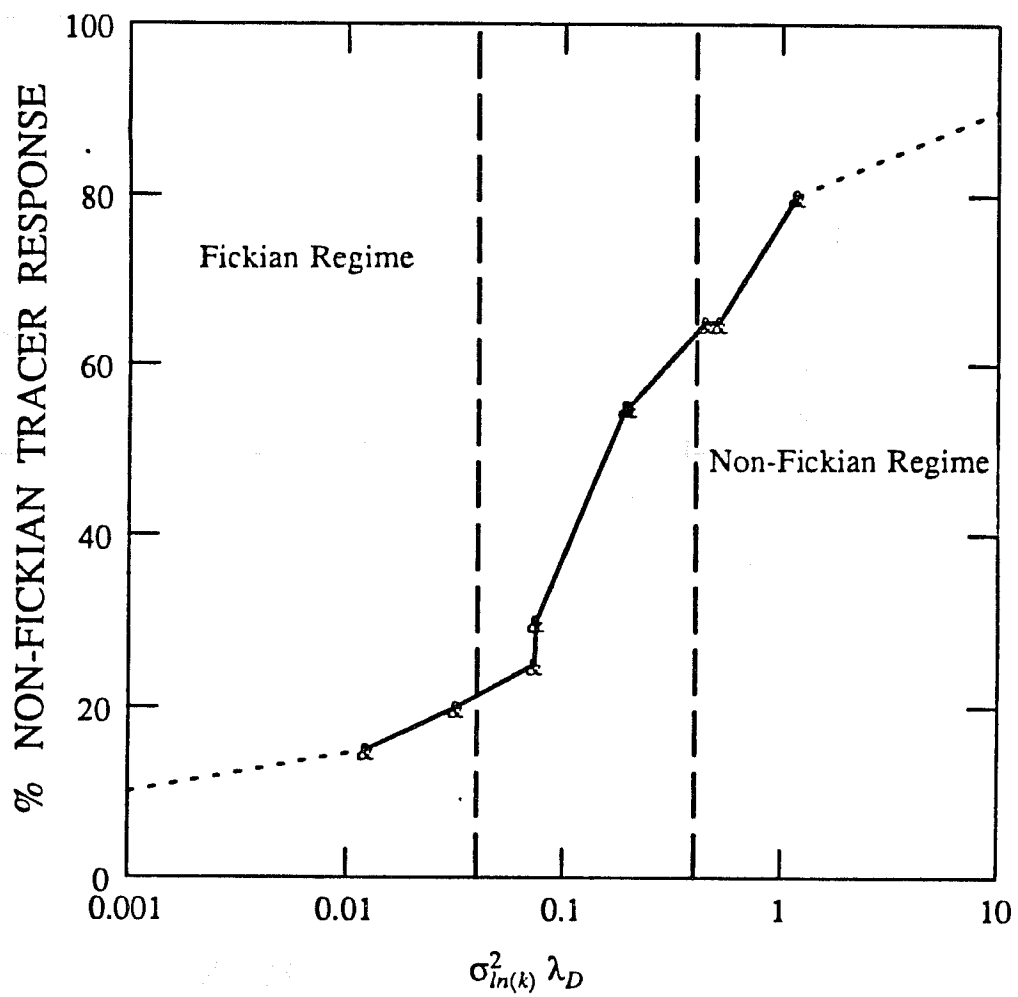


Fig. 4.33 Influence of heterogeneity index on nature of tracer response.

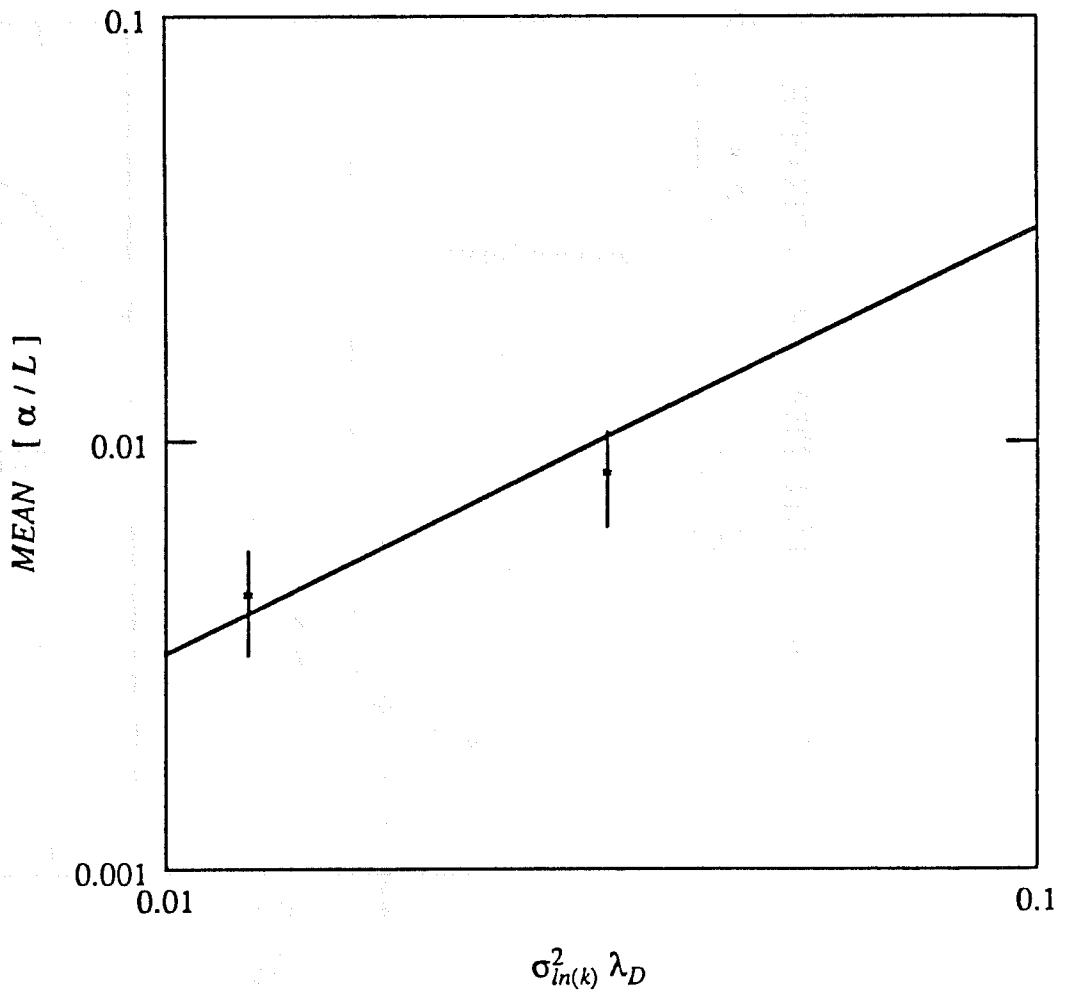


Fig. 4.34 Comparison of computed Fickian dispersivities with analytical results.

analytical result of Gelhar and Axness (1983) for two-dimensional isotropic media:

$$\frac{\alpha}{L} = 0.32 \sigma_{ln(k)}^2 \lambda_D \quad (4.4.16)$$

Also shown are the 95% confidence limits on the mean value of  $\alpha/L$ . The agreement between simulation results and predictions of stochastic theory are reasonable in view of the limited number of Monte-Carlo runs used for averaging.

For the non-Fickian examples, (i.e.  $V_{DP} = 0.50$ ,  $\lambda_D = 16/15$ ;  $V_{DP} = 0.65$ ,  $\lambda_D = 6/15$ ; and  $V_{DP} = 0.65$ ,  $\lambda_D = 16/15$ ) it was possible to match most tracer breakthrough curves with a two-layered model. In each case, the dispersivity,  $\alpha$ , was fixed at an arbitrary value of 1 ft to make the problem convection dominated. The regression program developed by Abbaszadeh-Dehghani and Brigham (1982) was then used to fit the simulated breakthrough data. Each match yielded four parameters, two for each *pseudo*-layer - the fractional  $\phi h$  and  $kh$  products. These results are summarized in Tables 4.8-4.10. No trend was observed in any of these parameters as a function of  $V_{DP}$ ,  $\lambda_D$  or a combination of the two. This suggests that a pseudo-layered interpretation model can at least be used to reproduce tracer response, though it is clear that the parameters obtained apply only at that scale and only for the specific realization under study. These parameters can also be used in conjunction with simple models for computing displacement performance, such as those described by Pande *et al.* (1987).

Since the tracer flow simulation code assumes that the wells are distributed over the entire grid-block, it is reasonable to expect that the effective pore volume available for tracer flow is less than the actual value. Another way of expressing this is to state that the sum of the pseudo-layer ( $\phi h / \Sigma \phi h$ ) values will be less than one. This was observed to be true (Tables 4.8-4.10) for the heterogeneous system simulations. For the homogeneous system case (i.e., Fig. 4.23b), regression calculated fractional  $\phi h$  was also found to be less than 1.

## 4.7. DISCUSSION OF RESULTS

A Monte-Carlo simulation approach has been used to demonstrate how pressure and tracer test data show different degrees of sensitivity to the presence of a heterogeneous permeability field. A parametric connection between the two test responses has been established empirically using the concept of heterogeneity index. This parameter also forms the basis of a proposed reservoir description procedure, which is outlined in the following.

1. From transient pressure data, compute  $k_{inj}$  and  $k_{prd}$ . Calculate  $k_{ss}$  from steady-state data, or use the geometric mean of  $k_{inj}$  and  $k_{prd}$  as a working approximation.
2. Compute dimensionless permeability difference  $\Delta k_D$  from Eq. (4.3.11), and estimate heterogeneity index  $\sigma_{ln(k)}^2 \lambda_D$  from Eq. (4.3.12).
3. Predict the qualitative nature of the tracer test response (i.e. Fickian or non-Fickian) using the criteria derived from Fig. 4.33.
4. If Fickian behavior is expected, calculate the approximate effective dispersivity from Eq. (4.4.16). If non-Fickian behavior is anticipated, then tracer test data may be needed to quantify the nature of heterogeneities.
5. When tracer test data are available, verify the results of Step 3, or compute *pseudo*-layer properties.

TABLE 4.8

PSEUDO-LAYER PARAMETERS FROM SIMULATED TRACER TEST DATA  
 SHOWING NON-FICKIAN BEHAVIOR;  $V_{DP} = 0.50$ ,  $\lambda_D = 16/15$

Run	Layer 1		Layer 2	
	$kh/\Sigma kh$	$\phi h/\Sigma \phi h$	$kh/\Sigma kh$	$\phi h/\Sigma \phi h$
1	0.89	0.75	0.05	0.16
2	0.59	0.52	0.27	0.28
3	Fickian		-	-
4	0.74	0.63	0.08	0.12
5	Fickian		-	-
6	0.76	0.50	0.15	0.38
7	Fickian		-	-
8	0.58	0.53	0.34	0.39
9	0.78	0.60	0.20	0.35
10	0.44	0.40	0.55	0.58
11	Fickian		-	-
12	0.42	0.42	0.50	0.52
13	0.83	0.72	0.13	0.24
14	Fickian		-	-
15	0.44	0.39	0.44	0.55
16	0.48	0.40	0.50	0.55
17	0.50	0.31	0.33	0.50
18	0.72	0.70	0.18	0.22
19	0.50	0.44	0.44	0.48
20	Fickian		-	-

TABLE 4.9

PSEUDO-LAYER PARAMETERS FROM SIMULATED TRACER TEST DATA  
 SHOWING NON-FICKIAN BEHAVIOR;  $V_{DP} = 0.65$ ,  $\lambda_D = 6/15$

Run	Layer 1		Layer 2	
	$kh/\Sigma kh$	$\phi h/\Sigma \phi h$	$kh/\Sigma kh$	$\phi h/\Sigma \phi h$
1	0.55	0.44	0.42	0.47
2	0.46	0.35	0.36	0.45
3	0.50	0.38	0.45	0.48
4	0.61	0.54	0.34	0.41
5	Fickian		-	-
6	Fickian		-	-
7	0.55	0.37	0.36	0.48
8	0.50	0.33	0.28	0.37
9	0.78	0.72	0.20	0.35
10	No convergence		-	-
11	0.80	0.77	0.14	0.21
12	Fickian		-	-
13	0.56	0.35	0.30	0.50
14	0.45	0.40	0.50	0.54
15	0.80	0.75	0.12	0.20
16	Fickian		-	-
17	0.78	0.52	0.15	0.42
18	0.75	0.51	0.18	0.35
19	0.57	0.65	0.40	0.31
20	Fickian		-	-

TABLE 4.10

PSEUDO-LAYER PARAMETERS FROM SIMULATED TRACER TEST DATA  
 SHOWING NON-FICKIAN BEHAVIOR;  $V_{DP} = 0.65$ ,  $\lambda_D = 16/15$

Run	Layer 1		Layer 2	
	$kh/\Sigma kh$	$\phi h/\Sigma \phi h$	$kh/\Sigma kh$	$\phi h/\Sigma \phi h$
1	0.43	0.39	0.56	0.60
2	0.48	0.39	0.47	0.54
3	Fickian		-	-
4	0.45	0.38	0.53	0.51
5	0.63	0.63	0.27	0.34
6	Fickian		-	-
7	0.68	0.55	0.27	0.40
8	0.56	0.48	0.38	0.45
9	No convergence		-	-
10	0.66	0.52	0.18	0.29
11	Fickian		-	-
12	0.46	0.39	0.48	0.52
13	0.54	0.50	0.40	0.42
14	0.72	0.51	0.18	0.33
15	0.75	0.52	0.20	0.40
16	0.78	0.40	0.15	0.50
17	Fickian		-	-
18	0.73	0.55	0.22	0.39
19	0.67	0.52	0.30	0.44
20	0.50	0.46	0.44	0.49

Simulation results reported here are based on a  $V_{DP}$  range of 0.35-0.65, and a  $\lambda_D$  range of 1/15-16/15 (i.e.  $60 < \lambda < 1000$  ft). Such  $V_{DP}$  values are believed to be representative of actual field conditions, even though these are less than typical core  $V_{DP}$  bounds, because a reduction in variance occurs (due to averaging effects) when core measurements are scaled up to grid-block values (Journel and Huijbregts, 1978). However, the same degree of confidence cannot be assigned to the  $\lambda$  values used. The uncertainty arises from the lack of information regarding permeability correlation length scales under reservoir conditions. Data from groundwater aquifers suggest that  $\lambda$  may be of the order of tens of kilometers (Hoeksema and Kitanidis, 1985), and may also be scale dependent because of nested scales of variation in rock properties (Gelhar, 1986).

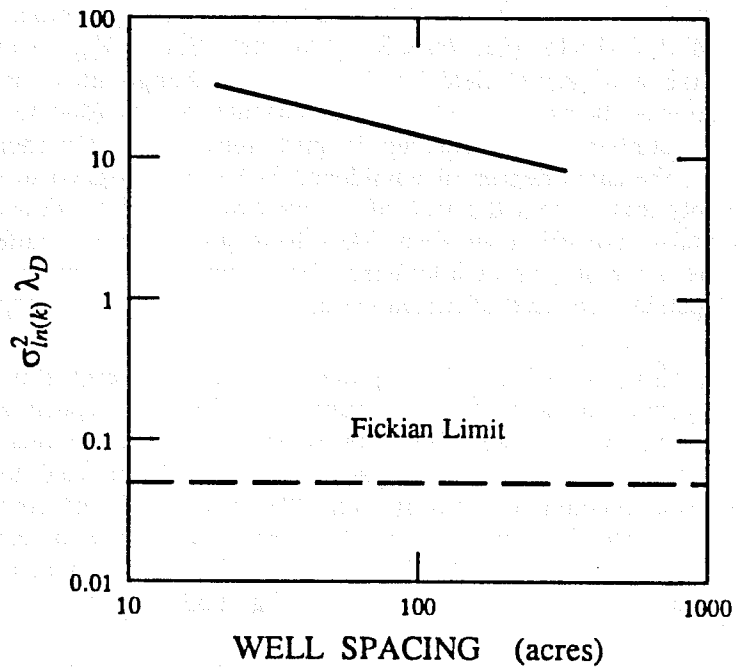
Da Costa e Silva (1985) presented data on permeability variation and spatial continuity from a North Sea oil reservoir. He fitted a spherical semi-variogram model (Table 4.1) to permeability measurements, and estimated  $\sigma_{ln(k)}^2 = 0.85$ , and  $\lambda = 3.4$  miles (5.4 km). These parameters have been used to calculate heterogeneity indices as a function of well spacing. The results of this computation, shown in Fig. 4.35(a), indicate that under typical field scale displacement conditions (i.e. when well spacing is of the order of 10-100 acres), non-Fickian behavior can be expected to be the norm based on the criterion derived from Fig. 4.33.

This data set can also be used to calculate correlation length scales required for Fickian behavior to be observed when the variance is known, assuming that the Fickian limit corresponds to a  $\sigma_{ln(k)}^2 \lambda_D$  value of  $4 \times 10^{-2}$ . Fig. 4.35(b) shows  $\lambda$  as a function of well spacing at the Fickian limit for the North Sea data set discussed previously. It is clear that  $\lambda$  values must be quite small for Fickian behavior to be observed. Based on limited field measurements of correlation length scales (i.e. Da Costa e Silva, 1985; Hoeksema and Kitanidis, 1985) this does not appear to be true, although more field studies are required to substantiate such general remarks.

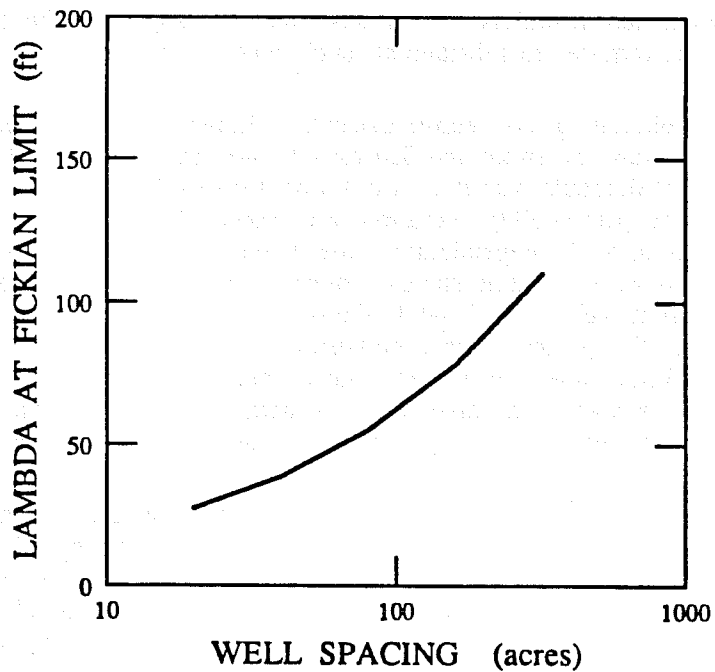
Simulations of convective tracer flow in heterogeneous media reported in this study, as well as those of Smith and Schwartz (1980), show that tracer breakthrough curves may exhibit considerable variation from one Monte-Carlo run to another, even when the statistics of permeability variation are known. This occurs because a convective flow process is strongly dependent on the actual permeability network used. Two different realizations with the same statistics might be such that one has a high permeability streak running from well to well, while the other has a similar streak along the other diagonal. Thus, even though the average measures (variance, correlation length scale) would be the same in both cases, their tracer flow behavior would be completely different. It is apparent that some additional statistical parameter which measures the *connectivity* effect would reduce such uncertainty, though it is not obvious what that parameter should be.

Under such conditions, only qualitative comments regarding tracer or miscible fluid flow (e.g. Fickian as opposed to non-Fickian) can be made with any reasonable degree of certainty. Quantitative predictions (e.g. time to breakthrough etc.) will have too high an uncertainty to be of practical use. These observations are obviously more appropriate when the scale of heterogeneities is no longer negligible compared to interwell distances, i.e. when tracer flow is non-Fickian. It also explains the lack of any definite correlation of *pseudo-layer* properties with  $V_{DP}$  and  $\lambda_D$ , as observed from the non-Fickian tracer test interpretations.

Thus the general use of the convection-diffusion equation for modeling tracer (and miscible fluid) displacement in heterogeneous media is open to question. In the groundwater literature, the current philosophy is to obtain some knowledge of the spatial



4.35 (a) Heterogeneity index as a function of well spacing.



4.35 (b) Correlation length scales required for Fickian behavior.

Fig. 4.35 Heterogeneity index and correlation length scales computed for a North Sea oil-field data set.

variation and continuity of the permeability field and then use this with results from stochastic theory to calculate the components of the dispersion tensor (Gelhar, 1986). Such an approach may be useful in the context of contaminant transport, but its applicability in petroleum reservoir engineering seems limited because of the small number of wells available for sampling the permeability distribution. The alternative is to ignore the dispersion formulation, and view spreading of the tracer slug as being purely the result of convective effects in a heterogeneous flow field. This modeling approach also requires a detailed knowledge of the permeability field. However, by using information from cores, logs and pressure tests, permeability values can be obtained at some pilot points (wells). Conditional simulation (Journel and Huijbregts, 1978) can then be used to construct the entire permeability field with some interpolation in the inter-well region while honoring known information at the wells. This semi-stochastic methodology has the advantage of better representing the physics in that no pseudo-mixing has been introduced, as in the dispersion formalism. Hewett (1986) has used similar ideas to match field displacement performance for fractal rock property distributions.

The need for well-designed field tests for detecting reservoir heterogeneities is paramount. A single-well pressure test would only reveal some average permeability in its drainage area, but the combination of several such tests has the potential of revealing structures in permeability variation, albeit in some averaged sense. Even though there are limits to detection with well tests, procedures such as those developed in this section can yield simple measures of in-situ permeability variation. That, in itself, is an important first step in describing a reservoir and forecasting its performance.

## 5. CONCLUSIONS AND RECOMMENDATIONS

*Major findings from this work are summarized. Some avenues for future research on the use of well testing for reservoir description are suggested.*

### 5.1. CONCLUSIONS

The results from Section 3, dealing with well test analysis for noncommunicating layered systems with a log-normal permeability distribution, suggest the following conclusions:

1. Conventional pressure drawdown or buildup testing in an injection-production system is insensitive to the degree of layering and permeability contrast. On the other hand, well-to-well tracer test response is influenced by the number of layers (which affect the number of concentration peaks) as well as the degree of permeability variation (which affects tracer breakthrough time).
2. Tracer tests can provide information regarding individual layer properties, but a conventional pressure test can only yield an integrated property (e.g. total transmissivity). However, the combined analysis of transient pressure and individual layer flow rate data has the potential of providing layer properties.
3. The buildup responses of layered systems with no-flow and constant pressure outer boundaries are significantly different. This is particularly true in the presence of high permeability contrast between layers, when differential depletion can be significant in the bounded system case and lead to the characteristic hump on a Horner buildup graph, but will be neutralized by fluid recharge in the injection case.

The results from Section 4, dealing with well test analysis in single-layer areally heterogeneous systems with log-normal spatially correlated permeability distributions, suggest the following conclusions:

1. The geometric mean of effective permeabilities around injection and production wells in a 5-spot pattern, as calculated from transient pressure data, reasonably approximates the steady-state inter-well permeability.
2. By combining permeability measurements over different spatial scales (i.e. around the injection and production wells and across the interwell region), a simple measure of heterogeneity called the heterogeneity index, defined as the product of permeability variance and a dimensionless correlation length, can be computed.
3. Tracer test data can be matched with solutions of the convection-diffusion equation to calculate an effective dispersivity only for small values of the heterogeneity index.
4. When the heterogeneity index is large, preferential flow paths are generated in the system, which cause tracer concentration-time data to resemble the response of a layered medium.

5. A reservoir description procedure, based on the concept of heterogeneity index and a combined analysis of pressure and tracer test data, is proposed.

In addition to these specific conclusions, some general observations regarding the use of well test data for reservoir description may also be made. Single-well transient pressure test data will yield a permeability which is a localized average. Several such measurements may be used to create a permeability map, either with simple interpolation methods, or with more sophisticated techniques such as kriging. The simultaneous analysis of transient flow rate and pressure data also offers a powerful tool for reservoir definition, particularly in the presence of vertical stratification.

Permeability measurements from several single-well tests can also be used to calculate the heterogeneity index and qualitatively predict tracer flow behavior. Tracer test data, if available, add an extra dimension to the level of information that can be obtained, which is offset to some extent by the time required to conduct such a test. However, it is possible to obtain some idea regarding the higher permeability streaks from an analysis of initial tracer returns, and tie this with pressure test data in order to construct a rough permeability frequency distribution, using a layered-system model. The use of such a model only implies that the convective flow response is *similar* to that of a noncommunicating layered system, even though the actual medium may be different. This simplistic modelling approach honors the physics of a discrete-flow-channel behavior and is suitable for computing displacement performance, at least over the scale from which the data were obtained. Real systems are certainly more complex, but the limitations of simple analytical modelling preclude the consideration of more complicated physical geometries.

Information from pressure and tracer tests needs to be integrated with core and well-log data so that a unified picture of the reservoir can be obtained. The major difficulty in this process currently lies in the lack of proper scaling methods for averaging transport properties (e.g. permeability). Fortunately, such questions are beginning to be addressed in a systematic manner. As we begin to understand more regarding the detection and representation of heterogeneities, it is also necessary to realize that reservoir description is best achieved by synthesizing information from a multitude of sources, as well as a variety of scales.

## 5.2. RECOMMENDATIONS

This work considered vertical and areal permeability variations separately. In most real reservoir settings, the physical system would be three-dimensional in nature and include both vertical *and* areal variations in permeability. Hence, a three-dimensional geometry should form the basis for the next generation of comparative studies similar to this research.

Point permeability measurements often indicate a multi-modal frequency distribution, as well as anisotropy. Moreover, porosity variations can perhaps be correlated in some simple way to permeability variations. These features should be incorporated in reservoir descriptions for input to Monte-Carlo simulation studies.

In order to obtain a better definition of the wellbore pressure response, a hybrid grid arrangement (Pedrosa and Aziz, 1986) should be utilized. Moreover, a better method for modelling solute transport, other than the USGS code used in this study, should be implemented. While the USGS simulator effectively reduces numerical dispersion, it can have mass balance errors because of a nonconservative finite-difference formulation of the convection-diffusion equation. Moreover, the extension of this method to three-dimensional geometries is quite complex. A possible alternative is the random walk method (Prickett *et al.*,

1981), which also minimizes numerical dispersion, and is easily adaptable to any existing fluid flow simulation code.

The influence of permeability correlation length scale on fluid transport has been well established through theoretical studies such as this work. However, the structure of actual permeability fields (i.e. whether permeability variation can be modelled with a bounded semi-variogram or as a fractal process), and their relation to depositional environments, is not well known. There is thus a critical need for field studies which address these aspects.

When the continuum hypothesis of flow through porous media does not hold (because of variations in material properties over all scales), a reformulation of the fundamental equations of fluid transport may be necessary. Recently, Wheatcraft and Tyler (1987) have applied fractal mathematics to model solute transport under such conditions. The applicability of this concept in reservoir engineering should be investigated.

## NOMENCLATURE

$a$	distance between like wells in a 5-spot	( $L$ )
$A$	pattern area	( $L^2$ )
$c_t$	total system compressibility	( $L^2 M^{-1}$ )
$C$	concentration	( $L^3 L^{-3}$ )
$C_{inj}$	concentration of injected tracer slug	( $L^3 L^{-3}$ )
$C^s$	concentration of source or sink fluid	( $L^3 L^{-3}$ )
$\bar{C}$	effluent concentration	( $L^3 L^{-3}$ )
$\bar{C}_l$	layered system effluent concentration	( $L^3 L^{-3}$ )
$C_D$	dimensionless wellbore storage	
$\bar{C}_D$	dimensionless tracer concentration	
$d$	distance between injection and production wells	( $L$ )
$D$	dispersion coefficient tensor	
$D$	dispersion coefficient	( $L^2 T^{-1}$ )
$F$	geometric factor, dimensionless	
$h$	formation thickness, or lag of semi-variogram	( $L$ )
$I_0$	modified Bessel function of the first kind of order zero	
$I_1$	modified Bessel function of the first kind of order one	
$k$	permeability tensor	
$k$	permeability	( $L^2$ )
$k_{inj}$	effective permeability around injection well	( $L^2$ )
$k_{prd}$	effective permeability around production well	( $L^2$ )
$k_{ss}$	steady-state interwell permeability	( $L^2$ )
$K_0$	modified Bessel function of the second kind of order zero	
$K_1$	modified Bessel function of the second kind of order one	
$L$	characteristic flow length	( $L$ )
$m$	slope of semi-log pressure-time graph	( $M L^{-2}$ )
$p$	pressure	( $M L^{-2}$ )
$p_{wf}$	flowing well pressure	( $M L^{-2}$ )
$p_{ws}$	shut-in well pressure	( $M L^{-2}$ )
$p_i$	initial reservoir pressure	( $M L^{-2}$ )
$\Delta p_{ss}$	steady-state pressure drop between wells	( $M L^{-2}$ )
$q$	well flow rate	( $L^3 T^{-1}$ )
$r$	radial distance	( $L$ )
$r_o$	effective well-bore radius	( $L$ )
$s$	skin factor, dimensionless	
$S$	storativity	( $L^3 M^{-1}$ )
$t$	time	( $T$ )
$t_p$	producing time	( $T$ )
$\Delta t$	shut-in time	( $T$ )
$T$	transmissivity	( $L^4 T M^{-1}$ )
$V$	velocity vector	
$v, V$	velocity	( $L T^{-1}$ )
$V_{DP}$	Dykstra-Parsons coefficient, dimensionless	
$W$	width of streamtube	( $L$ )
$x$	spatial coordinate vector	
$x$	spatial coordinate	
$\bar{x}$	average distance of travel	( $L$ )
$y$	spatial coordinate	
$z$	natural logarithm of permeability	
$\alpha$	dispersivity	( $L$ )

$\gamma$	semi-variance of $z$
$\lambda$	correlation length scale ( $L$ )
$\lambda_D$	dimensionless correlation length scale
$\mu$	viscosity ( $M L^{-1} T^{-1}$ )
$\phi$	porosity, dimensionless
$\sigma_{\eta}^2$	measure of mixing within streamtube
$\sigma_{\ln(k)}$	variance of log-permeability $z$
$\sigma_x$	variance of spatial location ( $L^2$ )
$\Psi$	streamline index
$\rho$	autocorrelation function

## REFERENCES

1. Abbaszadeh-Dehghani, M. and Brigham, W.E. (1982) : *Analysis of Unit-Mobility Ratio Well-to-Well Tracer Flow to Determine Reservoir Heterogeneity*, Stanford University Petroleum Research Institute Report SUPRI-TR-36, Stanford - condensed version published in *J. Pet. Tech.* (Oct. 1984), 1753-1762.
2. Abou-Kassem, J.H. and Aziz, K. (1985) : "Analytical Well Models for Reservoir Simulation," *Soc. Pet. Eng. J.*, **25**, 573-579.
3. Arya, A., Hewett, T.A., Larson, R.G. and Lake, L.W. (1985) : "Dispersion and Reservoir Heterogeneity," paper SPE 14364 presented at the SPE 60th Annual Technical Conference and Exhibition, Las Vegas, Sept. 22-25.
4. Aziz, K. and Settari, A. (1979) : *Petroleum Reservoir Simulation*, Elsevier Applied Science Publishing Company, London and New York.
5. Baldwin, D.E. Jr. (1966) : "Prediction of Tracer Performance in a Five-Spot Pattern," *J. Pet. Tech.*, 513-517.
6. Bear, J. (1972) : *Dynamics of Flow in Porous Media*, American Elsevier Publishing Company, New York.
7. Beck, J.V. and Arnold, K.J. (1977) : *Parameter Estimation in Engineering and Science*, John Wiley and Sons, New York.
8. Bennion, D.W. and Griffiths, J.C. (1966) : "A Stochastic Model for Predicting Variations in Reservoir Rock Properties," *Soc. Pet. Eng. J.*, **6**, 9-16.
9. Bourdet, D., Ayoub, J.A. and Pirard, Y.M. (1984) : "Use of Pressure Derivative in Well Test Interpretation," paper SPE 12777 presented at the SPE 54th California Regional Meeting, Long Beach, Apr. 11-13.
10. Brigham, W.E., Reed, P.W. and Dew, J.N. (1961) : "Experiments on Mixing During Miscible Displacement in Porous Media," *Soc. Pet. Eng. J.*, **1**, 1-8.
11. Brigham, W.E. and Smith, D.H. (1965) : "Prediction of Tracer Behavior in Five-Spots," paper SPE 1130 presented at the SPE 40th Annual Fall Meeting, Denver, Oct. 3-6.
12. Brigham, W.E. (1973) : "Mixing Equations in Various Geometries," paper SPE 4585 presented at the SPE 48th Annual Meeting, Las Vegas, Sept. 30-Oct. 3.
13. Brigham, W.E. and Abbaszadeh-Dehghani, M. (1987) : "Tracer Testing for Reservoir Description," Distinguished Author Series, *J. Pet. Tech.*, 519-527.
14. Carslaw, H. and Jaeger, J.C. (1959) : *Conduction of Heat in Solids*, Oxford at Clarendon Press.

15. Coats, K.H. and Smith, B.D. (1964) : "Dead-end Pore Volume and Dispersion in Porous Media," *Soc. Pet. Eng. J.*, 4, 73-84.
16. Cobb, W.M., Ramey, H.J., Jr. and Miller, F.G. (1972) : "Well Test Analysis for Wells Producing Commingled Zones," *J. Pet. Tech.*, 27-37.
17. Craig, F.F. (1971) : *Reservoir Engineering Aspects of Waterflooding*, Monograph Series, 3, Society of Petroleum Engineers, Dallas.
18. Crank, J. (1957) : *The Mathematics of Diffusion*, Oxford at Clarendon Press.
19. Da Costa e Silva, A.J. (1985) : "A New Approach to the Characterization of Reservoir Heterogeneity based on the Geomathematical Model and Kriging Technique," paper SPE 14275 presented at the SPE 60th Annual Technical Conference and Exhibition, Las Vegas, Sept. 22-25.
20. Dagan, G. (1979) : "Models of Groundwater Flow in Statistically Homogeneous Porous Formations," *Water Resources Res.*, 15, 47-63.
21. Desbarats, A.J. (1987) : "Numerical Estimation of Effective Permeability in Sand-Shale Formations," *Water Resources Res.*, 23, 273-286.
22. Dykstra, H. and Parsons, R.L (1950) : "The Prediction of Oil Recovery by Water Flood," *Secondary Recovery of Oil in the United States*, American Petroleum Institute, Washington, D.C.
23. Earlougher, R.C., Jr., Kersch, K.M. and Kunzman, W.J. (1974) : "Some Characteristics of Pressure Buildup Behavior in Bounded Multiple Layer Reservoirs Without Crossflow," *J. Pet. Tech.*, 1178-1186.
24. Earlougher, R.C., Jr. (1977) : *Advances in Well-Test Analysis*, Monograph Series, 5, Society of Petroleum Engineers, Dallas.
25. Ehlig-Economides, C.A. and Joseph, J.A. (1985) : "A New Test for Determination of Individual Layer Properties in a Multi-layer Reservoir," paper SPE 14167 presented at the SPE 60th Annual Fall Technical Conference and Exhibition, Las Vegas, Sept. 22-25.
26. Fischer, H.B., List, J.E., Koh, R.C.Y., Imberger, J. and Brooks, N.H. (1979) : *Mixing in Inland and Coastal Waters*, Academic Press, New York.
27. Garder, A.O., Peaceman, D.W. and Pozzi, A.L., Jr. (1964) : "Numerical Calculation of Multidimensional Miscible Displacement by the Method of Characteristics," *Soc. Pet. Eng. J.*, 4, 26-36.
28. Gelhar, L.W., Gutjahr, A.L. and Naff, R.L. (1979) : "Stochastic Analysis of Macrodispersion in a Stratified Aquifer," *Water Resources Res.*, 15, 1387-1397.
29. Gelhar, L.W. and Axness, C.L. (1983) : "Three-dimensional Stochastic Analysis of Macrodispersion in Aquifers," *Water Resources Res.*, 19, 161-180.

30. Gelhar, L.W., Mantoglou, A., Welty, C. and Rehfeldt, K.R. (1985) : *A Review of Field Scale Solute Transport Processes in Saturated and Unsaturated Porous Media*, Electrical Power Research Institute Report RP-2485-05, Palo Alto.
31. Gelhar, L.W. (1986) : "Stochastic Subsurface Hydrology : From Theory to Applications," *Water Resources Res.*, **22**, 135S-145S.
32. Goggin, D.J., Chandler, M.A., Kocurek, G.A. and Lake, L.W. (1986) : "Patterns of Permeability in Eolian Deposits," paper SPE/DOE 14893 presented at the SPE/DOE Fifth Symposium on Enhanced Oil Recovery, Tulsa, Apr. 20-23.
33. Golub, G.H. and Pereyra, V. (1972) : *The Differentiation of Pseudo-inverses and Non-linear Least-squares Problems whose Variables Separate*, Stanford University Computer Science Department Report 72-261, Stanford.
34. Gringarten, A.C. (1985) : "Interpretation of Transient Well Test Data," in *Developments in Petroleum Engineering-1*, Dawe, R.A. and Wilson, D.C. eds., Elsevier Applied Science Publishing Co., London and New York, 133-196.
35. Gutjahr, A.L., Gelhar, L.W., Bakr, A.A. and McMillan, J.R. (1978) : "Stochastic Analysis of Spatial Variability in Subsurface Flow," *Water Resources Res.*, **14**, 953-959.
36. Hewett, T.A. (1986) : "Fractal Distribution of Reservoir Heterogeneity," paper SPE 16170 presented at the SPE 61st Annual Technical Conference and Exhibition, New Orleans, Oct. 5-8.
37. Hoeksema, R.J. and Kitanidis, P.K. (1985) : "Analysis of the Spatial Structure of Properties of Selected Aquifers," *Water Resources Res.*, **21**, 563-572.
38. Horner, D.R. (1951) : "Pressure Buildup in Wells," *Proc.*, Third World Pet. Cong., The Hague, **II**, 503-523.
39. Jensen, J.L., Lake, L.W. and Hinkley, D.V. (1985) : "A Statistical Study of Reservoir Permeability: Distributions, Correlations and Averages," paper SPE 14270 presented at the SPE 60th Annual Technical Conference and Exhibition, Las Vegas, Sept. 22-25.
40. Journel, A.G. and Huijbregts, C.J. (1978) : *Mining Geostatistics*, Academic Press, London.
41. Konikow, L.W. and Bredehoeft, J.D. (1978) : *Computer Model of Two-Dimensional Solute Transport and Dispersion in Ground Water*, U.S. Geological Survey Techniques of Water Resources Investigation, Book 7, Chapter C2.
42. Kumar, A. and Ramey, H.J., Jr. (1974) : "Well-Test Analysis for a Well in a Constant-Pressure Square," *Soc. Pet. Eng. J.*, **14**, 107-116.
43. Larsen, L. (1981) : "Wells Producing Commingled Zones with Unequal Initial Pressures and Reservoir Properties," paper SPE 10325 presented at the SPE 56th Annual Technical Conference and Exhibition, San Antonio, Oct. 5-7.

44. Law, J. (1944) : "A Statistical Approach to the Interstitial Heterogeneity of Sand Reservoirs," *Trans.*, AIME, **155**, 202-222.
45. Lee, W.J. (1983) : *Well Testing*, Textbook Series, **1**, Society of Petroleum Engineers, Dallas.
46. Lefkovits, H.C., Hazebroek, P., Allen, E.E. and Matthews, C.S. (1961) : "A Study of the Behavior of Bounded Reservoirs Composed of Stratified Layers," *Trans.*, AIME, **222**, 43-55.
47. Long, J.C.S., Remer, J.S., Wilson, C.R. and Witherspoon, P.A. (1982) : "Porous Media Equivalents for Networks of Discontinuous Fractures," *Water Resources Res.*, **18**, 645-658.
48. Luster, G.R. (1985) : *Raw Materials for Portland Cement : Applications of Conditional Simulation or Coregionalization*, Ph.D. dissertation, Stanford University, Stanford.
49. McBratney, A.B. and Webster, R. (1986) : "Choosing Functions for Semi-variograms of Soil Properties and Fitting them to Sampling Estimates," *J. Soil Sc.*, **37**, 617-639.
50. Mandelbrot, B.B. (1982) : *The Fractal Geometry of Nature*, W.H. Freeman and Company, San Francisco.
51. Matthews, C.S. and Russell, D.G. (1967) : *Pressure Buildup and Flow Test Analysis*, Monograph Series, **1**, Society of Petroleum Engineers, Dallas.
52. Miller, C.C., Dyes, A.B. and Hutchinson, C.A. (1950) : "The Estimation of Permeability and Reservoir Pressure from Bottom-hole Pressure Buildup Characteristics," *Trans.*, AIME, **189**, 91-100.
53. Muskat, M. (1937) : "Use of Data on Buildup of Bottom-hole Pressures," *Trans.*, AIME, **123**, 44-50.
54. Pande, K.K., Ramey, H.J., Jr., Brigham, W.E. and Orr, F.M., Jr. (1987) : "Frontal Advance Theory for Flow in Heterogeneous Porous Media," paper SPE 16344 presented at the SPE 57th Annual California Regional Meeting, Ventura, Apr. 8-10.
55. Pedrosa, O.A. and Aziz, K. (1986) : "Use of a Hybrid Grid in Reservoir Simulation," *SPERE*, **1**, 611-620.
56. Perkins, T.K. and Johnston, O.C. (1963) : "A Review of Diffusion and Dispersion in Porous Media," *Soc. Pet. Eng. J.*, **3**, 70-80.
57. Prickett, T.A., Nyamik, T.G. and Lonquist, G. (1981) : *A Random-Walk Solute Transport Model for Selected Groundwater Quality Evaluations*, Illinois State Geological Survey, Bulletin 65.
58. Raghavan, R. (1986) : "Behavior of Wells Completed in Multiple Producing Zones," paper SPE 12378 presented at the SPE International Meeting on Petroleum Engineering, Beijing, China, Mar. 17-20.

59. Raghavan, R., Topaloglu, H.N., Cobb, W.M. and Ramey, H.J., Jr. (1974) : "Well-Test Analysis for Wells Producing from Two Commingled Zones of Unequal Thickness," *J. Pet. Tech.*, 1035-1043.
60. Ramey, H.J., Jr., Kumar, A. and Gulati, M.S. (1973) : *Gas Well Test Analysis under Water Drive Conditions*, American Gas Association, Arlington.
61. Ramey, H.J., Jr. (1976) : "Practical Use of Modern Well Test Analysis," paper SPE 5878 presented at the SPE 46th Annual California Regional Meeting, Long Beach, Apr. 8-9.
62. Ramey, H.J., Jr. (1982) : "Pressure Transient Testing," Distinguished Author Series, *J. Pet. Tech.*, 1407-1413.
63. Ramey, H.J., Jr. (1983) : Unpublished Note, Department of Petroleum Engineering, Stanford University, Stanford, CA.
64. Richardson, J.G., Sangree, J.B. and Sneider, R.M. (1987) : "Deepwater Fans," Technology Today Series, *J. Pet. Tech.*, 402-403.
65. Rosa, A.J. and Horne, R.H. (1983) : "Automated Type-Curve Matching in Well Test Analysis using Laplace Space Determination of Parameter Gradients," paper SPE 12131 presented at the SPE 58th Annual Technical Conference and Exhibition, San Francisco, Oct. 5-8.
66. Schwartz, F.W. (1977) : "Macroscopic Dispersion : The Controlling Factors," *Water Resources Res.*, **13**, 743-752.
67. Smith, L. and Schwartz, F.W. (1980) : "Mass Transport, 1. A Stochastic Analysis of Macroscopic Dispersion," *Water Resources Res.*, **16**, 303-313.
68. Smith, P.J. and Brown, C.E. (1984) : "The Interpretation of Tracer Test Response from Heterogeneous Reservoirs," paper SPE 13262 presented at the SPE 59th Annual Technical Conference and Exhibition, Houston, Sept. 16-19.
69. Stalkup, F.I. and Ebanks, W.J., Jr. (1986) : "Permeability Variation in a Sandstone Barrier Island-Tidal Channel-Tidal Delta Complex, Ferron Sandstone (Lower Cretaceous), Central Utah," paper SPE 15532 presented at the SPE 61st Annual Technical Conference and Exhibition, New Orleans, Oct. 5-8.
70. Stehfest, H. (1970) : Algorithm 368, "Numerical Inversion of the Laplace Transform," *Communications of the ACM*, **13**, 47-49.
71. Tariq, S.M. (1977) : *A Study of the Behavior of Layered Reservoirs with Wellbore Storage and Skin*, Ph.D. dissertation, Stanford University, Stanford.
72. Taylor, G.I. (1920) : "Diffusion by Continuous Movements," *Proc.*, London Math. Soc., **20**, 196-212
73. Tiab, D. and Kumar, A. (1980) : "Application of the  $p_D'$  function to Interference Analysis," *J. Pet. Tech.*, 1465-1470.

74. Warren, J.E. and Price, H.S. (1961) : "Flow in Heterogeneous Porous Media," *Soc. Pet. Eng. J.*, **1**, 153-169.
75. Warren, J.E., Skiba, F.F. and Price, H.S. (1961) : "An Evaluation of the Significance of Permeability Measurements," *J. Pet. Tech.*, 739-744.
76. Warren, J.E. and Skiba, F.F. (1964) : "Macroscopic Dispersion," *Soc. Pet. Eng. J.*, **4**, 215-230.
77. Willhite, G.P. (1986) : *Waterflooding*, Textbook Series, **3**, Society of Petroleum Engineers, Dallas.
78. Yuen, D.L., Brigham, W.E. and Cinco-L., H. (1979) : "Analysis of Five-Spot Tracer Tests to Determine Reservoir Layering," U.S. DOE Report SAW 1265-8, Washington, D.C.
79. Wheatcraft, S.W. and Tyler, S.W. (1987) : "Solute Transport in Heterogeneous Aquifers that Exhibit Fractal Characteristics," *EOS, Trans.*, AGU, **68**, 299.

## APPENDIX A

### CALCULATION OF EFFECTIVE PERMEABILITY FROM SIMULATED TRANSIENT PRESSURE DATA

This appendix presents the procedure used for computing effective permeabilities around injection and production wells from simulated transient pressure data, which are analyzed in Section 4.3.1. The example data set, shown in Fig. A.1, is for the case of  $V_{DP} = 0.50$ , and  $\lambda_D = 6/15$ .

Since a semi-log straight line on a pressure-time graph, which corresponds to the infinite-acting radial flow period, can be represented as a line of zero slope on a pressure derivative graph, its identification becomes much easier on the derivative graph. Hence, pressure data were first converted to pressure derivatives according to the formula:

$$\frac{\partial p}{\partial(\ln t)} \approx \frac{P_{i+1} - P_{i-1}}{\ln(t_{i+1} / t_{i-1})} \quad (\text{A.1})$$

Production and injection well pressure derivative data are shown in Figs. A.2(a) and A.2(b). For the production well case, an apparent straight line is indicated between  $t = 0.11$  days, and  $t = 0.73$  days, and for the injection well case, a similar linear segment is indicated between  $t = 0.03$  days, and  $t = 0.37$  days. Regression fitted straight lines for these linear portions yield slopes of  $m_{prd} = 1608$  psi/log-cycle, and  $m_{inj} = 553$  psi/log-cycle. Permeabilities can be calculated from these slopes with Eq. (4.3.7) expressed in oil-field units:

$$k = \frac{162.6 q\mu}{mh} \quad (\text{A.2})$$

which yields  $k_{prd} = 4.3$  md, and  $k_{inj} = 12.5$  md.

Checking for internal consistency was then done in the following manner. For the production well case (Fig. A.2a), the duration of the semi-log straight line is given by  $0.11 \leq t \leq 0.73$  days. The corresponding dimensionless times can be calculated with Eq. (4.3.10) expressed in oil-field units:

$$t_{Do} = \frac{6.33 \times 10^{-3} kt}{\phi\mu c_t r_o^2} \quad (\text{A.3})$$

For  $k_{prd} = 4.3$  md, one obtains  $5.0 \leq t_{Do} \leq 37.3$ . Similarly for the injection well case (Fig. A.2b), the duration of the semi-log straight line is  $0.03 \leq t \leq 0.37$  days. Since  $k_{inj} = 12.5$  md, Eq. (A.3) gives  $4.0 \leq t_{Do} \leq 49.1$ . These values are consistent with the bounds  $3 \leq t_{Do} \leq 50$  obtained from the homogeneous system simulation shown in Fig. 4.7.

When such bounds were violated, the duration of the approximate semi-log straight line (as indicated from the pressure derivative graph) was adjusted by a trial-and-error procedure, and permeabilities recalculated, till dimensionless time limits mentioned in the preceding paragraph were satisfied.

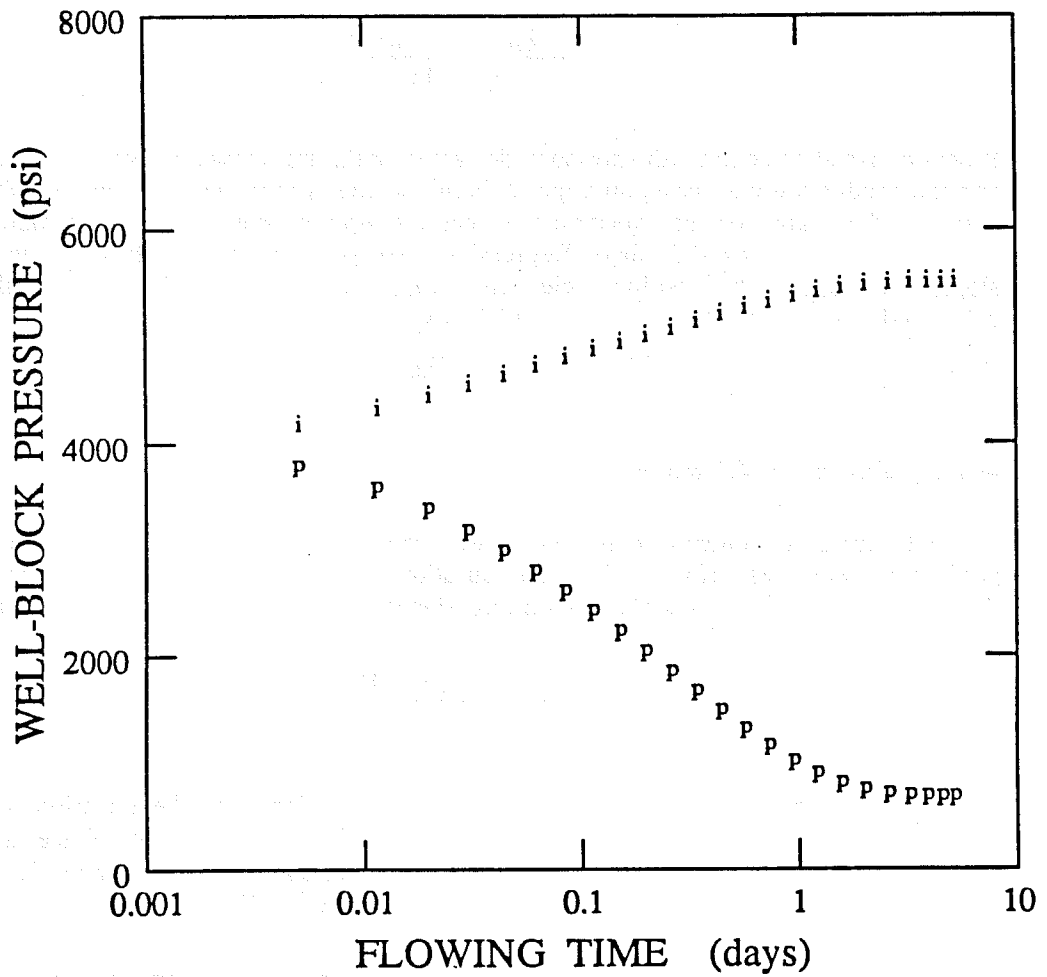
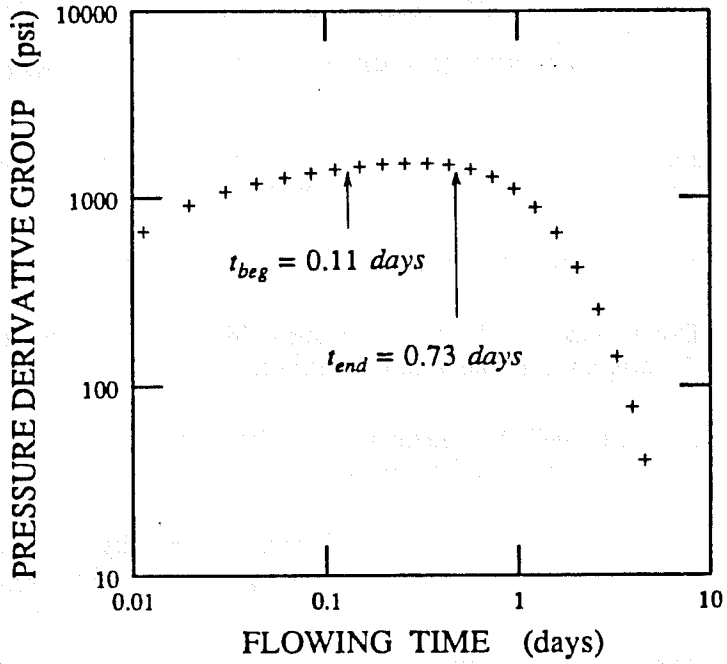
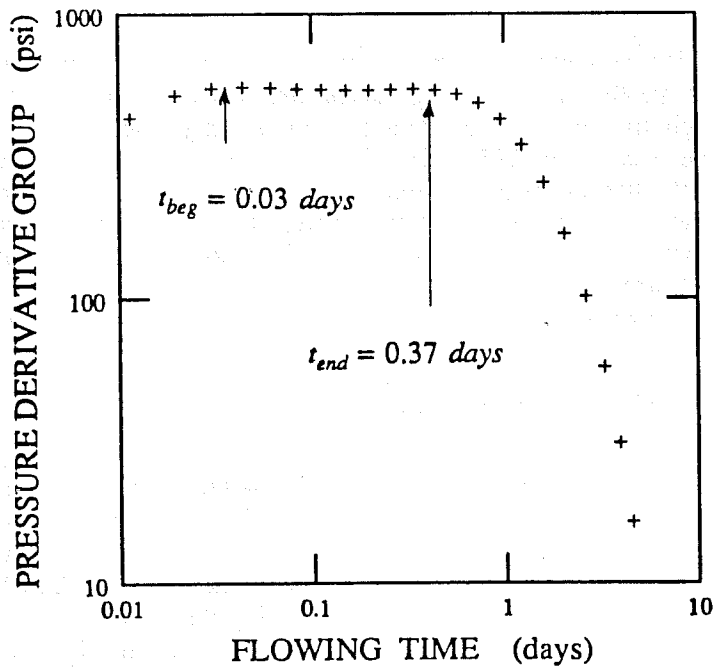


Fig. A.1 Pressure behavior, example permeability calculation



A.2(a) Production well response.



A.2(b) Injection well response.

Fig. A.2 Pressure derivative behavior, example permeability calculation.

## APPENDIX B

### EFFECT OF GRID REFINEMENT ON SIMULATED PRESSURE AND TRACER TEST RESPONSES

This appendix discusses the effect of grid refinement on simulated pressure and tracer test responses. The procedure adopted for this purpose was as follows:

1. Select permeability distribution on  $15 \times 15$  grid.
2. Divide each grid block into 4 sub-grid blocks, and assign the same permeability as the original grid-block to each sub-grid block.
3. Simulate well test responses in the refined ( $30 \times 30$ ) grid, and compare with responses obtained from the coarse ( $15 \times 15$ ) grid.

Simulations were carried out for three different permeability fields, one for each corresponding to (a)  $V_{DP} = 0.35$ ,  $\lambda_D = 1/15$ , (b)  $V_{DP} = 0.50$ ,  $\lambda_D = 6/15$ , and (c)  $V_{DP} = 0.65$ ,  $\lambda_D = 16/15$ .

#### B.1 PRESSURE TEST RESPONSE

The interpretation methodology used was the same as that described in Section 4.3.2. The middle-time data were analyzed as the infinite-acting response to calculate effective permeabilities around injection and production wells. The steady-state pressure drop between injection and production wells was also utilized to calculate steady-state interwell permeabilities.

Effective permeabilities thus computed are presented in Table B.1. Also tabulated for comparison are the corresponding values obtained from the coarse grid ( $15 \times 15$ ) simulations. Even though the two sets of data are not exactly equal, there is good general agreement between the two (within 10%). This indicates that the coarse grid was sufficient to capture the essence of the heterogeneous permeability field, at least for the purpose of estimating effective permeabilities. Although not shown here, the qualitative nature of fine- and coarse-grid simulated pressure responses were similar. Injection and production well responses were fairly symmetrical around the level of initial pressure when  $V_{DP}$  and  $\lambda_D$  were small. For larger values of these parameters, the variability between well responses was greater.

#### B.2 TRACER TEST RESPONSE"

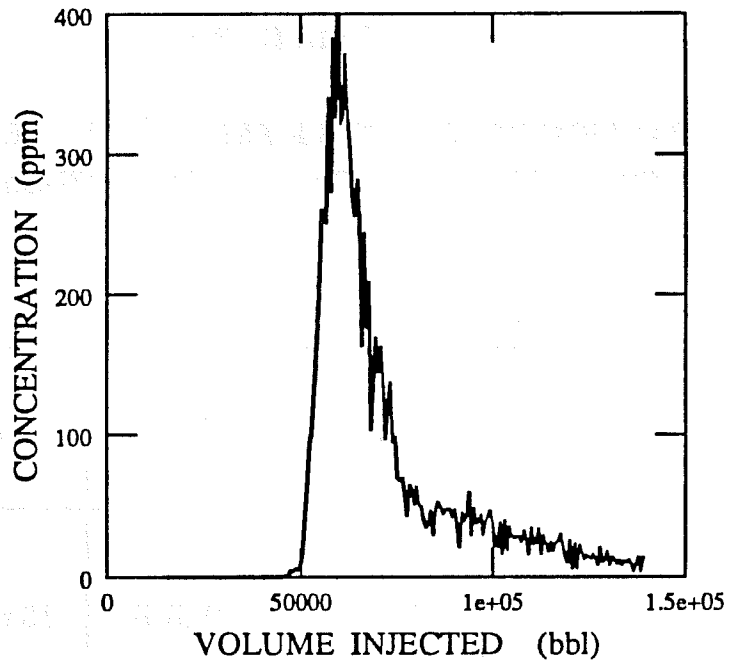
Figures. B.1 through B.3 show tracer breakthrough curves from the fine grid ( $30 \times 30$ ) simulations. Also shown for comparison are tracer responses from the coarse grid ( $15 \times 15$ ) simulations. For a small  $V_{DP}$  and small  $\lambda_D$  (Fig. B.1), both simulations produced similar early-time responses, with a concentration peak at around 60000 bbl. However, the fine-grid simulation showed smaller peaks later, indicating the presence of other flow paths which were not revealed in the coarse-grid run. Both simulations could be matched with a Fickian model (with the same value of dispersivity), but such an interpretation is only approximate for the fine-grid case, as it does not take into account the smaller flow channels.

**TABLE B.1**

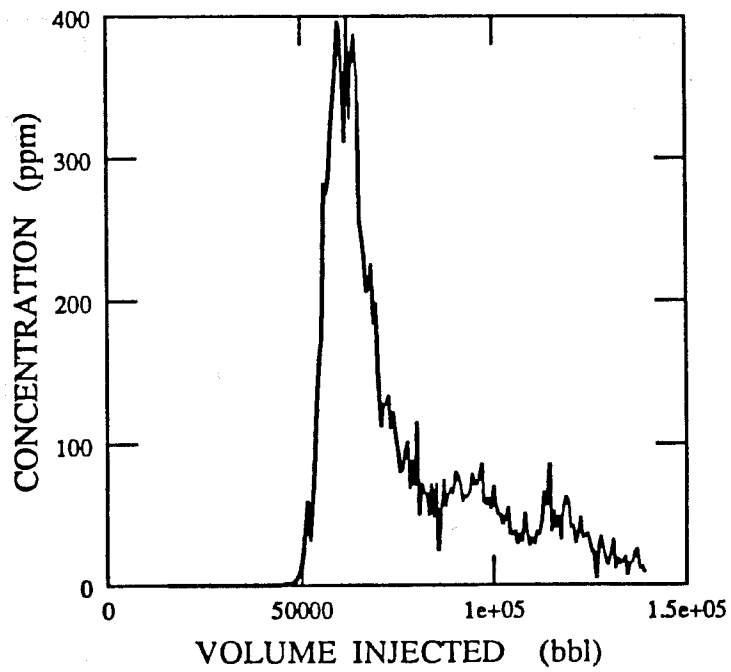
**COMPARISON OF EFFECTIVE PERMEABILITIES OBTAINED  
FROM FINE AND COARSE GRID SIMULATIONS**

	$k_{inj}$	$k_{prd}$	$k_{ss}$
$V_{DP} = 0.35$ $\lambda_D = 1/15$	10.9 (10.2)	9.0 (8.9)	10.6 (9.8)
$V_{DP} = 0.50$ $\lambda_D = 6/15$	8.0 (7.7)	9.4 (9.5)	8.5 (9.4)
$V_{DP} = 0.65$ $\lambda_D = 16/15$	9.5 (9.7)	19.9 (20.1)	13.5 (13.2)

Numbers in parenthesis are results from coarse grid simulations.

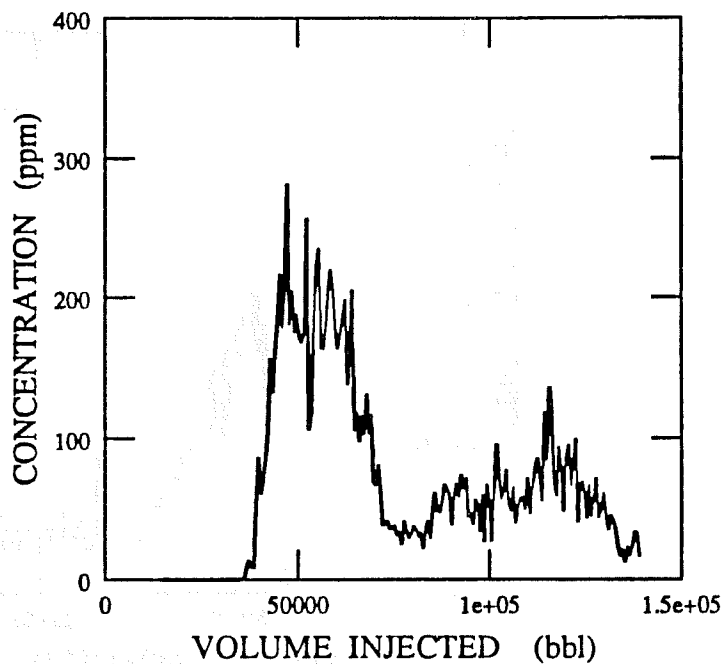


B.1 (a) Coarse-grid simulation, run 2.

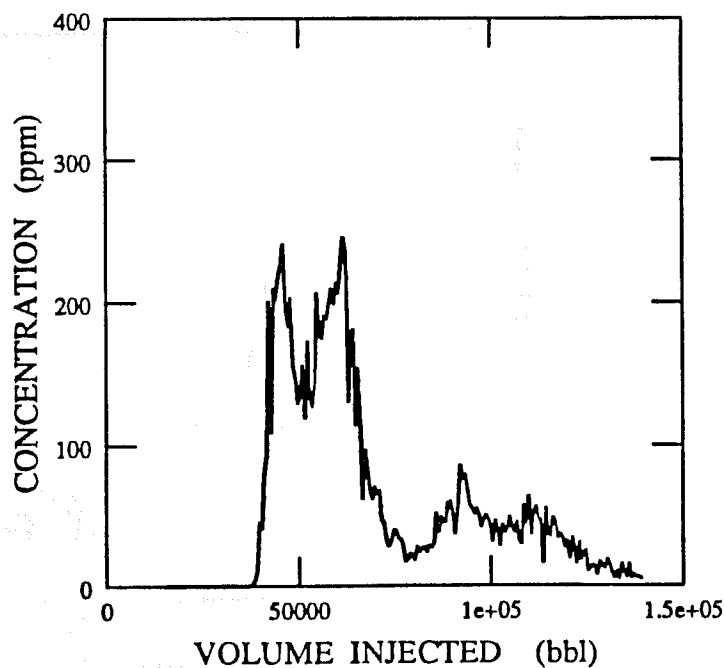


B.1 (b) Fine-grid simulation.

Fig. B.1 Tracer breakthrough curve,  $V_{DP} = 0.35$ ,  $\lambda_D = 1/15$ .

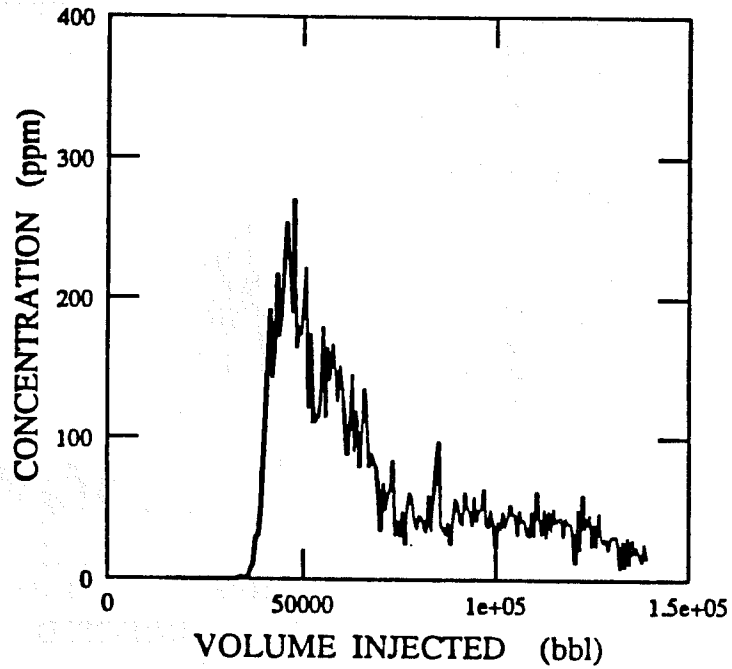


B.2 (a) Coarse-grid simulation, run 4.

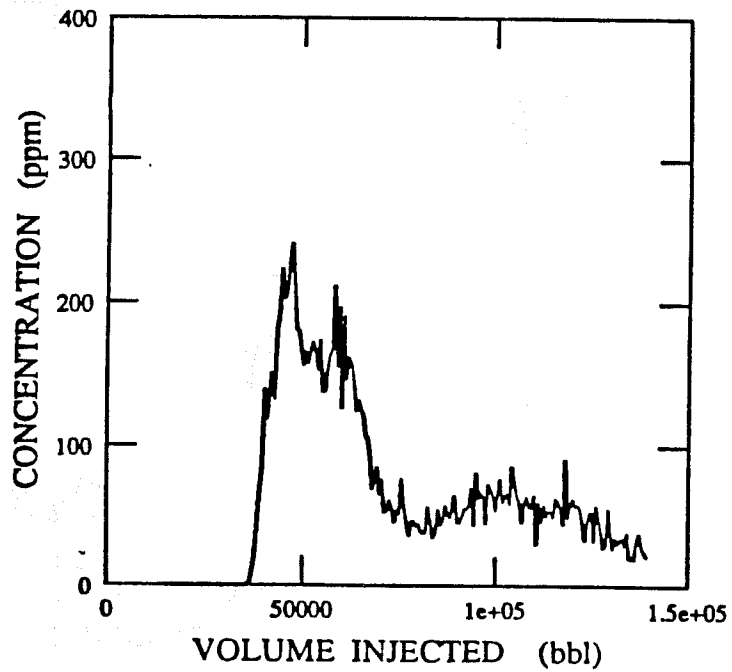


B.2 (b) Fine-grid simulation.

Fig. B.2 Tracer breakthrough curve,  $V_{DP} = 0.50$ ,  $\lambda_D = 6/15$ .



B.3 (a) Coarse-grid simulation, run 7.



B.3 (b) Fine-grid simulation.

Fig. B.3 Tracer breakthrough curve,  $V_{DP} = 0.65$ ,  $\lambda_D = 16/15$ .

In Fig. B.2, where both  $V_{DP}$  and  $\lambda_D$  are greater than that in Fig. B.1, the fine-grid simulations clearly produces a greater resolution in delineating two major flow paths which appeared as one in the coarse-grid simulation (around 60000 bbl). Moreover, the second peak of the coarse-grid run (around 120000 bbl) is seen a little earlier in the fine-grid run. A possible explanation for such behavior is that this flow path has also been divided into two, and its second half has not appeared in the fine-grid simulation due to the limited time-scale shown. The responses from the most heterogeneous case reported (Fig. B.3) show a similar trend, in that the fine-grid simulation is able to provide a better resolution of the nature of flow paths present in the system.

The overall features of tracer responses simulated with fine- and coarse-grids are thus seen to be similar. In both cases, greater heterogeneity produces more preferential flow paths (and concentration peaks). While the coarse-grid runs reported here may be matched with a two-layer model, at least three layers are required to match the fine-grid simulations. This also underscores the fact that not much information can be derived from parameter estimation of multi-modal tracer breakthrough curves, while effective dispersivities computed for the Fickian behavior cases can at least be used as a first estimate for computing tracer flow performance.





c  
c  
c  
c  
c  
c  
50  
c  
c  
c  
c  
60  
c  
c  
c  
c  
70  
80  
90  
c  
c  
c  
c  
c

```
****      standardize the normal values      ****  
****      so that mean equals 0 and variance 1      ****
```

```
sum = 0.  
sumsq = 0.  
do 50 ix = halfn+1, halfn+nx  
do 50 iy = halfn+1, halfn+ny  
    sim(ix,iy,2) = ( sim(ix,iy,2) - xmean ) / sdv  
    sum = sum + sim(ix,iy,2)  
    sumsq = sumsq + sim(ix,iy,2) ** 2  
continue  
xmean = sum / float(nx*ny)  
var = (sumsq - sum ** 2 / float(nx*ny) ) / float(nx*ny-1)  
sdv = dsqrt ( var )
```

```
****      calculate the lognormal values      ****
```

```
sum = 0.  
sumsq = 0.  
do 60 ix = halfn+1, halfn+nx  
do 60 iy = halfn+1, halfn+ny  
    sim(ix,iy,1) = dexp(sim(ix,iy,2)*lgstd+lgmean)  
    sum = sum + dlog(sim(ix,iy,1))  
    sumsq = sumsq + dlog(sim(ix,iy,1)) ** 2  
continue  
xmean = sum / float(nx*ny)  
var = (sumsq - sum ** 2 / float(nx*ny) ) / float(nx*ny-1)  
sdv = dsqrt ( var )
```

```
****      write output      ****
```

```
write (6,*) nx, ny  
ia = halfn + 1  
ib = halfn + nx  
ic = halfn + ny  
do 80 iy = ia, ic  
    j = iy - halfn  
    do 70 ix = ia, ib  
        i = ix - halfn  
        kx(i,j) = sim(ix,iy,1)  
    continue  
continue  
write (6,90) ((perm(i,j),i=1,nx),j=1,ny)  
format(15(f5.1))
```

```
****      calculate experimental variogram      ****
```

```
call gamma ( perm, nx, ny )  
end
```



